7-2020

# Phenotypic Switching of Bacterial Cells in Extreme Environments

Sudip Nepal
*University of Arkansas, Fayetteville*

Phenotypic Switching of Bacterial Cells in Extreme Environments

A dissertation submitted in partial fulfillment
of the requirements for the degree of
Doctor of Philosophy in Microelectronics-Photonics

by

Sudip Nepal
Tribhuvan University
Bachelor of Science in Physics, 2005
Tribhuvan University
Master of Science in Physics, 2008
University of Arkansas
Master of Science in Physics, 2015

July 2020
University of Arkansas

This dissertation is approved for recommendation to the Graduate Council.

Pradeep Kumar, Ph.D.
Dissertation Director

Kartik Balachandran, Ph.D.
Committee Member

Woodrow L. Shew, Ph.D.
Committee Member

Jiali Li, Ph.D.
Committee Member

Rick Wise, Ph.D.
Ex-Officio Member

The following signatories attest that all software used in this dissertation was legally licensed for use by Sudip Nepal for research purposes and publication.

| | |
|---|---|
| Sudip Nepal, Student | Dr. Pradeep Kumar, Dissertation Director |

This dissertation was submitted to http://www.turnitin.com for plagiarism review by the TurnItIn company's software. The signatories have examined the report on this dissertation that was returned by TurnItIn and attest that, in their opinion, the items highlighted by the software are incidental to common usage and are not plagiarized material.

| | |
|---|---|
| Dr. Rick Wise, Program Director | Dr. Pradeep Kumar, Dissertation Director |

**Abstract**

A large number of terrestrial microbial lives thrive in extremes of environmental conditions, including extremes of pressure, temperature, salinity, pH, and a combination of them. For example, all the marine biomass thrive at high hydrostatic pressure depending on depth. The temperature in the ocean can be very high near the hydrothermal vents and salinity and pH depends on the composition of salt in the surrounding areas. On the surface, hot springs, lakes and geysers provide high temperature conditions, while many places are permafrost regions with subzero temperatures. There is an emerging body of work on the viability, genomics, and metagenomics of these organisms, also called extremophiles due to their love for extremes of physicochemical conditions. However, these studies only provide a small window into their adaptation. A better insight into their adaptation to these conditions can be obtained by investigating the effect of these environments on cellular processes of mesophiles, organisms that are not adapted to extremes. Usually, extremes of environmental conditions lead to stresses on mesophilic cells, and therefore, application of these environments may reveal the bottleneck cellular processes that are prone to fail. The effect of pressure, temperature, and salinity on various cellular processes including metabolisms, growth, cell division, and gene expression of a mesophilic bacterium, *Escherichia coli* was studied. This work provides a quantitative picture of these cellular processes of phenotypes obtained under different extremes, and sets a foundation for long-term laboratory evolution of a mesophilic bacterium to the extremes of environmental conditions. Furthermore, the results presented here are also useful in assessing the kind of microbial lifeforms that may exist elsewhere in our solar system, such as Mars, Europa, Ceres, and Enceladus, where the presence of liquid water is known.

## Dedication

This dissertation is dedicated to my parents, Bijaya Doranga and Nar Maya Doranga, who showed the correct path in every step of my life, and always encouraged me to do scholarly work. They are truly the greatest source of my inspiration.

**Acknowledgement**

I would like to show my utmost gratitude to my dissertation advisor, Dr. Pradeep Kumar, for his incomparable support, encouragement, teaching, mentoring, advice, and guidance. Prior to joining his lab, I had no idea of biophysics, research, scientific writing, handling of instruments, experiments, data analysis, and software. He constantly encouraged, taught, mentored, and advised me to formulate a research question and answer it by experiments, models, and simulations. I want to thank Dr. Kumar for making me able to solve related research questions with proper guidance and discussion. I admire his readiness and excitement to discuss research questions, plans, results, and presentations. His description of the problems that emerged during the course of experiments and analysis were easy to understand, and made me realize the amount of research that needs to be carried out to understand the natural phenomena. I further want to mention that Dr. Kumar is very friendly and understood my feelings, problems, strengths, and weaknesses. He always praised the strengths and encouraged me to overcome the weaknesses. Besides research and classes, in every meeting, he talked about great scientists and their accomplishments to motivate me. He shared his experiences as a researcher without hesitation. His passion, hardwork, and philosophy about life inspired me to a great extent and left a memorable impression on me.

I want to express sincere acknowledge to Dr. Rick Wise, Director of Microelectronics-Photonics graduate program, for his invaluable suggestions and advice. Dr. Wise always helped me in every academic and research situation during my graduate school life. I am grateful for his seminars, advising, and encouragement. I want to show my earnest respect to Dr. William Oliver, Physics department chair, for providing me a space to work in the Physics department. I am extremely thankful to Dr. Julia Kennefick for providing teaching assistantships and Stephen Skinner for setting up laboratories and guidance on teaching. I wish to express my indebtedness to Paula Prescott and Renee Hearon for helping me in every aspect of the administration perspective and guidance for the documentation required by the department and the university.

I am wholeheartedly thankful to my dissertation committee members, Dr. Jiali Li, Dr. Woodrow L. Shew, and Dr. Kartik Balchandran, for their enourmous support, guidance and suggestions during the project, which inspired me in every aspect of the research.

During my research, I used some facilities outside our laboratory. I am thankful to Dr. Basanta Raj Wagle for helping me with RT-qPCR protocol and experiments, Dr. Betty Martin for teaching me transmission electron microscopy and helping with the imaging, and Dr, Jianhong Zhou for the help with cell cytometry. I worked on different research projects closely with undergraduate REU students. I enjoyed working with Sara Diletti and Kiona Henderson. I am thankful to Sara Diletti for working with me on a gene expression study.

I am thankful to my lab colleagues Navita Sinha, Khanh Nuygen, and Steven Murray for fruitful discussion, help in experimentations, coursework, suggestions, guidance, and encouragement to perform research. I express my genuine thanks to my brother Suraj Nepal and my sister Suman Nepal for all the love, care, and kindness. I sincerely thank my helpful friends Desalegn Debu, Shiva Pangeni, Mahesh Pangeni, Amrit Pangeni, Prashant Acharya, Bhuwan Khatri, Lakhi Sharma, Samir Jha, Khusbu Jha, Binod Regmi, Kavita Lamsal, Sandip Shrestha, Nawaraj Dulal, and Ranjan Parajuli. I would like to take this opportunity to express gratitude to my family members Narendra Ghimire, Sambridhi Ghimire, Sarthak Ghimire, Shanvi Nepal, Bhawana Poudel, Shiva Kumari Acharya, Prakash Pangeni, Paru Poudel, Bhawagan Pokharel, Dipa Aryal, Ramesh Khatiwada, Shanti Acharya, Deepak Regmi, Shesh Kanta Aryal, Mina Khanal, Dharmagat Pangeni, and Debi Regmi for their support and encouragement.

Finally, I would like to thank my wife, Jyoti Acharya, and my daughter, Adrisha Nepal, for all the care, love, patience, and support during my time in graduate school. I further want to thank everyone who helped me directly or indirectly during my graduate school.

I wish to acknowledge the Arkansas Bioscience Institute for providing partial financial support for the project from the grant provided to Dr. Pradeep Kumar.

**Table of Contents**

**List of Figures**

**List of Tables**

**List of Symbols**

$\tau$= Relaxation time

$\tau_R$= Critical relaxation time

C= Constant

T= Time

$\ell_0$= Initial length of bacteria

$\ell$(T)= Length of bacteria at time

$\ell$= Length of bacterial cell

$< \ell >$ = Average cell length

$P(\ell)$ = Probability distribution

$\tau_d$ = Population doubling time for bacteria

$\tau$= Relaxation time

$\sigma$ = Standard deviation

$\epsilon$ = Error on Gaussian distribution

$m$ = Counting number

$n$ = Counting number

$\Psi$ = Pressure

$k_1(\Psi)$ = Pressure dependent growth rate

$k_2(\Psi)$ = Pressure dependent division rate

$t$ = Time

$\gamma_{L\to H}$ = Switching rate from low-pressure to high-pressure phenotype

$\gamma_{H\to L}$ = Switching rate from high-pressure to low-pressure phenotype

$\ell_0$ = Average length corresponding to 1 atm pressure and 37 °C

$CV_L$ = Coefficient of variation in length

$h$ = Hour

$\ell$ = Length of bacteria

$\ell_b$ = Length at birth

$C_t$ = Threshold cycle

$\ell_d$ = Length at division

$\Delta$ = Added mass

$\tau_{sd}$ = Time between successive divisions

$n_d$ = Number of cells

$r$ = Division ratio

$\rho$ = Repression factor

$F_I$ = Normalized maximum fluorescence intensity

$F_B$ = Normalized background fluorescence intensity

$F_{UI}$ = Normalized fluorescence intensity of master culture

n = Number of generations

**List of Abbreviations**

A-T: Adenine-Thiamine

A: Adenine

ADP: Adenosine Di-Phosphate

AMP: Adenosine Monophosphate

ATCC: American Type Culture Collection

atm: Atmospheric Pressure

ATP: Adenosine Triphosphate

C: Cytosine

cDNA: Complementary Deoxyribonucleic Acid

CV: Coefficient of Variation

DNA: Deoxyribonucleic Acid

*E. coli* : *Escherichia coli*

EXP: Experiments

FAD: Flavin Adenine Dinucleotide

FITC: Fluorescein Isothiocyanate

FMN: Flavin Monomolecule

FSC: Forward Scatter

G-C: Guanine-Cytocine

G: Guanine

GFP: Green Fluorescent Protein

GTP: Guanosine 5-Tri-Phosphate

HGT: Horizontal Gene Transfer

IPTG: Isopropyl $\beta$-D-1-Thiogalactopyranoside

LB: Luria Broth

Mpa: Mega Pascal

n.d.: Not Defined

NAD: Nicotinamide-Adenine Dinucleotide

NADP: Nicotinamide Adenine Dinucleotide Phosphate

NGS: Next Generation Sequencing

NI: National Instruments

OD: Optical Density

OGT: Optimal Growth Temperature

PDS: Potential Division Site

pH: Potential of Hydrogen

PI: Propidium Iodide

rDNA: Ribosomal Deoxyribonucleic Acid

RNA: Ribonucleic Acid

rRNA: Ribosomal Ribonucleic Acid

RT-qPCR: Reverse Transcriptase Quantitative Polymerase Chain Reaction

SSC: Side Scatter

T: Thiamine

TEM: Transmission Electron Microscopy

TMG: Thiomethyl Galactosidase

UV: Ultraviolet

µL: Micro Liter

µm: Micro Meter

µM: Micro Molar

**List of Published Papers Used in this Dissertation**

1. **Part of Chapter 2 was originally published as:**

    - **Sudip Nepal** and Pradeep Kumar. Dynamics of Phenotypic Switching of Bacterial Cells with Temporal Fluctuations in Pressure. *Physical Review E* 97.5 (2018): 052411.

2. **Part of Chapter 3 was originally published as:**

    - **Sudip Nepal** and Pradeep Kumar. Growth, Cell Division, and Gene Expression of *Escherichia coli* at Elevated Concentrations of Magnesium Sulfate: Implications for Habitability of Europa and Mars. *Microorganisms* 8.5 (2020): 637.

# 1 Introduction

## 1.1 Introduction to Bacteria

"What is the origin of life?" is a fundamental question. Biologists, biophysicists, and biochemists have been working on this topic from different perspectives. Some researchers support that life might have originated in places with extremes of physicochemical conditions, such as places with very high temperatures [1, 2, 3], or places with high pressures [4, 5]. While others have argued that the extreme conditions may be irrelevant for the perspective of the origin of life [6]. The proper and satisfactory description of origin of life and its evolution is still lacking in the scientific community. Therefore, the study of the effect of extreme conditions on cellular responses of mesophiles, organisms that thrive in moderate conditions, is useful for understanding the origin of life and the mechanisms of adaptation and evolution of living systems.

Bacteria constitute a large fraction of animal biomass on Earth. The total biomass of bacteria is estimated to be $\approx 70$ gigaton, which is roughly 70% of the total biomass of all the animal biomass on the Earth [7]. The presence of bacteria is important on Earth in different perspectives. Bacteria carry various roles in ecological cycles. They recycle dead plants and animals by decomposing, feed other microbes and eukaryotes; nitrification bacteria fix nitrogen and help to maintain nitrogen cycle. Furthermore, cyanobacteria liberate oxygen during photosynthesis, probiotics bacteria protect the health of higher animals not only by breaking food but also by preventing foreign infections. On the other hand, harmful bacteria are one of the reasons for several diseases and may kill other organisms. The study of bacteria is crucial to understand the mechanism of living systems, and is beneficial in medical, ecological, evolutionary, and extraterrestrial life perspectives.

Nature has created a plethora of environmental conditions on Earth. Both bacteria and archaea can thrive in almost all existing environmental conditions. The traces of bacteria are found in every existing environmental condition on the Earth, including geysers and hot

springs of Yellowstone National Park [8, 9], icy surfaces in Antarctica [10], hydrothermal vents [11] in the ocean, rocky subsurfaces inside the Earth [12, 13], and water droplets in the clouds [14, 15].

## 1.2 Extremophiles

Many environmental conditions on Earth, characterized by the extremities of physicochemical conditions, are not suitable for all life forms. However, a large number of organisms can still thrive in such environments and, hence, are called extremophiles. The study of extremophiles might help to understand the mechanistic view of origin, evolution [16], and the possibility of extraterrestrial life [17]. A summary of different extremophiles is presented below.

### 1.2.1 Piezophiles

Bacteria that can survive at high pressure are called piezophiles. One such example of high-pressure conditions existing on the Earth is deep-sea environments, where the hydrostatic pressure depends on the depth of the ocean. Challenger Deep of the Mariana trench is the deepest part of the Earth with a depth of 10899 m and a pressure of 108 MPa. Deep-sea environments pose several challenges for the microbial community including high pressure, low temperature, and low nutrition. Despite these harsh conditions, some bacteria and archaea can grow optimally. Zobel and Morita in 1957 found the first trace of a barophilic bacterium [18]. Several bacterial strains isolated and studied from the Challenger Deep. The first pure isolation of the bacterial strain was obtained in 1979 is MT41 [19]. In 1997, two more strains isolated and studied are DB21MT-2 and DB21MT-5 and these strains grow optimally at pressures of 70 and 80 MPa, respectively [20], and are called obligately barophiles. The DNA sequencing, DNA-DNA relatedness study, and the fatty acid analysis of the extracted bacteria showed that the strains DB21MT-2 and DB21MT-5 are closely related to *Shewanella benthica* and genus *Moritella*, respectively [21]. Further taxonomic and

gene sequencing study of the thousands of microbes collected from the mud samples revealed that the seabed ecosystem consists of several extremophiles including alkaliphiles, thermophiles, and psychrophiles [22].

### 1.2.2 Thermophiles

Thermophiles live and grow at a higher temperature than most of the existing organisms on the Earth. The naturally occurring geothermal heated regions found on the Earth serve as home for a large number of thermophiles. A variety of thermophiles are found in hot springs and several thermophilic organisms are extracted and studied from hot springs around the globe [23, 24, 25, 26, 27, 28]. The spring in the Uzon Caldera of Kamchatka is an excellent example of the extreme environment for the growth of extremophiles due to high temperature (75 °C) and acidic environment of pH about 1.0 [29]. Volcanic activities create several hot springs near the Caldera regions. Kamchatka peninsula in the far east of Russia is one such example of extreme environments existing on Earth for thermophiles and acidophiles. The temperature of hot springs varies from $60 - 100$ °C and pH can be as low as 1.0 [30]. Mutnovsky, a complex volcano, situated in the southern part of Kamchatka peninsula, Russia, consists of several ions including $Fe^{3+}$, $Mg^{2+}$, $Al^{3+}$, $Ca^{2+}$, $K^{+}$, $Na^{+}$, and $SO_4^{2-}$. Out of these ions, $SO_4^{2-}$ is the most abundant ion present in the peninsula [31]. The abundance of sulfate ions makes the springs acidic and the energy source for sulfur-reducing bacteria. *Methanopyrus kandleri* is hyperthermal archaea found in hydrothermal vents at the coastal areas of California which can grow at temperature of 122 °C [32].

Figure 1 is the grand prismatic spring in the Yellowstone National Park, USA. The temperature at the center of the spring is around 70 °C. The temperature slowly falls off from the center to the edge creating a temperature gradient. Diverse bacterial species are found due to the variation in temperature. The different colors at different parts of the spring arise due to a variety of bacteria present in the spring.

The outermost layer of grand prismatic spring has *Calothrix sp.*, a bacterium that lives

Figure 1: The grand prismatic spring located in the Yellowstone National Park.(Source: http://www.yellowstonepark.com/things-to-do/grand-prismatic-midway-geyser-basin).

at temperature below 30 °C. The cell contains a dark brown pigment in scytonemin which protects the bacteria from UV radiation [33]. The second layer contains *Phoridium sp.*; a bacterium that thrives at temperatures between 45 and 60 °C. These cells produce pigments with rusty brown mats [34]. Another layer is composed of *Chloroflexus sp.* bacteria which can grow in the temperature range of $52 - 60$ °C, and they produce green and brown color pigments bacteriochlorophyll c, bacteriochlorophyll, and carotenoids [35]. *Thermus aquaticus* is another chemotrophic bacterium which produces yellow pigment, and the bacteria thrives at the temperature of 70 °C [36, 37]. The bacterium, *Synechococcus sp.*, grows at the extreme heat, near the places where the temperature of the lake is 72 °C. These bacteria secrete chlorophyll a and phycobiliproteins, which are green and yellow-orange fluoresce at the wavelength range of $570 - 620$ nm [38]. All these bacterial strains are autotrophic except *Thermus aquaticus*. The color of the spring appears dark red and orange during summer

because of the dominance of autotrophic bacteria and their pigments that help to save them from the intense radiation from the Sun. In winter, the color of the spring appears dark green due to the photosynthesis process and production of the chlorophylls by the cells [39]. The presence of bacteria in hot environments like hot springs has both ecological and evolutionary importance.

### 1.2.3 Psychrophiles

Bacteria not only thrive in moderate and hot places but also in the area where the temperature is always low. Antarctic surfaces are one such area where environment is generally cold and dry. The atmosphere is harsh due to the presence of negligible amounts of liquid water, low light, high pressure, a small amount of salt, and a low concentration of chemicals. Several organisms cannot survive under these conditions. Despite harsh conditions, psychrophilic bacteria thrive in the Antarctic ice [40, 41]. Recent studies revealed that methane reservoirs [42] and aquifers [43] are present beneath the surface of Antarctica. These findings indicate that the Antarctic subsurface is a potential place for the habitat of methanogens, and suggest a possibility of the existence of an ecosystem. The extremophiles in cold environments open the possibility of extraterrestrial life in places, where an icy world is present including, Europa, Ceres, and Enceladus.

### 1.2.4 Acidophiles

Low pH is one of the extreme environmental conditions which exists both naturally and artificially. Acidophiles are further divided into two categories — (i) extreme acidophiles which thrive at pH less than three and (ii) moderate acidophiles that can survive at a pH range of $3-5$ [44]. Life in acidic medium is challenging due to large ionic strength, lack of essential chemicals, and lack of nutrients. Bacteria living in an acidic medium utilize the available iron or sulfur as a source of energy [45]. One of the challenges for archaea and bacteria thriving at low pH is to maintain the stability and functionality of enzymes and

proteins. To take advantage of low surrounding pH, acidophiles create a pH gradient across the cell membrane. The gradient thus formed is further utilized to produce adenosine triphosphate (ATP) by driving protons inside the cells through F0F1 ATPase [46]. Figure 2 is an acidic river, Rio Tinto, in southwestern Spain. The river serves as a shelter for extremophiles because of low pH $(1.1 - 3)$ and the presence of heavy metals. It appears red due to the presence of a high amount of ferric iron.

Figure 2: Rio Tinto, an acidic river in southwestern Spain. The red color of the river is due to the presence of ferric iron. (Source: https://www.nasa.gov/content/rio-tinto-spain).

The ecosystem at the Rio Tinto is limited to the organisms that can oxidize iron and sulfur. The microorganisms involved in the oxidation of iron (*Acidithiobacillus ferrooxidans*, *Sulfobacillus spp.*, and *Ferroplasma spp.*) and the oxidation of sulfur (*Desulfurella spp.*, *Desulfosporosinus spp.*, and *Thermodesulfobium spp.*), and the oxidation of carbon (*Acidiphilium spp.*, *Bacillus spp.*, *Clostridium spp.*, and, *Acidobacterium spp.*) were found in

the river [47]. Ferric iron helps to accept an electron for the process of oxidization. Low pH of the river is due to oxidation of sulfur by chemolithotrophic organisms, that reduce inorganic compounds to obtain the necessary energy from the river. The eukaryotes and prokaryotes present in the lake maintain the iron, sulfur, and carbon cycle in the lake environment.

### 1.2.5 Halophiles

Extremophiles that need high salt for optimal growth are called halophiles. Halotolerant bacteria grow optimally in low salt, and can grow and divide in high salt, albeit at a slower growth rate. Halophilic organisms exist in all three taxonomic domains — bacteria, archaea, and Eucarya. Salt is necessary for the growth and maintenance of cellular integrity [48]. When the salt level drops below 20 mM of magnesium chloride or 0.2 M of sodium chloride, the integrity of the cell breaks down, and the cellular components disaggregate [49]. Halophiles exhibit highly diversified metabolism, including oxygenic, anoxygenic, phototrophic, autotrophic, sulfur-reduction, denitrification, and fermentation [50]. *Halobacterium halobium* contains a membrane with purple color in its plasma, which uses light to create an electrochemical gradient by translocating the proteins [51]. The gradient thus generated is used for ATP synthesis.

### 1.2.6 Microbial Life Near Hydrothermal Vents

Hydrothermal vents are a part of the ocean where organisms experience both high hydrostatic pressure and high temperature. The temperature in the hydrothermal vents can be as high as 400 °C. The temperature decreases on increasing the distance from the vent. The hot anoxic hydrothermal fluid mixes quickly with the cold oxic seawater, creating chemical and thermal gradients [52, 53, 54]. These gradients serve as a home for several microbes, and gives rise to a strong symbiotic hydrothermal ecosystem. Some reactive chemicals from the inner part of the Earth react with the surrounding chemicals, creating new materials. Vents are rich in several chemicals with an abundance of sodium and chloride.

Other chemicals like lithium, potassium, rubidium, beryllium, bismuth, copper, zinc, and manganese are also available, but in lower concentrations compared to sodium and chlorine [55]. These chemicals play an important role in developing hydrothermal ecology. Magnesium and sulfate are not found in the vent tip and chimneys, but are abundant in the seawater. Figure 3 shows the interaction between the fluid present around a hydrothermal vent and the seawater. Quick decrease in temperature away from the vents due to mixing of the fluids with the cold seawater [56] makes a favorable environment for the growth of several microbes. The organisms present near the hydrothermal vents obtain energy from the interaction of electron donors (e.g., $H_2$, $H_2S$, $Fe^{2+}$, and $CH_4$) and electron acceptors (e.g., $O_2$, $CO_2$, $Fe^{3+}$, $SO_4^{2-}$, and $NO_3^-$) and their interactions.

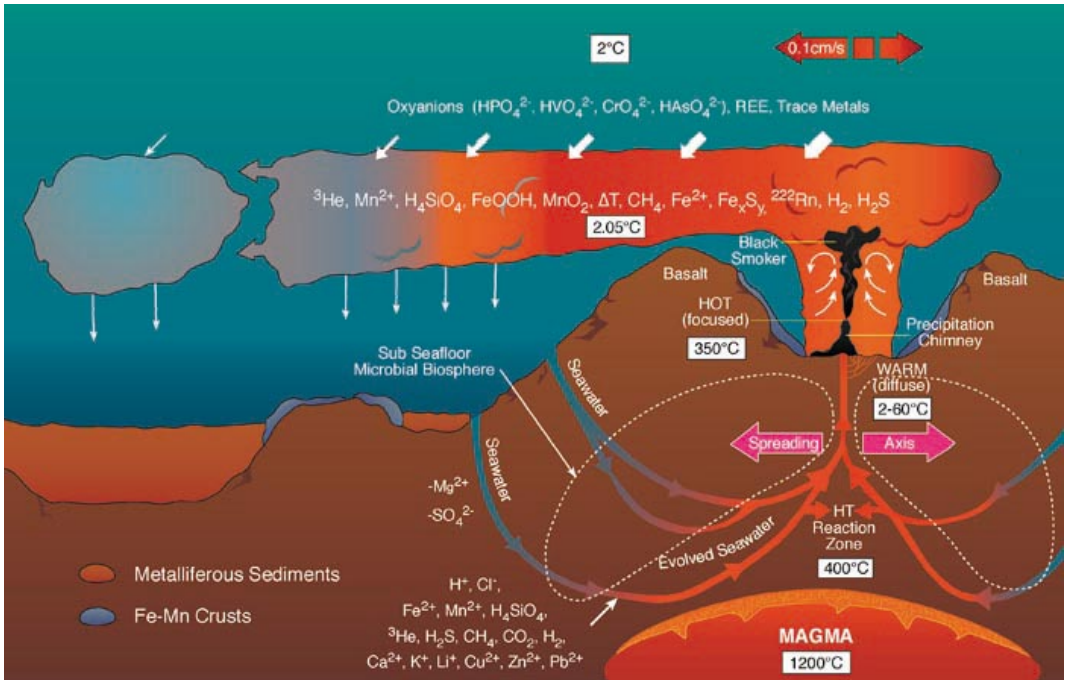


Figure 3: Chemistry around the hydrothermal vent and its interaction with the ocean water. (Source:pubs.acs.org/cen/hotarticles/cenear/981221/7651sci6xaa.ce.html).

Specifically, redox reactions provide necessary energy to the vent organisms [52]. Some redox reactions occur at high temperature near the tip of the vents. On the other hand, organic reductions are rare at such high temperature ranges. Even though organic reductions

are rare at high temperatures, some sulfate reducing anaerobic bacteria can take sulfate for the terminal electron acceptor and reduce it to sulfides [57]. It was shown that bacteria can reduce sulfate at 110 °C [58] at the rate of $19 - 61$ µM of $SO_{4^-}$ per day [59]. Metagenomics studies of sulfur-oxidizing bacteria revealed the presence of sulfur oxidation gene (*soxB*) with two enzymes present in the cell. The first enzyme is sulfite oxidase which oxidizes sulfite into sulfate and the second enzyme is sulfide dehydrogenate that catalyzes sulfite into sulfate of low-temperature found in two hydrothermal chimneys on the Southwest Indian Ridge [60]. In addition to high hydrostatic pressure and high temperature, the presence of minerals make the environment saline near the vents, and several halophile bacteria and archaea are reported to be found near hydrothermal vents [61, 62, 63].

Figure 4 is a recently discovered (2015) hydrothermal vent in the Gulf of California (150 km east to La Paz, Mexico). The vent is located at 3800 m below the ocean's surface. The crimson color organisms shown in the figure are giant tube worms, *Riftia pachyptila*. These tube worms surround the hydrothermal vents where the physiochemical conditions are favorable to them. They feed on chemosynthetic microorganisms [64] and can grow up to two meters long, living symbiotically with other organisms near the vents [65]. Trophosome of *Riftia pachyptila* provides shelter for *Candidatus Endoriftia persephone* [66] and several other monospecific endosymbiotic bacteria [67]. Tube worms generally make a cluster, as shown in Fig. 4, and it is known to provide a shelter for 60 different species [65]. 16S *rRNA* sequencing and phylogenic study of the organisms from a hydrothermal vent on Mid Atlantic ridge revealed that two symbiotic bacteria — one is sulfur reducing and another is methane reducing thrive symbiotically sheltering in a single mytilid organism [68].

### 1.3 Stability and Functionality of Biomolecules in Extreme Conditions

Stability and functionality of biomolecules in any environment are necessary for organisms to grow and reproduce. For any organism to adapt to extreme environments, biomolecules must also be able to function in those conditions. Micromolecules are biomolecules that are associated with metabolism or gene expression. Metabolite and

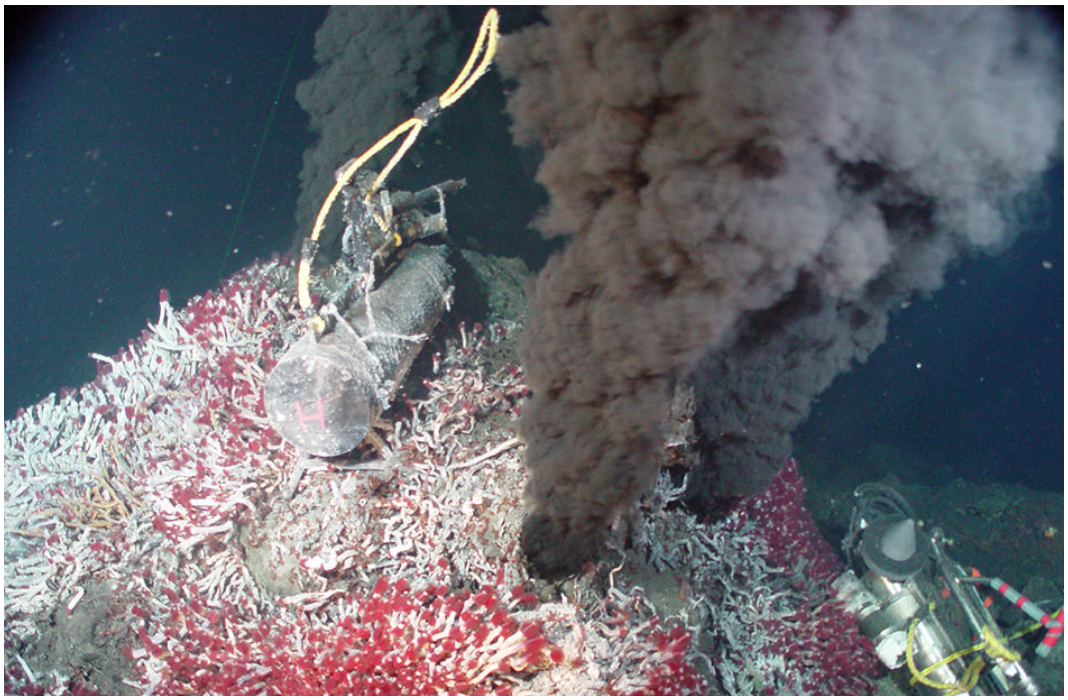

Figure 4: Hydrothermal vent in the Gulf of California showing black and white smokers. (Source: https://oceanservice.noaa.gov/facts/vents.html.)

coenzymes, are necessary for the production and functioning of macromolecules. Table 1 is a list of stability of some micromolecules at two temperatures, 95 °C and 105 °C, exposed for the duration of one and three hours, respectively [69]. Acetyl phosphate, NAD(P), ADP, ATP, and pyridoxal phosphate are unstable at a temperature higher than 100 °C. The micromolecules that decompose when heated at 95 °C for an hour decrease their remaining portion significantly when heated for three hours at 105 °C (FMN, Pyridoxal phosphate, Glucose 1, 6-phosphate, ATP, ADP, and AMP). Growth of hyperthermophilic bacteria and archaea above 100 °C suggests that they circumvent the instability of micromolecules in some way. Studies have shown that microorganisms use several ways to overcome the thermal instability of biomolecules, including multiple metabolites [70], catalytic enzymes [71], and by changing the physiochemical conditions in the cells [72].

The stability of major macromolecules like DNA, RNA, lipids, and proteins at a high temperature is important for the cells to function properly. Table 2 is a list of half-life of

Table 1: Thermal stability of metabolite/coenzymes.

| metabolite/coenzyme | Percentage remaining after | |
|---|---|---|
| | $1h$/95 °C | $3h$/105 °C |
| NAD | <5 | n.d. |
| FAD | 100 | 85 |
| FMN | 75 | 65 |
| Pyridoxal phosphate | 40 | 0 |
| Glucose | 100 | 100 |
| Glucose 6-phosphate | 100 | 70 |
| Glucose 1, 6-phosphate | 90 | 50 |
| Gluconate | 100 | 100 |
| 6-phosphogluconate | 100 | 90 |
| Glycerate | 100 | 100 |
| 3-phosphoglycerate | 100 | 100 |
| Acetate | 100 | 100 |
| Acetyl phosphate | < 10 | n.d. |
| CoASH | 100 | 45 |
| Acetyl-CoA | 100 | 75 |
| ATP | 40 | 0 |
| ADP | 50 | 0 |
| AMP | 95 | 60 |

some enzymes at temperatures $\geq$ 100 °C. The data presented here were obtained from Vielle et al. and Coolbear et al. [73, 74]. The half-life of the enzymes listed is higher than the doubling time of organism and, hence, it has relatively small effect on the enzymes.

Table 2: Thermal stability of some enzymes $\geq$ 100 °C

| Enzymes | Source | half-life (h) | Temperature |
|---|---|---|---|
| 3-phosphate dehydrogenase | *Thermotoga maritima* | >2 | 100 |
| Hydrogenase | *Pyrococcus furiosus* | 2 | 100 |
| Amylase | *Pyrococcus woesei* | 6 | 100 |
| Glutamate dehydrogenase | *Pyrococcus furiosus* | 10 | 100 |
| Cellobiohydrolase | *Thermotoga sp.* | 1.1 | 108 |
| Amylase | *Pyrococcus furiosus* | 2 | 120 |

Cell death of *Escherichia coli* at 50 °C regardless of the strains may be due to the instability of vital proteins at 50 °C [75]. The native structure and functionality of proteins remain intact in a range of environmental parameters in which they thrive. Proteins unfold

at low pH [76], high pH [77], high salinity [78], and extremes of temperatures [79] and pressures [80]. The stability of proteins depends on a number of parameters such as composition, the length of amino acid chain, and their hydrophobicity [81].

External driving forces due to physicochemical conditions can destabilize proteins, causing them to lose their native structure. The stability of globular proteins at room temperature is marginal [82, 83] and the marginal stability of the proteins are necessary to function. High temperatures may denature proteins and, hence, make them not functional [84]. pH also affects the stability and functionality of proteins [85]. Proteins may unfold at extremes of pH [86, 87]. A protein is neutral at the isoelectric point, defined by the pH, and it exhibits positive charge below and negative charge above the isoelectric point [88]. Studies have shown that similar to temperature, application of high pressures can also lead to denaturation of proteins [89].

### 1.4 Genomic studies of Extremophiles

Functionality and stability of DNA, RNA, and proteins are necessary for cellular processes. The first DNA sequencing of bacteriophage ΦX147 DNA was done in 1977 by Fred Sanger using the chain termination method, and it remains a dominant approach for 30 years [90, 91]. An ultra-high throughput, cheaper, and faster sequencing method was recently introduced called next generation sequencing (NGS) [92]. While many of the extreme conditions are hard to simulate in a laboratory, the advent of NGS has provided a small window into the adaptation of many extremophiles. Genetic study using a whole genome sequence is more convenient and faster due to the development of NGS [93]. The size of the genome is highly diverse, ranging from 582 base pairs in *Mycoplasma genitalium* [94] to 149 billion base pairs in *Paris japonica* [95]. The human genome has about three billion base pairs and the size of the genome and the complexity of the organism are not related in higher organisms. The robustness of the organism instead depends on the stability of macromolecules, namely nucleic acids, lipids, and proteins. Amino acid sequences of a

proteins are useful for the determination of their native structures, secondary structures, that essential parameters to define the functionality and stability of the proteins [96].

A DNA (di-oxiribose nucleic acid) is a double-stranded polymer composed of four nucleotides; Adenine(A), Thiamine(T), Guanine(G), and Cytosine(C). Adenosine-Thiamine and Guanine-Cytosine form opposite strands form hydrogen bonds, providing stability to the DNA. Adenine (A) and Thiamine (T) form two hydrogen bonds, while the Guanine (G) and Cytosine (C) form three hydrogen bonds [97]. Due to three hydrogen bonds between the G-C pair, a DNA with large number of G-C pairs has higher thermal stability and, hence, a large denaturation temperature than a DNA with large number of A-T pairs [98, 99]. The genome of wild-type *E. coli* (optimal growth temperature 37 °C) has around 50% of G-C content. *Sulfolobus*, sulfur-reducing bacteria, are spherical and lacking peptidoglycan layer with G-C composition of $60 - 68\%$ can grow in low pH and at high temperature [100]. *Thermus thermophilus*, an extremophile with optimal growth temperature of 65 °C [101], has 70.1% of G-C content in the coding regions of the genome [102]. A recent study of 722 mesophilic and 93 extremophiles (Thermophiles/hyperthermophiles) showed that the optimal growth temperature is directly correlated to the percentage of G-C content in bacteria [103]. The results further signify that the optimal growth condition of an organism depends on the thermal stability of DNA. The continuous exposure of the stress on a bacteria for a long time might change the genome structure. The genomes of the organisms that belong to a family are related and its matching fraction differs according to the strains. The genomes of organisms of the same family with 50% identical pairs over 50% of the genome length are conserved genomes. The different strains of *E. coli* have wide differences in their genomes [104].

There are many other factors that lead to stability of proteins at extreme conditions. Genomic studies have found the number of salt bridges forming amino acids increases in organisms that thrive at high temperatures [105]. For example, a recent study found that the numbers of cystine amino acids, that can form disulfide bond, increases with increasing

optimal growth temperature of organisms [106]. Proteins of halophiles are relatively stable at high salt concentrations regardless of the lower hydrophobicity, and the water activity. The formation of salt bridges in halophilic bacteria provides halostability of proteins [107]. The additional salt bridges compensate for the presence of low hydrophobicity and water activity making halophiles viable in high salt environments.

## 1.5 Laboratory Experiments on Adaptation of *E. coli*

Adaptive evolution in laboratory, whereby a mesophilic bacteria is kept under a constant extreme conditions, is another approach to study their adaptation to extreme conditions. The genome of bacteria is dynamic, and in *E. coli*, they are rearranged by deletion, inversion, and duplication during laboratory evolutionary experiments [108]. The rearrangement of the genome leads organisms to adapt and evolve in a set of new environmental conditions. Several laboratory evolution experiments were carried out for cells under different stresses, to understand the effect of long term stress on cells. In Table 3, a list of some adaptive evolution experiments that were carried out in the laboratories. In many of these studies, cells were able to adapt to a new set of environmental conditions after few hundreds of generations. Such an approach has many advantages, including characterization of the temporal evolutionary dynamics of cells as they adapt to the new set of conditions.

## 1.6 Extraterrestrial Life

Bacteria are ubiquitous in the water bodies on Earth, regardless of the other extreme environmental conditions. Liquid water, organic molecules, semipermeable membranes, and energy sources are the basic requirements for the existence of any life form [116]. Water has a crucial relationship with terrestrial life. It serves as a solvent for ions, and organic and inorganic compounds. Presence of water in the solar bodies makes the life tenable there. Several planetary bodies have emerged as the candidates for life beyond Earth, due to the discovery of the presence of water. These include Mars, Europa, Enceladus, and Ceres.

Table 3: Adaptive evolution studies carried out in *E. coli* at different environmental stresses

| Environmental Stresses | | | |
|---|---|---|---|
| *E. coli* REL606 | Temperature (41.5 °C) | 2000 generations | [109] |
| *E. coli* PQ30 | UV light | 80 UV light cycles | [110] |
| *E. coli* REL606 and REL607 | Freeze-Thaw | 150 cycles | [111] |
| *E. coli* Several Strains | Osmotic stress | n.d. | [112] |
| *E. coli* MG1655 | Temperature (48.5 °C) | 620 generations | [113] |
| *E. coli* MG1655 | Rich media, ethanol 5%(v/v) | $30 - 160$ generations | [114] |
| *E. coli* W3110 | M9 media, ethanol 7%(v/v) | 1000 generations | [115] |

Mars once had a molten core similar to Earth, in which magnetohydrodynamics effects created a magnetic effect [117]. Later the magnetosphere vanished, and the atmosphere was swept away by the solar wind [118]. Due to the lack of a protective atmosphere, the surface is bombarded by solar radiations. Presence of little water, very low surface temperature and atmospheric pressure, and high radiation on the surface of the present day Mars make it an inhospitable place for life [119]. However, the possibility of life on Mars cannot be ignored until it is proven by analyzing a physical sample from the Mars. Laboratory experiments of bacteria and archaea under simulated Mars conditions may help understand the possibility of life on the surface or the subsurface regions of Mars. A methanogenic archaea isolated from a permafrost place on Siberia survived under the simulated Martian conditions and, hence, raised possibility of the life on Mars [120]. In another study, a methanoutotrophic archaea, *wolfeii*, could survive a wide range of pH, temperature, and hydrostatic pressure [121, 122], again suggesting the possibility of methanogens in the subsurface regions of Mars. In addition Mars is a planet with an abundance of ferric iron, giving it a characteristic orange-red color. The aqueous solutions of the salts of iron creates a low pH environment. Bacteria thriving at low pH exhibit different metabolism compared to mesophilic bacterium. Some are chemolithoorganoheterotrophic, chemolithotrophic, and chemolithomixotrophic

metabolism and the starch breaking enzymes like amylase and glucoamylase are found in acidophiles [48]. Moreover, the microorganisms get their energy from the organic and inorganic compounds as well as proton consumption. These attributes are important to the astrobiological studies of the conditions where oxygen is low and water contains several ions.

Europa, Jupiter's Galilean moon, has liquid water on it and, hence, is a potential candidate to search for the life beyond Earth [123, 124, 125, 126, 127]. In 2016, the Hubble telescope detected a 100 km tall plume of water emerging from the equatorial surface [125, 128, 129]. Figure 5(A) is plume of water rising from the surface and Fig. 5(B) is the patterns made by the ice.

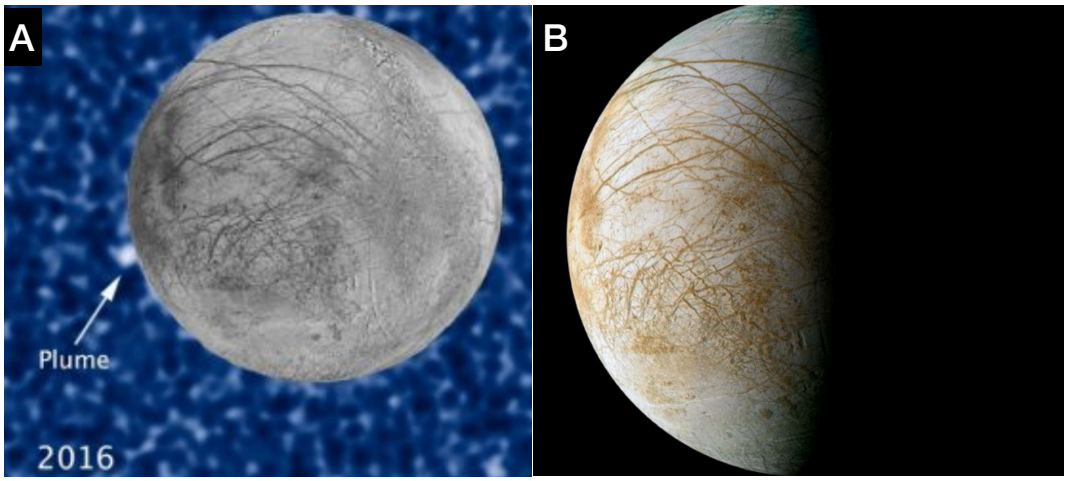


Figure 5: Presence of water on Europa, A. ice patterns on the surface and B. plumes of water on its equator. (Source: https://www.space.com/36464-jupiter-moon-europa-water-plume-hubble.html).

Another vital aspect of life, if it may exist at all on Europa, is the requirement of the inorganic substances necessary to support life. Magnesium sulfate is abundant in the surface of the Europa [130, 131, 132] that might have formed due to radiation present along with sulfuric acid and sulfur dioxide [133]. These conditions make the ocean on Europa acidic. Therefore, the life in the ocean of Europa must be adapted to high hydrostatic pressure, presumably low temperatures, and low pH. The study of the extremophiles and their growth and viability in extreme conditions provide rich information about the extremophiles and

possibility of existence of extraterrestrial life.

## 1.7 Dissertation Overview

The first chapter is a broad literature review of different organisms and their growth habitats, metabolisms, stability of biomolecules, and their characterization in different extreme conditions that exist on Earth. The chapter further discusses the possibility of life on other planetary bodies.

The second chapter discusses the cellular responses of *E. coli* at high hydrostatic pressure. Specifically, it discusses the dynamics of phenotypic switching of two phenotypes with temporal oscillations in pressure. The experimental results of the phenotypic switching of bacteria at high pressure is explained using a two-state switching model.

The third chapter discusses the growth, morphology, plasmolysis, death, and gene expression of *E. coli* at elevated concentrations of $MgSO_4$. The reversibility of the cells grown at 1.25 M $MgSO_4$ are also studied.

The fourth chapter focuses on the dynamics of cell division upon the removal of the slat stress. The underlying phenomenon of cell division of highly heterogeneous population of bacteria cells is studied using experiment, theory, and simulations.

The fifth chapter deals with the effect of temperature on the multistability on gene expression of the *lac* operon. The chapter discusses the ranges of bistability in the temperature and thio-methyl galactosidase (TMG) space using a set of experiments.

# 2 Dynamics of Phenotypic Switching of Bacterial Cells with Temporal Fluctuations in Pressure

## 2.1 Introduction

Bacteria experiences physicochemical fluctuations continuously, and they respond to those fluctuations on a day by day basis [134]. These environmental fluctuations may cause cells to change the morphology and growth rate. The extent of deviations in growth rate and morphology depends on the intensity of fluctuations. If the change around bacteria is high, they experience cell death [135]. Obligately barophilic bacteria are known to survive and grow optimally at the bottom of the oceans where the depth is about 11800 m, and the pressure is as high as 1200 Mpa [20]. At elevated pressure, the growth rate of *Escherichia coli* (*E. coli*), a mesophilic bacterium, decreases [136, 137], and the growth is completely inhibited at 600 atm. A fraction of cells grown at high pressure undergo lack of cell division resulting in an increase in cell length [138, 139]. Cells die at a pressure of 900 atm [139, 140]. It is shown that FtsZ and MreB depolymerize at high pressure inhibiting cell division process [141, 142]. Pressure also affects the dynamics of motility of bacterial cells. The motion of cells in a media decreases with the increase in pressure and the counterclockwise rotation of *E. coli* shifts to clockwise motion at high pressure [143]. The loss in motility of cells is due to the lack of formation of the flagella at high pressure [144]. Although cellular processes of cells shut down completely at 1000 atm[145], the integrity of cells remain intact at pressure as high as 5000 atm due to the stability of pectin methylesterase, an enzyme associated with cell wall integrity [146].

At a high pressure of 1000 atm, the bonds remain intact [80]. Hence, the primary structure micromolecules like lipids, saccharides, coenzymes, metabolites, and peptides remain unchanged. Hydrogen bonds are stable at pressure as high as 1000 atm [147]. The macromolecules with a strong bond remain structurally and functionally sound, but the molecules with weak pressure might break at high pressure and, hence, change the primary structure. For example, multimeric proteins are bound with a weak bond, and pressure

denatures these proteins [148]. The secondary and tertiary structure might change at high pressure. It is known that the tertiary structure of supercoiled DNA changes at high pressures [149]. Pressure affects the ions and stability of the ions in cells [148] and, hence, several proteins are aggregated at high pressure losing its functionality [150]. Effect of extreme conditions on several proteins is well studied [2, 150, 151, 152]. Several proteins undergo denaturation at hydrostatic pressures above 2000 atm and the denaturation of proteins is temperature dependent [80, 147, 150, 153, 154]. Proteins are functional when they are in native structure and even a partial denaturation might lose the functionality of protein at moderate pressures [151]. Recent investigations showed that long $5'$ untranslated regions, the structural motifs, conduct the structural stability of RNA in deep sea viruses [155]. Supercoiled DNA was found to be twisted at high hydrostatic pressure and, hence, modify the tertiary structure and raises an issue on the effect of high hydrostatic pressure on the stability of DNA and the adaptation of organisms especially thriving in deep sea environments [156]. Pressure and temperature not only affect the stability of several biomolecules but also change the reaction rate and the synthesis of biomolecules. At high pressure, the synthesis of macromolecules like RNA and protein is inhibited [157, 158, 159].

Synthesis of biomolecules is a fundamental process in the cell, and the products are used for the growth, metabolism, transportation, and virulence. RNA synthesis is inhibited at high pressure in deep-sea viruses [145]. The gene expression in *E. coli* changes with the applied pressure. For example, transcription of several genes including stress response are changed in *E. coli* O157:H7 strain at high pressure [160]. These regulations provide resistance to the organism in high pressure and increase the survivability. The polypeptide synthesis reduces significantly at the pressure of 550 atm [161]. The decrease in polypeptide synthesis hinders the formation of amino acids and proteins and, in turn, the biomass growth. Furthermore, heat shock and cold shock proteins are upregulated at high pressure [162]. The purpose of these proteins is to repair the DNA if broken due to stresses. Another study has shown that several genes are also upregulated at high pressures [163]. Beside morphology,

growth, and gene expressions, cells also experience oxidative stress at high pressure [164] and, the gene upregulations are related to decrease of the oxidative stress in a cell.

Cell division, the reproduction mechanism in bacteria, is a complex process due to involvement of several proteins. The division site on cell is sensed by cell division inhibitor protein MinC, which is accompanied by two proteins MinD and MinE [165]. Cells contain three potential division sites altogether — two are located at the pole of cells and one at the middle of cells [166]. Ftsz protein forms a ring at the division site [167], which helps in pinching of the cell membrane for the division process. MreB, a cytoskeleton protein, helps to maintain the overall cell integrity by depolymerizing at high pressure [142].

The study of the bacteria under high pressure in hydrothermal vents is important in the perspective of the origin of life [168, 169, 170]. Bacteria at high pressure switch their phenotype to longer cell phenotype stochastically [136]. The switching was assumed to be irreversible at continuous application of high pressure. Phenotypic switching was first observed in *Candida albicans* [171]. Later, several studies were deployed to understand the phenotypic switching mechanism by studying the variation in growth, direction, texture, color, and shape of the colonies of bacteria grown from an isogenic population [172]. The phenotypic switching caused by deviation in environments are generally reversible when the growth condition is restored. In some cases, the switching property in cells can propagate over several generations either in the form of memory or in the form of acquired epigenetic [173, 174]. The switching mechanism of bacteria is important for evolutionary perspective [175] and the selection of population in harsh conditions to counteract the pressure stress [176]. Bacteria switch their phenotype depending on the nutrients, and cells persist short term memory on gene expression depending on the previous nutrient source [177]. The time scale for memory is important for the adaptation of bacteria in different nutrient conditions. This chapter deals with the reversibility study of bacterial cells at two oscillatory pressures — (i) a fast oscillation and (ii) a slow oscillation, to answer the switching timescale of cells at two different durations. Another interesting question is

whether the process of phenotypic switching has a memory or not. The cell division process and elongation at high pressure are supposedly conducted by a large number of genes. However, the experimental results of cell division and switching of bacteria at oscillating high pressure can be described by using a simple two-state model.

## 2.2 Materials and Methods

### 2.2.1 Sample and Media

MC4100 [178] strain of *E. coli* used in the pressure study was obtained from American Type Culture Collection(ATCC). Bacterial stock was inoculated in a solid Luria Bertani Broth (LB) media and harvested at 37 °C for 16 h. A single colony from the solid media was transferred to LB liquid media and incubated in a shaker at 200 rpm, which was maintained at 37 °C. The cells were grown until the optical density ($OD_{600}$) reached $0.4 - 0.6$. Then the sample was diluted immediately to $OD_{600} \approx 0.05$, and about 500 µL was transferred into a rectangular quartz cuvette (volume: 500 µL, Spectrocell) and loaded into the high-pressure system.

### 2.2.2 Experimental Setup

The schematic of the experimental setup of the high-pressure system is shown in Fig. 6. The system contained a high-pressure chamber, piston, water bath, thermocouple, data acquisition card, and water regulation system. The piston and water bath were used to control temperature and pressure, respectively. The uncertainties of the measurements of temperature and pressure were on the order of 0.2 °C and 10 atm, respectively.

The temperature of the high-pressure chamber (ISS) was regulated using circulating pipes connected to a water bath. A thermocouple was inserted in the high-pressure chamber and connected to a data acquisition card (National Instruments), then to a computer. Temperature was monitored using a LabView, a software from National Instruments. A bacterial sample was loaded in a cuvette and capped with a flexible Teflon cap. A piston

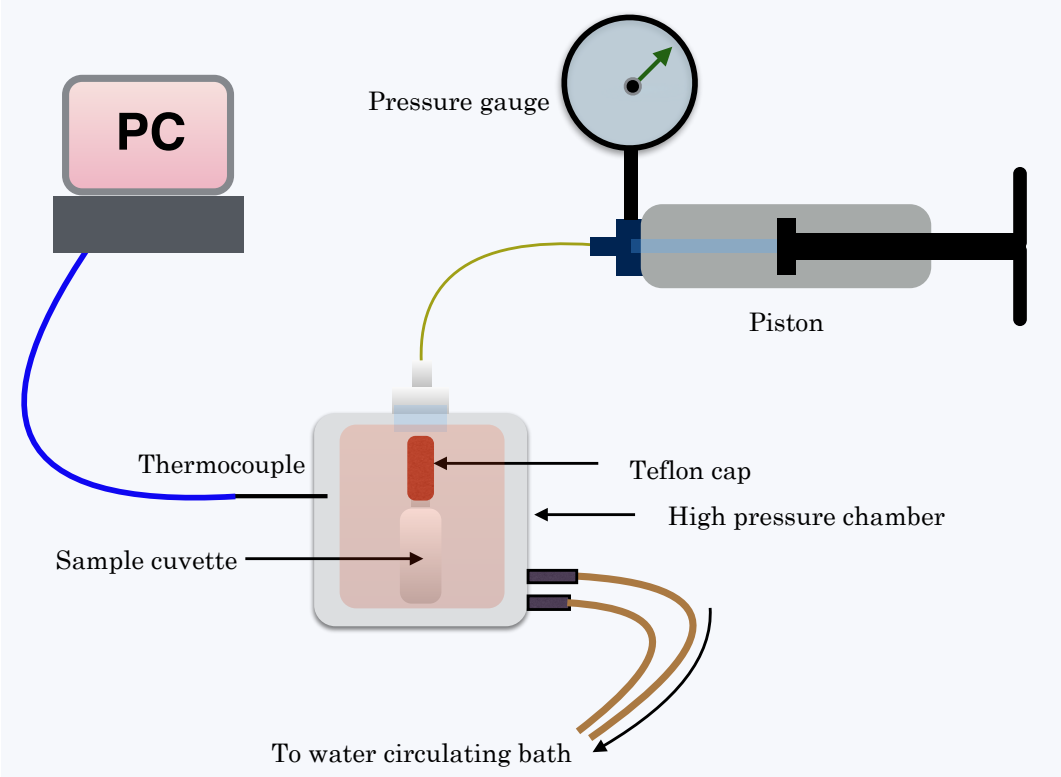


Figure 6: Schematic of high-pressure system.

(High Pressure Equipment (HiP), Inc.) with a small water reservoir was used to generate high pressure to the chamber. The pressure was monitored with the help of a pressure gauge. The temperature of the chamber was maintained earlier than applying pressure because the temperature equilibrium time scale was longer compared to the pressure equilibrium time.

### 2.2.3 Imaging and the Analysis of Images

The bacterial sample cultivated at high pressure was taken out at the end of the high pressure experiments. Slides of the bacterial samples were made right after the experiments, and images were acquired using a SPOT (SPOT Imaging Solution) camera attached on a Nikon EFD-3 microscope (Nikon Instruments) using a 40X objective. The obtained images were segmented using ImageJ [179] and converted into binary images. The binary image data were used to measure the contour length to obtain cell length data.

### 2.2.4 Error Estimation

The error of the mean cell length and the variance arise from various sources [180]. However, two dominating errors appeared from (i) finite optical resolution of the images which was about 0.25 µm and (ii) finite sampling (typically about two thousand cells were imaged for each experimental condition). In image processing, the standard deviation in cell length was estimated to be about 0.125 µm, due to finite resolution.

## 2.3 Results

### 2.3.1 Comparison of Morphology at Normal and at High Pressure

Cell morphology was studied at different ranges of pressures. Cells were removed from the pressure after five hours. The optical density ($OD_{600}$) was found to be 0.7. The sample was visualized under a microscope. Figure 7 is the representative images and corresponding probability distributions of bacterial cells at steady normal and high pressure. Figures 7(A) and 7(C) are the representative images and the corresponding probability distributions, respectively, for bacteria cultivated at atmospheric pressure. Figures 7(B) and 7(D) are the illustrative images and related probability distributions, respectively, for bacterial cells grown at pressure $\Psi = 400$ atm. The probability distribution, $P(\ell)$, of bacterial cell lengths is uniformly distributed for $\Psi = 1$ atm, and it has a longer tail and higher heterogeneity at $\Psi = 400$ atm. An earlier study suggested that DH5$\alpha$ strain of *E. coli* grows up to $\Psi = 700$ atm with a decrease in growth rate [136]. Similar behavior was obtained in case of MC4100 strain of *E. coli* studied here.

High hydrostatic pressure inhibits the cell division and, the cells appear longer. Cell length and fraction of the long cells depend on the extent and the duration of the pressure applied. Cells with a normal morphology switch to a new phenotype which is a combination of normal and elongated cells at high pressure. Cell length, ($\ell$), at a single-cell level were calculated, and probability distributions are presented in Figure 7(C) and Figure 7(D), determined by analyzing 4810 and 1571 cells, respectively.

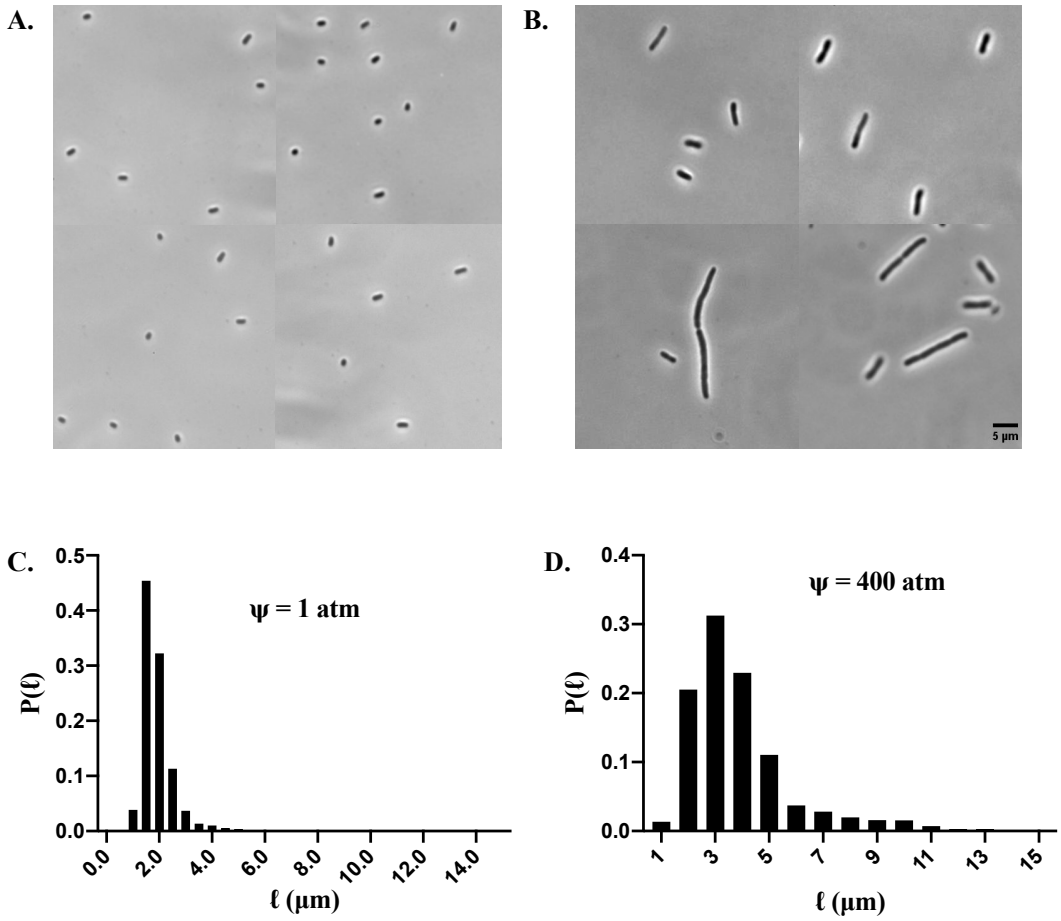


Figure 7: Representative images and corresponding probability distributions at $\Psi = 400$ and 1 atm.

The probability distribution, $\mathrm{P}(\ell)$, appears narrow and centered around $\ell = 1.8$ µm and wide and centered about $\ell = 2.5$ µm at $\Psi = 1$ and 400 atm, respectively. Most of cells had a length about 2 µm at $\Psi = 1$ atm. At high pressure, cell lengths were distributed in a wide range of $\ell$ ($1.8 \ - 12$ µm). The peak of the distribution was higher at normal and lower at high pressure, respectively. The coefficient of variation ($\sigma_\ell$) in cell length was calculated using cell length data and found to be $\sigma_\ell = 0.32$ and 0.52 for $\Psi = 1$ and 400 atm, respectively. The coefficient of variation of cell length at normal pressure was found consistent with the previous study of MG1655 in LB media, and it was reported that the coefficients of variation for the cell length at birth and division are 0.3188 and 0.3129, respectively [181].

Bacterial cells switch their phenotype stochastically according to the environmental

condition [182]. Switching in a fluctuating environment is important to prevent the collapse of the population [183]. The robustness of the population is altered when they switch to a new phenotype [184]. Bacteria switch to elongated cells, a new phenotype, due to inhibited cell division at high hydrostatic pressure. The elongated cells revert to the normal cells when the applied pressure stress is removed [136]. The phenotypic switching at continuously fluctuating pressure is poorly known. In order to explore the mechanism of phenotypic switching, two similar but complimentary sets of experiments were formulated. These experiments would be able to tell whether cells persist a phenotypic memory or not. The first set of experiments consisted of applying continuous pressure to the bacterial cells for 60 minutes and subsequently releasing the pressure for a time $\tau$. Five cycles of applying and releasing of the pressure were performed as shown in Fig. 8(A). The population doubling time ($\tau_d$) of bacteria at 400 atm is $\approx$ 115 min. When cells are exposed to one hour at $\Psi = 400$ atm, the cell cycle would not be completed; however, the growth of cells would have started. In the second set of experiments, cells were exposed for 300 min, a relatively longer period compared to the first set of experiments. Then, the pressure was released and applied for a duration, $\tau$, and five cycles of pressure application and relaxation were executed for a duration of $\tau$ as shown in Fig. 8(B). The relaxation time in each experiment was varied from 0 - 20 min. For simplicity, from here and onward, EXP I and EXP II will be used to denote the set of experiments I and the set of experiments II, respectively.

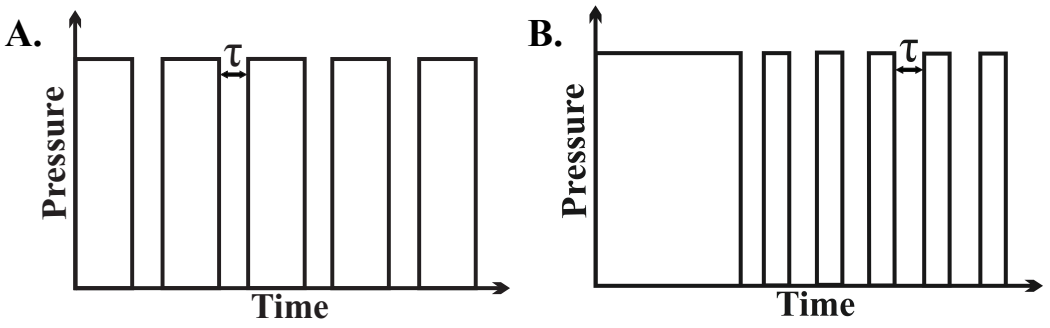


Figure 8: Experimental schemes for two set of experiments.

The exposure of cells at $\Psi = 400$ atm for a time less than $\tau_p$, switching of the population was insignificant compared to cells grown for three hours. The growth rate of cells changed but the overall morphology remained similar. Firstly, the initial phenotype of cells at the beginning of EXP I was different from those at the beginning of EXP II. Cells in EXP I were in a low-pressure phenotype, and cells in EXP II were in a high-pressure phenotype. Secondly, the nature of oscillatory pressure was different. In EXP I, cells were exposed for a longer pressure time (60 min) and relaxed to a shorter time (0 - 20 min), whereas, in EXP II, cells were exposed for a short pressure time and released for the same short duration (0 - 20 min). In case they had different memory, cell division dynamics and the fraction of the population switched to a new phenotype would be different in each set of the experiments. The purpose of those two different sets of studies was to find whether a bacterial cell exhibit a phenotypic memory of phenotypic switching at high pressure for a small number of generations. In the case of memory, cell fractions of high-pressure and low-pressure phenotype should be the same in different $\tau$'s.

Next, the dynamic response of phenotypic switching was studied using two sets of experiments (EXP I and EXP II). In either case, cells were stressed by applying oscillatory pressure. In EXP I, cells were oscillated starting from the low-pressure phenotype, and the pressure applied during the oscillation was longer (60 min). On the other hand, cells were oscillated starting from the high-pressure phenotype in EXP II and the pressure application during the oscillation was kept small (0 - 20 min). The two sets of experiments were performed for the same number of cycles of oscillatory pressure for better comparison.

### 2.3.2 Dynamics of Phenotypic Switching at Different $\tau$'s for EXP I

At the end of EXP I, cells were visualized, and binary images were analyzed to get the distribution of cell length data. Figures 9(A), 9(B), 9(C), 9(D), and 9(E) are the probability distributions of cell length distributions, $P(\ell)$, for $\tau = 0$, 5, 10, 15, and 20 min, respectively. The number of cells analyzed were 1571, 1950, 693, 2007, and 2212 for $\tau = 0$, 5, 10, 15, and

20 min, respectively. The probability distributions were used to describe the dynamics of the morphology of cells at different $\tau$'s.

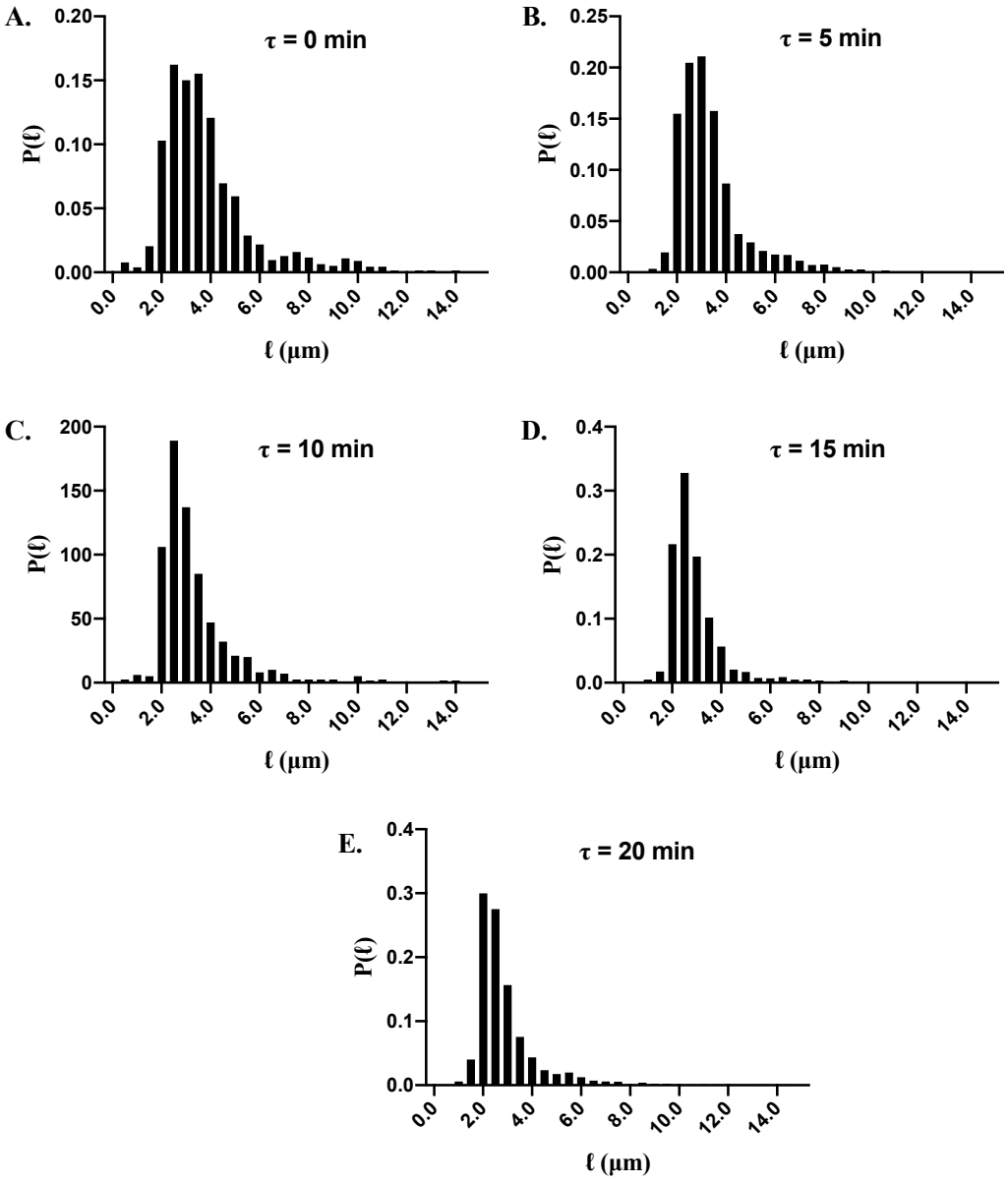


Figure 9: Probability distributions of cells from EXP I for different $\tau$'s.

The tail of the distribution was maximum when $\tau = 0$ min. On increasing $\tau$, the tail of the distribution decreased slowly and beyond $\tau = 10$ min, it remained unchanged. The tail represents the elongated cells and the decrease in the tail with the increase in $\tau$ shows that

the fraction of longer cell in the population was decreasing. Furthermore, the peak of the distribution was at $\ell \approx 3.75$ µm, at $\tau = 0$ min. The peak shifted slightly toward the smaller value of $\ell$ with increasing relaxation time. At $\tau = 20$ min, the peak of the distribution was at $\ell \approx 2.25$ µm. The height of the distribution increased on increasing $\tau$. The height of the distribution was 0.3 at $\tau = 0$ min, and it became maximum (0.7) when $\tau = 20$ min. The increase in height showed that the population of cells which have a length around mean value was increasing. At $\tau = 0$ min, the cells were at high-pressure phenotype and they slowly changed to low-pressure phenotype with an increasing relaxation time, $\tau$. The cell length distribution at $\tau = 20$ min was comparable to the distribution of control cells, the distribution of cells at $\Psi = 1$ atm.

To further quantify the dynamics of phenotypic switching and the morphology of cells, the mean length $\langle \ell \rangle$ and the variance ($\sigma_\ell^2$) were extracted from cell data. Mean length and the variance were further used to analyze the phenotypic switching of cells at different $\tau$'s.

Figures 10(A) and 10(B) are $\tau$ dependence of $\langle \ell \rangle$ and $\sigma_\ell^2$ of cells obtained from probability distributions of Fig. 9. The error bars on cell length are the standard error. Both $\langle \ell \rangle$ and $\sigma_\ell^2$ decreased monotonically with an increasing $\tau$. At $\tau = 20$ min, $\langle \ell \rangle$ and $\sigma_\ell^2$ were found to be 2.85 µm and 2, respectively. The results were comparable to the mean length and variance of control cells. The $\tau$ dependence length data $\langle \ell(\tau) \rangle$ were fitted with $\ell_0(1 + C * e^{-\tau/\tau_R})$. The fitted curves are presented as the blue lines in Fig. 10. In the exponential function, C is a constant and critical relaxation time, $\tau_R$, was found to be 10.8 min. The result showed that, when cells were exposed at high-pressure for a long time (60 min) and relaxed for a short period (10 min), the morphology of cells remained unchanged. In other words, cells did not feel the stress in their size and shape when they were exposed longer to pressure, followed by shorter relaxation time. The results remained unchanged on increasing the $\tau$ beyond 10 min. Similar fitting was done for the variance and, it was found that $\tau_R = 3.08$ min. The results indicated that the relaxation time scale of variance in length was much faster compared to the relaxation of mean length.

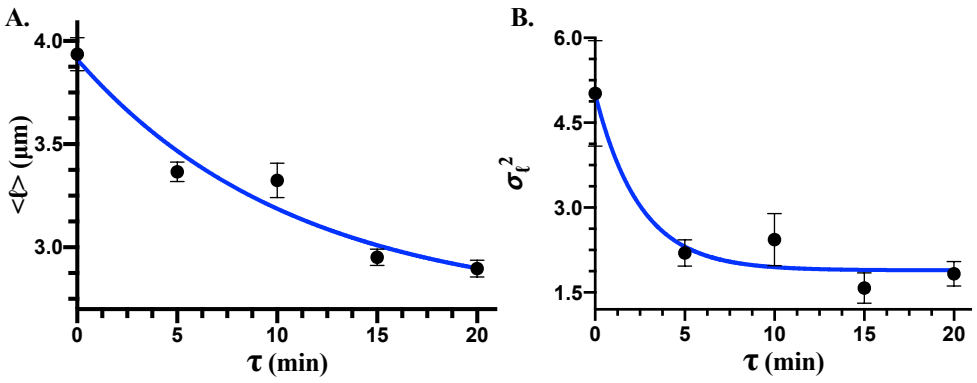


Figure 10: $\tau$ dependence of $\langle \ell \rangle$ and $\sigma_\ell^2$ of cell lengths for EXP I.

### 2.3.3 Dynamics of Phenotypic Switching at Different $\tau$'s for EXP II

After the completion of pressure cycles of EXP II, the images of cells were taken and analyzed to get the distribution of cell length. Figure 11(A), 11(B), 11(C), 11(D), and 11(E) are the probability distributions of cell length, P($\ell$), for $\tau$ = 0, 5, 10, 15, and 20 min, respectively. The number of bacterial cells analyzed to obtain the probability distributions were 1373, 1921, 1930, 1519, and 1525 for $\tau$ = 0, 5, 10, 15, and 20 min, respectively. The probability distributions are helpful to describe the dynamics of the morphology of cells at different $\tau$'s.

The tail of the distribution was maximum when $\tau$ = 0 min. Upon increasing relaxation time, $\tau$, the tail of the distribution decreased quickly and reached a minimum at $\tau$ = 5 min. The tail of P($\ell$) again increased slowly until $\tau$ = 10 min and remained the same for larger values of $\tau$'s. Long tail represents the presence of elongated cells, and the decrease in the tail with increasing $\tau$ shows that a fraction of longer cells in the population was decreasing. Furthermore, the peak of the distribution was at $\ell \approx$ 3.75 μm at $\tau$ = 0 min. The peak shifted slightly toward the smaller value of $\ell$. At $\tau$ = 20 min, the peak of the distribution was at $\ell \approx$ 2.25 μm. The height of the distribution was non-monotonic with $\tau$. Height was maximum (0.75) at $\tau$ = 5 min, and it decreased when $\tau$ = 10 min, and again started

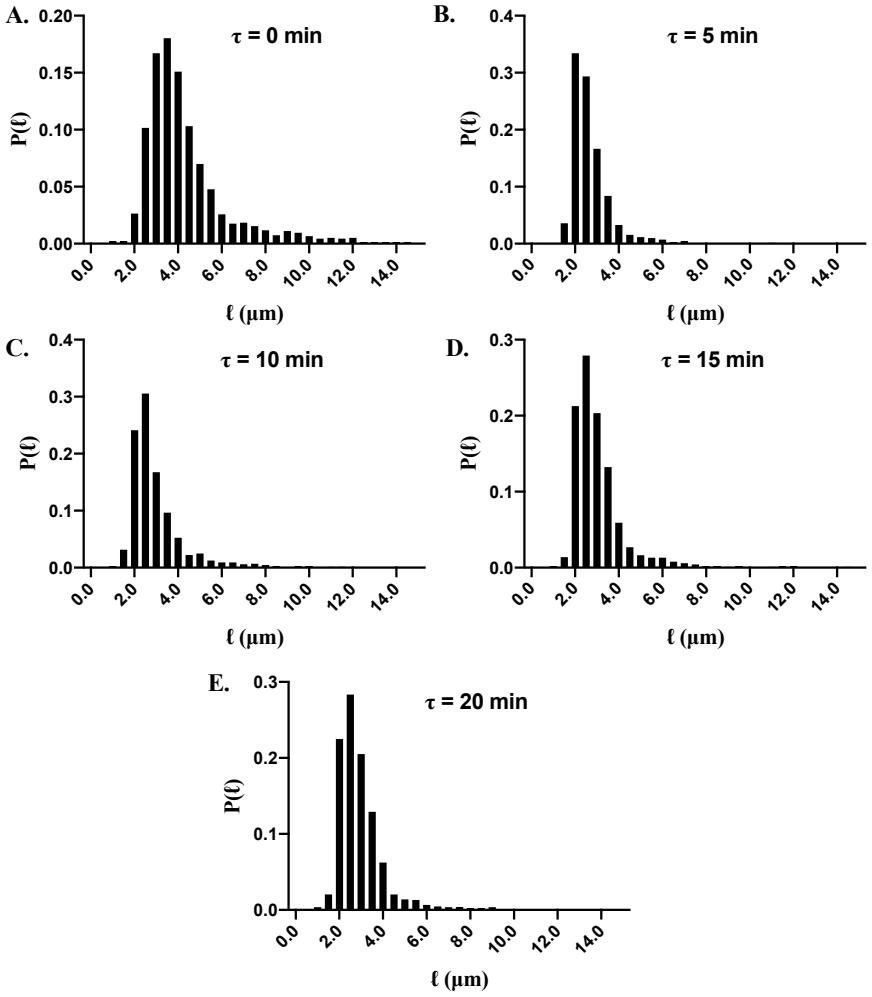


Figure 11: Probability distributions, P($\ell$), of cells from EXP II for different $\tau$'s.

increasing. The distribution at $\tau = 20$ min was comparable to the distribution of the control cells, the distribution of cells obtained by growing at continuous atmospheric pressure. To further quantify the dynamics of phenotypic switching and the morphology of cells, the mean length $\langle \ell \rangle$ and the variance ($\sigma_\ell^2$) were extracted from cell data. Mean length and variance were further used to analyze the phenotypic switching of cells at different $\tau$'s.

Figure 12(A) and 12(B) are $\tau$ dependence of $\langle \ell \rangle$ and $\sigma_\ell^2$ of cells obtained from probability distributions of Fig. 11 for EXP II. The error bars on cell length are the standard error. Both $\langle \ell \rangle$ and $\sigma_\ell^2$ decreased non-monotonically with increasing $\tau$. At $\tau = 5$ min, $\langle \ell \rangle$ and $\sigma_\ell^2$ were found to be minimum with values of 2.7 µm and 0.75, respectively. The blue lines

were obtained by fitting Akima splines through the experimental data points. At $\tau = 20$ min, the mean length and variance were comparable to those of the control cells.

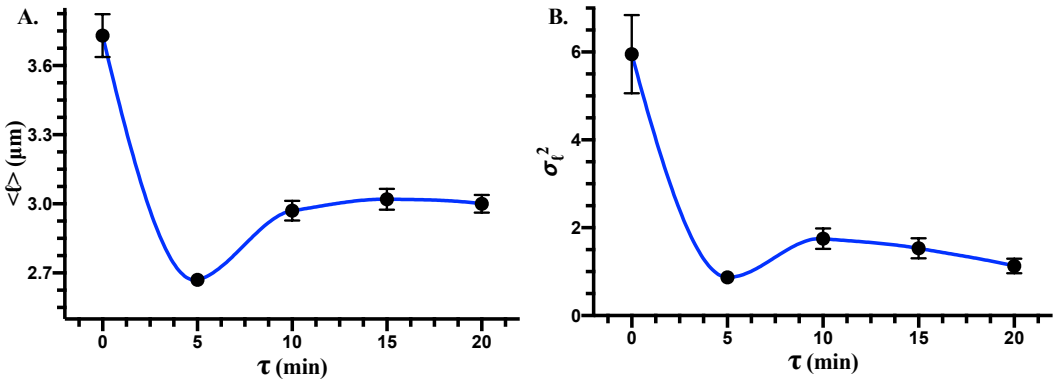


Figure 12: $\tau$ dependence of $\langle \ell \rangle$ and $\sigma_\ell^2$ of cell lengths for EXP II.

The behaviors of $\langle \ell \rangle$ and $\sigma_\ell^2$ were slightly different for EXP II compared to EXP I. Both $\langle \ell \rangle$ and $\sigma_\ell^2$ exhibited minima when $\tau = 5$ min. Hence, the exponential lines were not fitted to analyze the mean length and variance behaviors. Except for the minima, the overall result was comparable for both experiments. These quantities saturated slightly after 10 min regardless of the type of oscillation described here. To describe the results, a simulation model was developed.

## 2.4 Two-state Model of Phenotypic Switching at High Pressures

### 2.4.1 Introduction to Two-state Model

The elongation of cells in high pressure is reversible upon releasing the pressure [136]. The timescale for cells to achieve their normal length might be proportional to the duration of the pressure applied. The phenotypic switching of cells in high pressure studied earlier [136, 142] do not indicate the time scale of phenotypic switching with the temporal fluctuation of high pressure. The following section describes the time dependency of phenotypic switching of the bacterial cells in oscillatory pressure. Cell division cycles at high oscillatory pressure is divided into two different stages:

(1) A cell has length distribution centered around 2 µm, the average size of *E. coli*. The variation in cell length is due to the continuous growth of cells, followed by cell division. Cells elongate with a growth rate of $k_1$ and form potential division sites (PDS) [142] at the multiple locations separated by the fundamental unit($\ell_0$). The formation of the septum and Z-ring [165] is included in the formation of a potential division site. The formation of PDS is only possible when a cell grows and reaches a multiple of $\ell_0$.

(2) After the formation of PDS, it breaks at a rate of $k_2$, and a cell division event occurs. Cells can form multiple PDS and all PDS have equal probability of formation.

### 2.4.2 Cell Division Scheme

Formation of PDS is necessary for cell division; however, the formation of PDS alone does not guarantee division in short time scale. If a cell starts to grow from a length of $\ell_0$ and reaches to $2\ell_0$, a PDS is formed at the length $\ell_0 \pm \epsilon$ from a pole, where $\epsilon$ has a property of the Gaussian distribution with a zero mean and 0.1 µm standard deviation. Similarly, if a cell reaches to m $\ell_0$ length, there will form $(m-1)$ division sites. All the PDS have the same probability of division and the model assumes no preference of the PDS according to the location. For example, if a cell reaches $(m+n+1)\ell_0$ length, it contains $m+n$ division sites. Suppose, a cell divides at $m^{th}$ PDS, then the first daughter cell will have the length $\ell_1 = m\ell_0 \pm \epsilon$ and the second daughter cell will have the length $\ell_2 = n+1\ell_0 \mp \epsilon$. The first cell contains $m-1$ and the second contains $n$ division sites. Figure 13 is a schematic diagram of the phenotypic switching of cells at high pressure. There are two cell dynamics, as shown in Fig. 13. The first one is the growth, and the second is the division. The growth and division rates were faster at low pressure giving rise to the low-pressure phenotype, and the growth and division rates were slow at high pressure giving rise to high-pressure phenotype. The PDS were formed at a fundamental unit apart from each other and the pole of the cell, and cell division site had no priority over the location of the PDS.

Cell division for the normal cells is assumed to follow a sizer method [185, 186], where, a

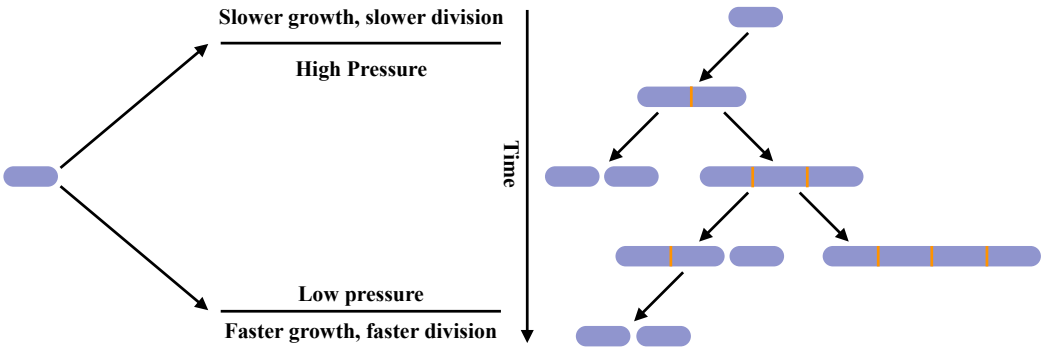


Figure 13: Schematic of two-state model of phenotypic switching.

cell starts dividing once it reaches critical length regardless of time and initial length ($\ell_0$). Cell division was hindered at high pressure resulting in an elongation of cells. Moreover, normal cells had low-pressure phenotype and under the stress of high hydrostatic pressure, the morphology changed to high-pressure phenotype. When the pressure was released, cell division resumed, and cells went back to low-pressure phenotype. An idea of PDS was introduced to model cell division for the oscillatory pressures, where cells would have possessed typical division at low pressure. Cells might not divide at high pressure due to depolymerization of FtsZ [141] and MreB [142] but formed PDS.

### 2.4.3 Model Simulation

Pressure dependent cell growth rate $k_1(\Psi)$ and cell division rate $k_2(\Psi)$ were considered to model the cell division process. These two rates determine the long term behavior on the change in phenotype of cells. The rate $k_1$ was obtained from the experimental results of population doubling time ($\tau_d$) of the bacteria cells using the experimental results. At $\Psi = 1$ and 400 atm, the doubling time, $\tau_d$, was found to be $\approx$ 30 and 115 min, respectively. Error minimizing method between the model and experiments was deployed to calculate the value of $k_2$. The growth of cells data was necessary to obtain those two parameters. The simulation performed was a stochastic time step of 0.01 min with $10^4$ starting cells. The growth equation used for the growth simulation is given by,

$$\frac{d\ell(t)}{dt} = k_1(\psi)\ell(t) \qquad \text{(Equation 1)}$$

### 2.4.4 Model Results

First of all, the growth and division parameters were obtained for $\Psi = 1$ and 400 atm. Table 4 represents the parameters for $\Psi = 1$ and 400 atm. The rate at which cells switch from low-pressure phenotype to high-pressure phenotype on the application of the pressure is denoted by $\gamma_{L\to H}$. Similarly, $\gamma_{H\to L}$ is the rate at which cells switch from high-pressure phenotype to low-pressure phenotype when the applied pressure is released.

Table 4: Model parameters used in simulation

| Pressure (atm) | $k_1(min^{-1})$ | $k_2(min^{-1})$ | $\gamma_{L\to H}(min^{-1})$ | $\gamma_{L\to H}(min^{-1})$ |
|---|---|---|---|---|
| 1 | 0.023 | 0.5 | 0 | 0.10 |
| 400 | 0.01 | 0.016 | 0.05 | 0 |

Cell length distributions at $\Psi = 1$ and 400 atm are presented in Fig. 14. The upper panel represents the images of the bacterial cells that were obtained from the simulation. The lower panel represents the corresponding probability distribution of cell length, P($\ell$). The heterogeneity on cell length was defined by the coefficient variance, $CV_L$. At $\Psi$= 1 and 400 atm, $CV_L$ were found to be 0.27 and 0.48, respectively. The experimental results of $CV_L$ were 0.32 and 0.54 for $\Psi = 1$ and 400 atm, respectively. The ratio of growth rate to the division rate ($k_2/k_1$) at $\Psi = 1$ and 400 atm were found to be 20 and 1.6, respectively. The results indicate that at low pressure, cells grow faster, and the division rate was much faster compared to the growth and cell division at high pressure. Cells at low pressure divided immediately after reaching a critical length and cells did not elongate. However, at high pressure, the growth rate was slower, and the division rate was much slower. Once cells grow, they have to wait for the division. Since growth is a continuous phenomenon, cells continuously grow regardless of the division. Hence, cells are elongated at high pressure. These results agree with the previous results that cells elongate at high pressure due to lack

of depolymerization of vital cytoskeletal proteins FtsZ and MreB [187, 188, 189].

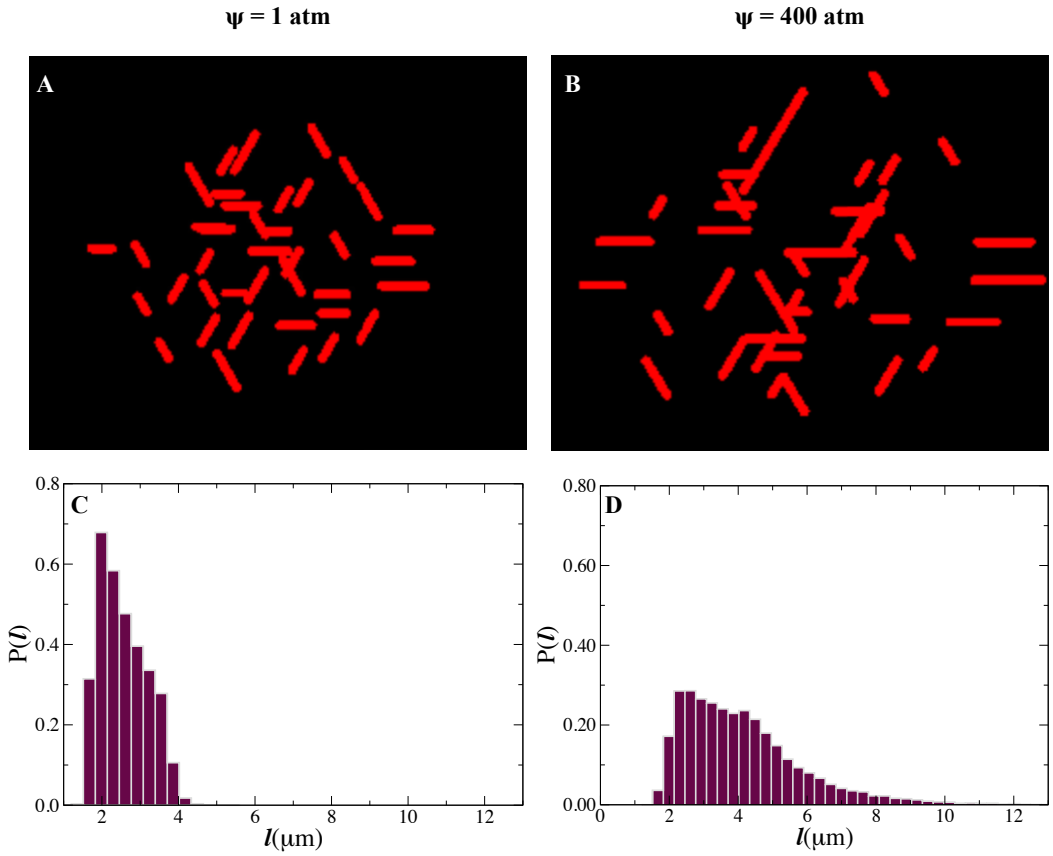


Figure 14: Model results on cell lengths at $\Psi = 1$ and 400 atm, and their corresponding probability distributions.

The model was simulated in case of EXP I and EXP II to understand the dynamics of phenotypic switching. Cell length data thus obtained for several $\tau$'s were plotted to get the probability distributions. Two new parameters were obtained from the simulations. They are $\gamma_{L\to H}$ and $\gamma_{H\to L}$, which are the switching rate for the low-pressure to high-pressure phenotype and high-pressure to low-pressure phenotype, respectively. A grid search algorithm was deployed in two-dimension to obtain the values of these rates, and found to be $\gamma_{L\to H} = 0.05$ $(\text{min})^{-1}$ and $\gamma_{H\to L} = 0.10$ $(\text{min})^{-1}$. The corresponding time scales were 20 and 10 min, respectively. The length data for different $\tau$'s for both the experiments were calculated. Figure 15 is the probability distributions of EXP I and EXP II at several $\tau$'s. The

upper panel consists of the probability distributions for EXP I and the lower panel consists of probability distributions for EXP II. The probability distributions were found to have a long tail at $\tau = 0$ min for both the experiments. For higher values of $\tau$, the length of the distribution was decreasing. The length data were extracted from the simulation at different values of $\tau$. Next, the mean length, variance in length, and standard errors were calculated and these data were compared with the experimental results.

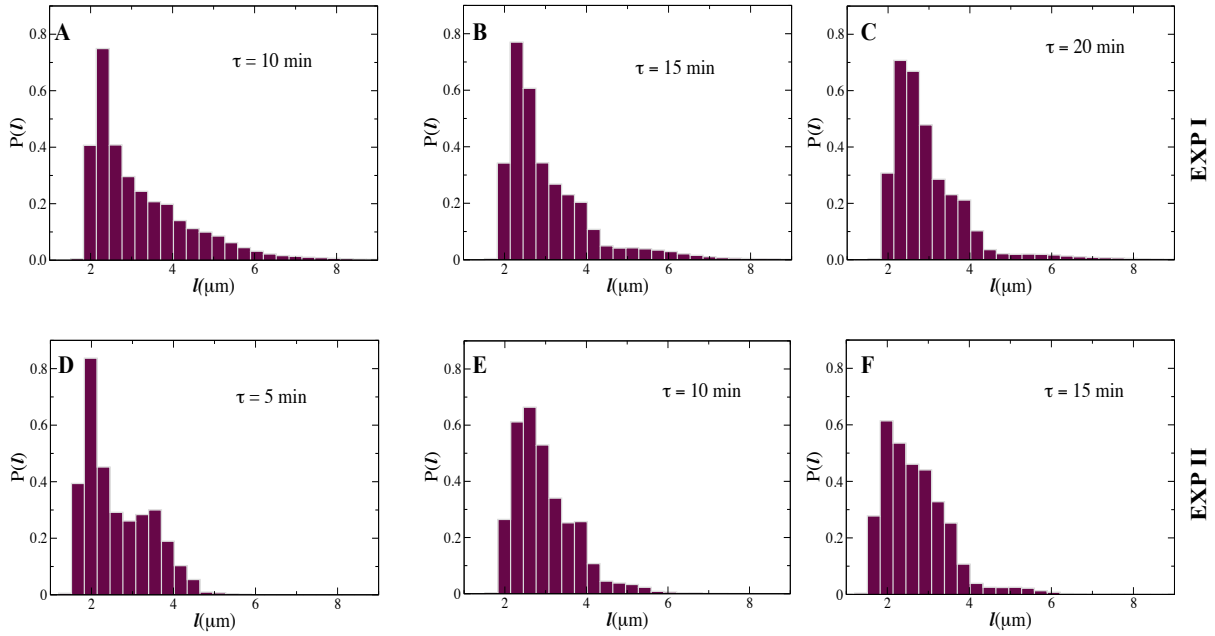


Figure 15: Probability distributions obtained from model for EXP I and EXP II.

From cell length data, the mean lengths at different $\tau$ were obtained. Figures 16(A) and 16(B) represent the $\tau$ dependence model results of $\langle \ell \rangle$ for EXP I and EXP II, respectively. Blue circles with the error bar and black squares are the experimental and model results, respectively. The red dotted line is an exponential fit to the experimental result and Akima spine for EXP I and EXP II, respectively. The error bars were estimated by calculating the standard errors. The model predicts the exponential behavior of cells for EXP I and a weak minimum for EXP II reasonably well. The model and the experimental results were consistent with each other.

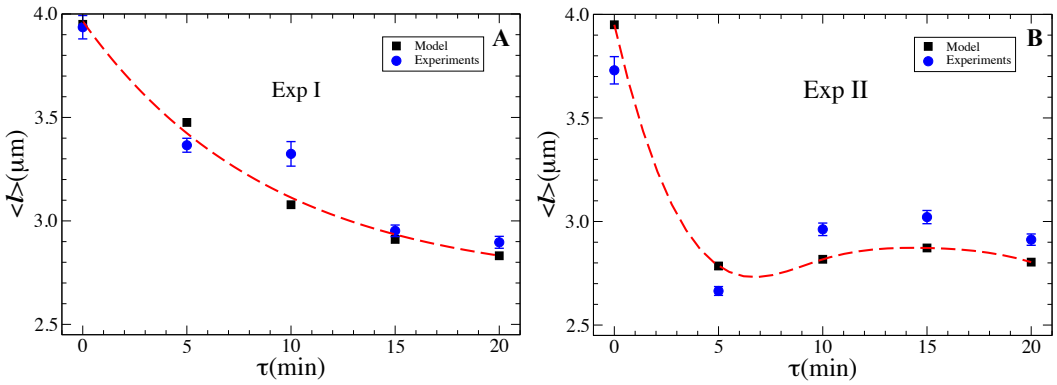


Figure 16: $\tau$ dependence experimental and model results of $\langle \ell \rangle$ for EXP I and EXP II.

## 2.5 Summary and Discussion

High hydrostatic pressure is an extra stress for bacterial cells. Cellular activities are inhibited at high pressures. Some proteins of cell might not be fully functional even though protein is intact at the range of pressure studied here. The cellular processes remain intact at a pressure of 500 atm, albeit at the slower rate. Growth and division do not completely shut down, but a large number of cells experience elongation due to lack of cell division. Growth and cell division processes are stochastic [190], and at high pressure, a two-state model predicted the increase in stochasticity [136]. The stochasticity in cell division leads to heterogeneity in bacterial population and it increases with the application of hydrostatic pressure. Heterogeneity in population measured from the experiments was $\mathrm{CV}_L = 0.54$. Here, a more physically intuitive model was presented and showed that the two-state model also predicts the behavior of cells in an oscillatory pressure. The model also finds the switching parameters for each set of experiments.

The experiments indicate that the relaxation of 10 min in either experiment does not affect cell morphology. The application of a long duration or a short duration exposure to cells followed by 10 min relaxation saturates behavior of cells. To switch the high-pressure phenotype to low-pressure phenotype, at least 5 min of relaxation was necessary for both the set of experiments. High pressure might have affected the kinetics of several biomolecules by

up or down-regulating them. The synthesis rate might have changed and would have affected the switching of cells. The model presented here uncovers the switching rate correlated with the growth and cell division. Although a cell division process is exceptionally complex, the model assumes a simple mechanism for the physical picture. It relies on two major events — growth and division. The model further does not take account of regulations of other vital processes like ATP synthesis, molecule intake rate, and maintenance of the membrane potential. However, the model predicts the experimental behavior of switching, growth, and reversibility dynamics correctly. The model assumes the fact that growth rate is one of the fundamental parts for the division, and it might have included several other vital aspects like protein synthesis, accumulation, binding, and organization. The model further predicts the behavior of cells when releasing the applied pressure.

The model further indicates that the switching rate of cells when the pressure is applied ($\gamma_{L\to H} = 0.05$ (min)$^{-1}$) is smaller (half) than the rate when the pressure is removed ($\gamma_{H\to L} = 0.10$ (min)$^{-1}$). It makes physical sense because at high pressure, all cells may not be elongated, but in releasing the pressure, all the longer cells switch back to normal. Also, the growth rate of bacteria at high pressure ($\approx$ 0.0087 min$^{-1}$) is much lower compared to the growth rate at low pressure ($\approx$ 0.034 min$^{-1}$). The timescale does not signify the presence of phenotypic memory at the range of pressure and the time of application of pressure studied here [177]. As opposed to the memoryless process, the bacterial critical relaxation time scale would be different for both of the experiments. The critical timescale is about 10 minutes for saturation in both the cases.

Several proteins are integrated for the mechanism of cell division. Localization of several proteins are required for the cell division process including FtsN [191], FtsQ [192], FtsK [193], FtsL [194, 195], FtsA [196], FtsZ [197], and MreB [198]. Cell division inhibitor proteins MinC and MinD, along with SulA, play an essential role in the formation of the septal ring [199].The effects of polymerization and depolymerization of several proteins at high pressure are unknown. The filament formation time of MreB and FtsZ proteins is very

small at atmospheric pressure [200, 201] and the depolymerization of MreB and FtsZ at pressure of 500 atm might have caused cells to elongate. Growth at 400 atm is significantly small compared to atmospheric pressure, and cell division for a fraction of cells is inhibited. The stochasticity in cell division at high pressure is known [136]. However, the mechanism of stochasticity is known only in the perspective of gene expression [202]. The complete mechanism of cell division integrated with other cellular processes such as the formation of a protein that localizes acts as a ring helps in the division. Hence, the complete answer to the mechanism is complex and further investigations are required.

# 3 Growth, Cell Division, and Gene Expression of *Escherichia coli* at Elevated Concentrations of Magnesium Sulfate: Implications for Habitability of Europa and Mars

## 3.1 Introduction

Europa, a Galilean moon of Jupiter, possesses a liquid water ocean in contact with a rocky core [123, 124, 125, 126, 127], making it a compelling candidate in our solar system for search of life beyond Earth. Due to low surface temperature, it has a thick layer of ice crust, and a global ocean that may run $100 - 200$ km deep. Depending on the depths, the hydrostatic pressure at the seafloor ranges from $130 - 260$ MPa [203]. A recent study on composition of Europa using spatially resolved spectra suggested that the surface is rich in sodium and potassium chloride, and magnesium sulfate ($MgSO_4$) present on it is a product product of radiation, and not a constituent of brines [133]. Other investigations using the data from Galileo's Near Infrared Mapping Spectrometer of the surface and geochemical models have predicted that $Mg^{2+}$, $Na^+$, $SO_4^{2-}$, and $Cl^-$ are the most dominant ions in the ocean of Europa [131, 204]. Several experiments were conducted to understand the ionic composition of Europa's ocean using the measurements of the surface [205]. These studies showed that if sodium sulfate and magnesium sulfate have endogenic origin, the ocean would be rich in sulfate and poor in sodium, and would have low pH. These studies have suggested that the concentration of $Mg^{2+}$and $SO_4^{2-}$ could be as large as 2.9 M and 3.6 M, respectively, at certain temepratures [131, 204].

Several studies in the past indicated that Mars regoliths contain hygroscopic salts of Mg, Ca, Fe, and Na [206, 207, 208, 209]. These hygroscopic salts can absorb water from the atmosphere and, hence, brines might be formed [210]. The presence of sulfate in the regoliths of Mars can be as high as 30% by weight [209, 211]. These results suggest that organisms must adapt at high concentrations of magnesium sulfate and other salts, including the physicochemical conditions present on Mars and Europa, to flourish as life on these planetary bodies. There are several physicochemical conditions present on Earth at which organisms

are thriving including, extremes of salinity, pressures, pH, temperatures, and combinations of them [20, 22, 212, 213]. However, the environmental conditions present on Mars and Europa are unknown in terrestrial life. Earth has rare but rich epsomic environments including Basque and the Spotted lakes in Canada and Qaidam Basin in China [214, 215, 216, 217]. Metagenomic studies of the samples from the Qaidam Basin showed that there is a change in microbial community according to the concentration of $Mg^{2+}$ [218]. Metagenomic studies further revealed the presence of a large number of Firmicutes, Bacteroidetes, and Proteobacteria in epsomic environments present in the Spotted lakes and the Qaidam Basin [218, 219]. The subgroups of Firmicutes and proteobacteria phylum has diverse microbial systems containing both mesophiles and extremophiles. Some subgroups can tolerate high magnesium sulfate due to the external epsomic environments. The isolated bacterial samples from Great Salt Plains (OK, USA), Hot Lake (WA, USA), and the Basque Lakes (BC, Canada) can tolerate high concentrations of magnesium sulfate [220, 221, 222, 223].

The studies on extremophiles provide rich information regarding the mechanism of growth, genomics, and adaptation of these bacteria under extreme conditions. However, these studies fail to provide the information regarding adaptation of mesophilic bacteria under high salt conditions. Some cellular functions of non-salinotolerant bacteria might be non-functional at high salt conditions. Chapter 2 showed that *E. coli*, a mesophilic bactterium, can tolerate very high pressure by changing the cell division process stochastically. Similar effect was observed in a previous study, and it had shown that cells can tolerate high pressure in a temperature dependent manner [136]. Whether these cells can tolerate high salinity, similar to Mars and Europa conditions, or not is an intriguing subject of investigation.

High salt conditions create ions in aqueous solution creating ionic stresses. The presence of high ions further creates electrostatic imbalance on several proteins, and it might affect the stability, structure, and functionality of proteins [224]. The charged ligands binding phenomenon is affected at high salt conditions [225]. Proteins are soluble at low salt

concentrations and they precipitate at high salt known as salting out. The water activity, the ratio of partial vapor pressure of the solution to the partial vapor pressure of pure water, decreases with the addition of salt in a media [226]. Water activity had shown to be an important limiting factor to support life for both prokaryotes and eukaryotes. Life is not possible at water activity less than $\approx$ 0.61 [227]. *Escherichia coli* experience both ionic and osmotic stress at high salt. Hypersaline media causes osmotic stress on the cells. During the osmotic stress, bacteria actively regulate the volume to counteract the effects [228]. At high salt concentration, the volume of the cells may decrease by the process of plasmolysis [229, 230], and at extremely high concentration of the salt, cells may undergo death. A study had shown that cell death does not occur up to the concentration of 0.51 M of sodium chloride and the viability decreases on further increasing the amount of salt present in the media [231].

Regulation of expression of genes changes according to the surrounding environment. The global transcription factor (RpoS) regulates the expression of various genes when conditions like heat, oxidative, and osmotic stresses are presented to cells [232]. Cells have specific genes to regulate during different stresses. For example, *osmC*, an osmotically inducible gene, is upregulated at osmotic stress created by high salt [233]. The decrease in volume of cells at high salt requires active transport of water from inside to outside of the cell. The pure diffusion system of water is extremely slow. *aqpZ*, an aquaporin water channel, is necessary to regulate both inward and outward flow of water [234, 235]. Previous study investigated that *aqpZ* is downregulated under hyperosmolar conditions [236]. *corA*, a magnesium transporter gene, in *E. coli* expresses constitutively and establishes the magnesium concentration homeostasis inside the cell [237, 238, 239]. When the concentration of $Mg^{2+}$ is low in cytoplasm, *corA* is in an open configurational state allowing magnesium to pass inside. On the other hand, when the presence of $Mg^{2+}$ is high inside the cell, the configuration changes to off state and shuts off the transportation of magnesium. CysP, a thiosulfate transporter protein, is a part of ABC transporter complex and involves regulating

sulfate and thiosulphate which are necessary for the synthesis of amino acids containing sulfur [240, 241].

In the past, several studies were conducted to understand the effect of high osmolarity [230, 242, 243, 244] and low osmolarity [226, 245, 246] on cellular processes of *E. coli*. Sodium chloride was the most used common salt in these studies to understand the effect of salt on bacteria, and sucrose was widely used to investigate the osmotic stress. Other bodies of literatures are focused on the study of response of extremophiles in extreme conditions. The effect of magnesium sulfate on the cellular response and adaptation of bacteria is still elusive. The chapter discusses the cellular process and effect of magnesium sulfate on *E. coli*, a mesophilic bacterium, by studying the morphology, cell division, viability, plasmolysis, gene expression, and reversibility of bacteria upon the removal of applied salt stress

## 3.2 Materials and Methods

### 3.2.1 Cell Culture and Media

Wild-type MG1655 strain of *Escherichia coli* was obtained from the Coli Genetic Stock Center (Yale University, CT, USA). The media to culture cells was prepared by adding two carbon sources, 0.4% of glucose and 0.4% of succinate, and 2 mM of $MgSO_4$ in M9 minimal media. Cells were inoculated in solid Luria Bertani (LB) media with 1.5% of agar powder (BD Difco, Franklin Lakes, NJ, USA), and incubated at 37 °C for 16 h. A single colony of the cells was transferred to a liquid LB media and grown until optical density ($OD_{600}$) reached $0.5 \pm 0.1$. The sample was then transferred to M9 media containing 0.4% glucose and 0.4% succinate and a varying amount of magnesium sulfate. Glucose and succinate were provided to bacteria as carbon sources. The pH of the media was observed to decrease with increasing concentration of $MgSO_4$ and found to be 5.3 at 1.25 M. The media was passed through a 2.2 µm filter (Thermo Fisher Scientific, Carlsbad, CA, USA). Cells required 2 mM of magnesium sulfate for the growth, and the media with this concentration is referred to as

a control media. The $OD_{600}$ of the cells were measured at an interval of 30 min using UV/VIS spectrophotometer (PerkinElmer, Waltham, MA, USA).

### 3.2.2 Imaging and the Analysis of Images

When $OD_{600}$ of the sample reached one, the sample was dispensed on glass slides and phase-contrast images were obtained using a SPOT camera (SPOT Imaging Solutions, Sterling Heights, MI, USA) attached to a Nikon EFD-3 (Nikon Instruments, Tokyo, Japan) microscope with a 40X objective (Nikon Instruments, Tokyo, Japan). The images were taken without bias immediately after the experiments to minimize the error. The ImageJ [247] software was used to transform phase-contrast images to binary images. Binary images thus obtained were analyzed to obtain cell length data using a custom home brewed MATLAB code.

### 3.2.3 Transmission Electron Microscopy (TEM)

Cells obtained at different concentrations of $MgSO_4$ were centrifuged at 2000 rpm to reduce the error on morphology for eight min. The pellets were resuspended in phosphate buffered saline (PBS). A TEM grid was submerged into the sample for two minutes. Next, the grid with the sample was immersed in 2% lead acetyl for about two minutes, and subsequently dried for 24 h at room temperature. The dry sample was loaded to the TEM and was visualized.

### 3.2.4 Cell Death Assay

Bacterial samples were centrifuged at 8000 rpm for 5 min. The supernatant was discarded and the cell pellets were resuspended in PBS. The process of centrifugation and resuspension was repeated twice to wash the salt from the sample. The sample was then diluted to $OD_{600} \approx 0.1$, and 20 ng/mL of propidium iodide (PI) was added. The sample was then incubated in the dark for 20 min. The sample was then washed twice with PBS and representative fluorescence images were acquired. The fluorescence intensity data at the

single-cell level were obtained using BD Ariafacs Fusion cell cytometer (BD Bioscience, Franklin Lakes, NJ, USA).

### 3.2.5 Reversibility in a Liquid Media

To investigate the dynamics of reversibility of the cells after the removal of applied salinity stress, cell morphology, lag time, and growth measurements were performed every five generations. The samples were grown starting from $OD_{600} \approx 0.10$ to $OD_{600} \approx 1.0$ at different supplement levels of $MgSO_4$. The sample is diluted to $OD_{600} \approx 0.04$ in a fresh M9 control media and grown to $OD_{600} \approx 1.2$ (five generations). The optical density was measured every 30 min. The phase-contrast images were acquired to study the morphology. Cells were again diluted to $OD_{600} \approx 0.04$ and the process of growth was repeated. Each cycle of dilution and growth was termed as a passage. Those passages were repeated until the cells behaved normally in terms of morphology, growth rate, and lag time.

### 3.2.6 Primers and RT-qPCR

To understand how magnesium sulfate affects the gene expression of bacterial cells, the relative gene expression level of different genes was investigated as described in previous studies [248, 249]. In Table 5, the primers used in this study are listed. Primer 3 software was used with the sequence data available from the National Center for Biotechnology Information (NCBI) to design the primers, and the primers were tested with the NCBI Primer Blast, melt curve analysis, and in silico PCR [250]. The amplicon length of each primer was selected to be 150 bp. The primers thus designed were purchased from Integrated DNA Technologies (Coralville, IA, USA).

For the preparation of bacterial samples, a single colony was picked from petri dish and inoculated in M9 media. Bacteria were grown to the ($OD_{600} \approx 0.8$). Then the sample was diluted by 16 fold to M9 media, and cells were grown until $OD_{600}$ reached about 0.6. The total RNA was extracted using RNeasy mini kit (Qiagen, Germantown, MD, USA), and

total RNA was treated with DNAse (Thermo Fisher Scientific, Carlsbad, CA, USA). The treated RNA was then converted to complementary DNA (cDNA) using respective primers and with the help of iScript cDNA synthesis kit (Bio-Rad, Hercules, CA, USA). The amplification of cDNA was obtained using Quant Studio 3 real-time PCR system (Applied Biosystems, Thermo Fisher Scientific, Carlsbad, CA, USA) and iQ SYBR Green Supermix (Bio-Rad, Hercules, CA, USA). The threshold cycle data obtained were normalized to 16S *rRNA*, and the comparative fold measurements ($2^{-\Delta\Delta Ct}$) were calculated. The mean of the fold was calculated using three biological and two technical replicates. The error bars on the comparative fold expression were obtained from the standard error on $\Delta Ct$ for each gene.

Table 5: Primers used in this study.

| **Gene** | **Primer** | **Sequence (5′-3′)** |
|---|---|---|
| 16S *rRNA* | Forward | TCGTCAGCTCGTGTTGTGAA |
| | Reverse | AGGGCCATGATGACTTGACG |
| *corA* | Forward | AACATCGAGCAGAACCGCAT |
| | Reverse | AAAGATAATCGCGCCAGGGT |
| *cysP* | Forward | CGCCGTTTGAGCAACAATGG |
| | Reverse | TTTGTACGTCGGTCACCTGG |
| *osmC* | Forward | ATCGATTGATACCACCGCCG |
| | Reverse | GGGCATCCTGCTTTTGCTTT |
| *aqpZ* | Forward | AGCATTCACCAGGCGGTTAT |
| | Reverse | TCAGGGTTAAGGCCAGACCA |

## 3.3 Results

### 3.3.1 Growth and Death of Cell at high $MgSO_4$ Concentration

To investigate the effects of elevated concentrations of $MgSO_4$ on growth and death of *E. coli*, cells were cultivated in M9 media containing six different concentrations of $MgSO_4$, 2 mM, 0.41 M, 0.83 M, 1.25 M, 1.66 M, 2.07 M, and 2.50 M. The temperature of T = 37 °C was maintained in all the experiments. To study the growth, optical density ($OD_{600}$) of cells were monitored every 30 min. The $OD_{600}$ data were plotted to obtain the growth curves. To

calculate the mass doubling time, $\tau_d$, was obtained by fitting an exponential of the form $\mathrm{OD}_{600}(t) = \mathrm{OD}_{600}(0)2^{\frac{t}{\tau_d}}$ through the growth curves. Figures 17(A) and 17(B) are the growth curves and the mass doubling times of the cells for different concentrations of magnesium sulfate, respectively. The $\tau_d$ increased with the increase in magnesium sulfate concentration. The cells did not grow at $\mathrm{OD}_{600}$ greater than 1.25 M but cell death occurred. Therefore, the mass doubling times are not presented in the respective figure. Figure 17(C) is the survival fraction of the cells as a function of concentration of $MgSO_4$. Cells did not exhibit a significance decrease in viability up to 1.25 M, and the fraction of dead cells increases sharply beyond 1.25 M $MgSO_4$.

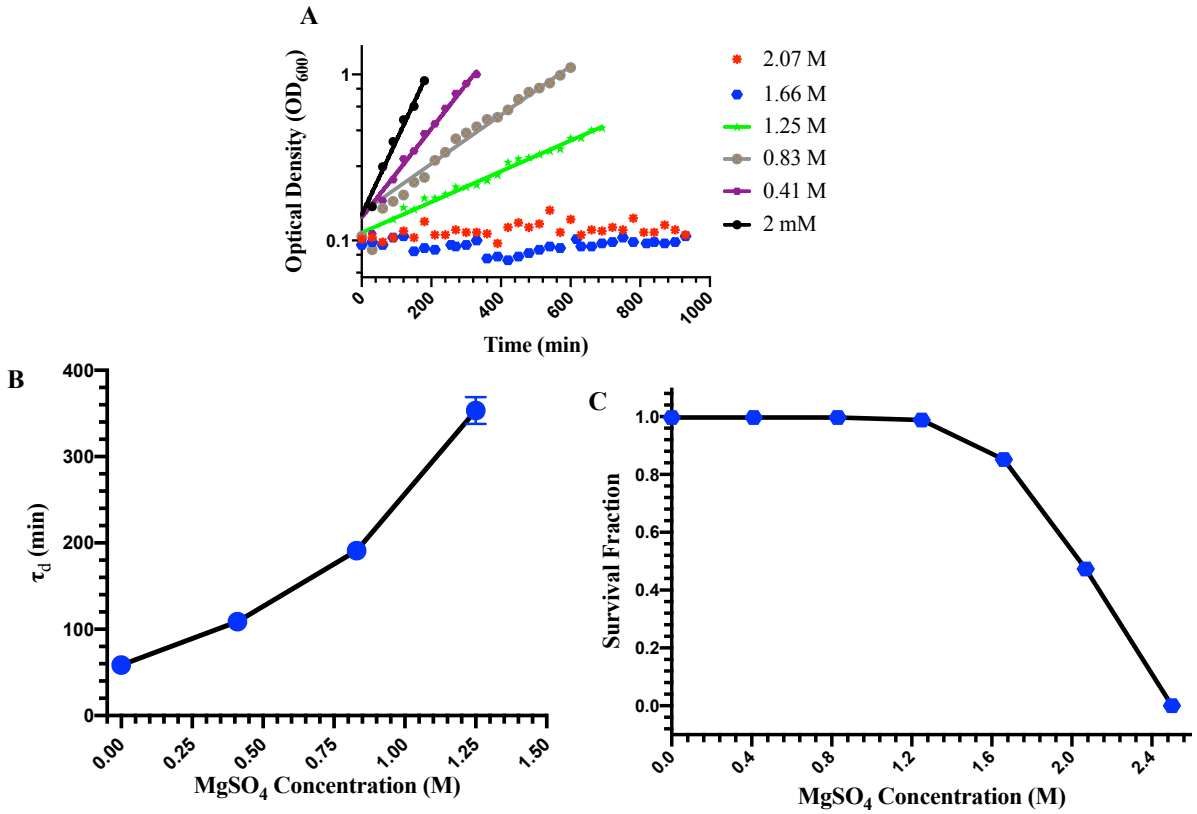


Figure 17: Growth and survival of *E. coli*: (A) growth curves, (B) mass doubling times, and (C) survival fractions at different concentrations of magnesium sulfate.

To investigate the death of *E. coli* at elevated $MgSO_4$, cells were grown at different salt concentrations from starting $\mathrm{OD}_{600} = 0.10$ to final $\mathrm{OD}_{600} = 1.0$. The sample was stained with

propidium iodide (PI) and a flow cytometer was used to obtain the fluorescence data. About $120,000$ cells were analyzed for each concentration. The fluorescence data thus obtained were used to calculate the survival fraction. The survival fraction remained unchanged up to 1.25 M $MgSO_4$ and then decreased sharply with the increase in $MgSO_4$ concentration. Cells cultivated at 2.5 M magnesium sulfate did not grow when the cells were transferred to a fresh M9 control media. These results show that *E. coli* is a halotolerant bacteria.

### 3.3.2 Cell Division, Cell Length, and Cellular Heterogeneity

To investigate the effect of magnesium sulfate on cellular morphology, cells were inoculated in liquid M9 media with the supplement of different levels of $MgSO_4$ and allowed to grow until OD reached 1. At $MgSO_4$ concentrations 1.66 M and 2.07 M, the cells did not exhibit any growth. The samples were incubated for 15 h before taking images and performing cell death assays. A small volume of the sample, 5 µL, was dispensed on multiple slides and imaged under microscope. Figure 18 represents illustrative images of bacteria cultivated at $MgSO_4$ concentrations of 2 mM (control), 0.41 M, 0.83 M, 1.25 M, 1.66 M, and 2.07 M. The size (length) of the cell was found to decrease with the increase in concentration. At 1.25 M $MgSO_4$, the morphology of cell was completely different compared to other concentrations. Cells switched to a new phenotype containing three different populations — (i) cells comparable to those grown in control media, (ii) cells smaller than the control cells, and (ii) filamentous cells (cells longer than the control cells). The filamentous cells consisted of several unit cells, and septum was formed but cells were not divided completely. Hence, the filamentous cells were counted as a single cell (Figure 18(D)).

The image data obtained at the end of experiments were analyzed using MATLAB to obtain the cell length. Figure 19 shows the probability distributions, $P(\ell)$, of cell length, $\ell$, for 2 mM (control), 0.41 M, 0.83 M, 1.25 M, 1.66 M, and 2.07 M concentrations of $MgSO_4$, respectively. Note that the range of $x$-axis for 1.25 M concentration in Fig. 19(D) is different compared to other figures. From 2 mM to 0.83 M $MgSO_4$ concentrations, the distributions

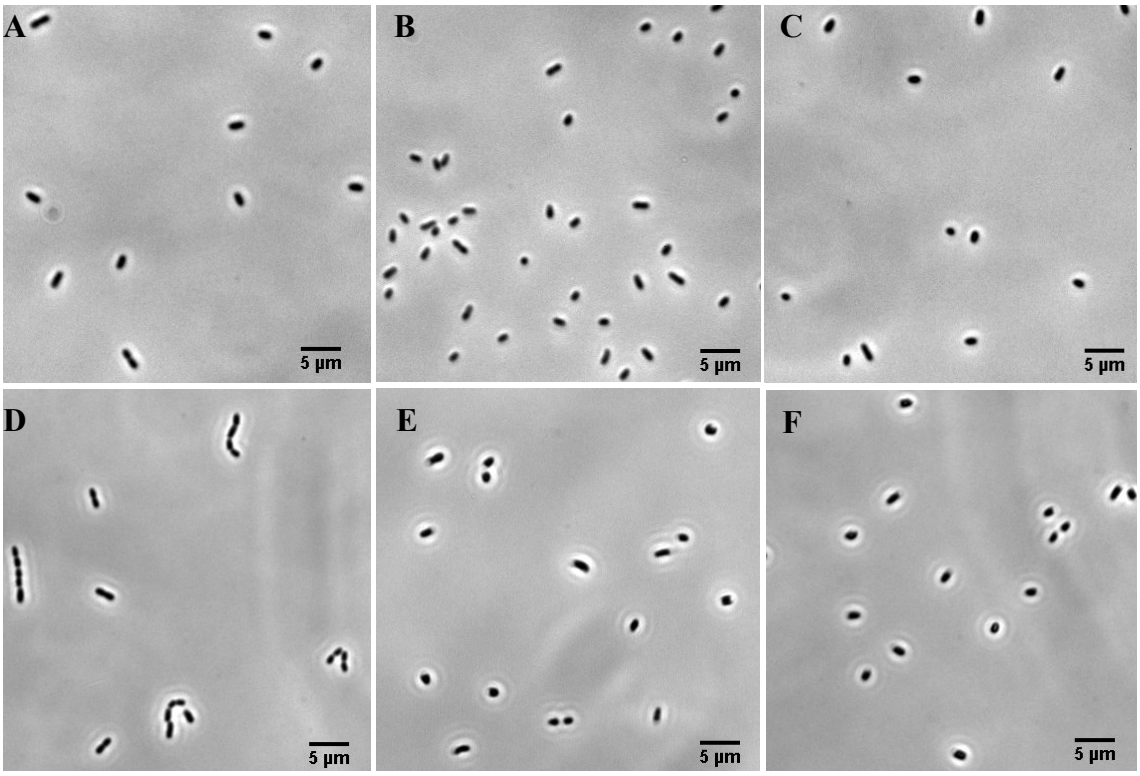


Figure 18: Representative images of *E. coli* at different $MgSO_4$ concentrations.

were similar. The one major difference on the distribution was the fraction of cells around 1.2 µm, increased with the increase in the salt concentration. The distributions were slightly shifted to a smaller value of cell length. At 1.25 M concentration, the distribution was a long tail. This long tailed behavior shows the fraction of long cells increased in the population. The distribution was over the short, long, and similar sized cells compared to the control (Fig. 19(A)). On further increasing the $MgSO_4$ concentration, the width of the distribution decreased. The cell death started at 1.25 M $MgSO_4$, and for the distributions $> 1.25$ M, cells did not grow, and the probability distributions were obtained from both alive and dead cells. Next, the average cell length and heterogeneity in cell length defined by variance will be discussed.

The length data for cells grown at different $MgSO_4$ concentrations were used to extract the average cell length, $\langle \ell \rangle$, and the variance, $\sigma_\ell^2$, on cell length. Figure 20(A) and 20(B)

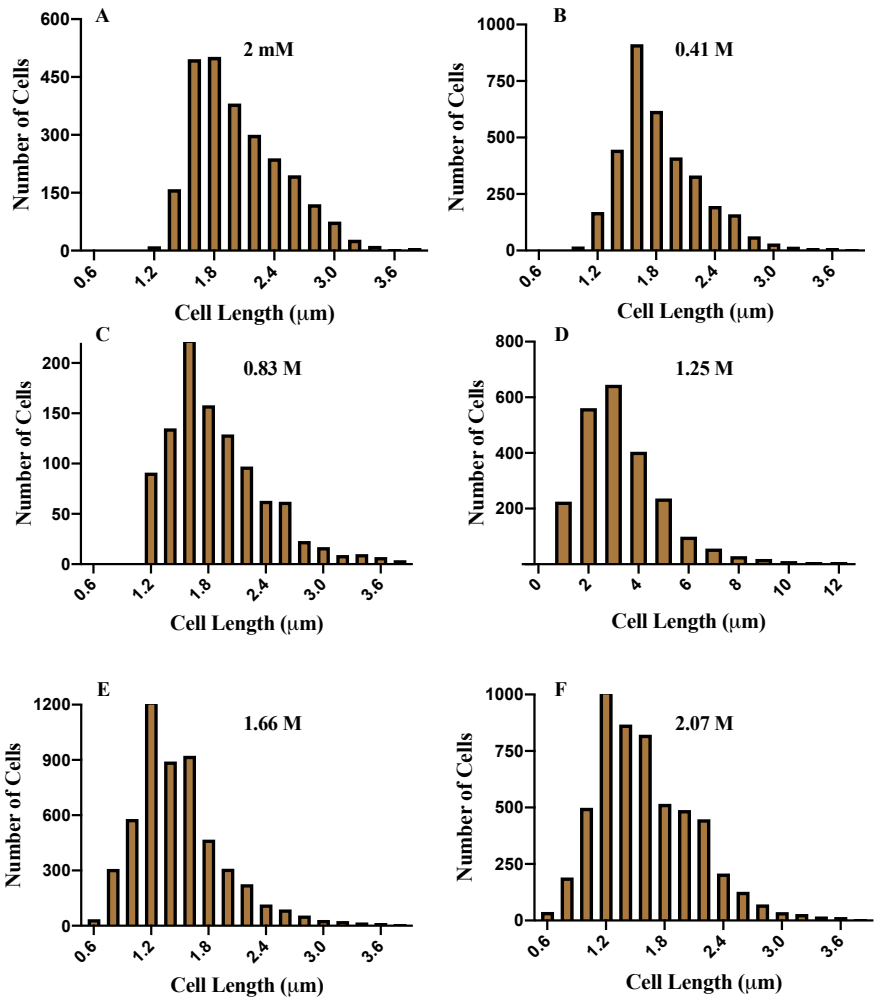


Figure 19: Probability distribution, P($\ell$), of cell length of *E. coli* at different concentrations of $MgSO_4$.

represent $\langle \ell \rangle$ and $\sigma_\ell^2$ of the cells as a function of $MgSO_4$ concentrations, respectively. The average length decreased slightly on increasing the concentration until 0.83 M, and it again increased to a maximum at 1.25 M. On further increasing the concentration, the average cell length was found to be decreasing. Similar non-monotonic behavior was observed in variance with a maximum at 1.25 M. The long cells contributed to an increase of the average length of the cells and both the short and long cells contributed to an increase the variance at 1.25 M $MgSO_4$. Both the average and the variance of cell length exhibit a maximum at 1.25 M because cells do not grow for concentrations $> 1.25$ M and part of the population of

cells undergo cell death.

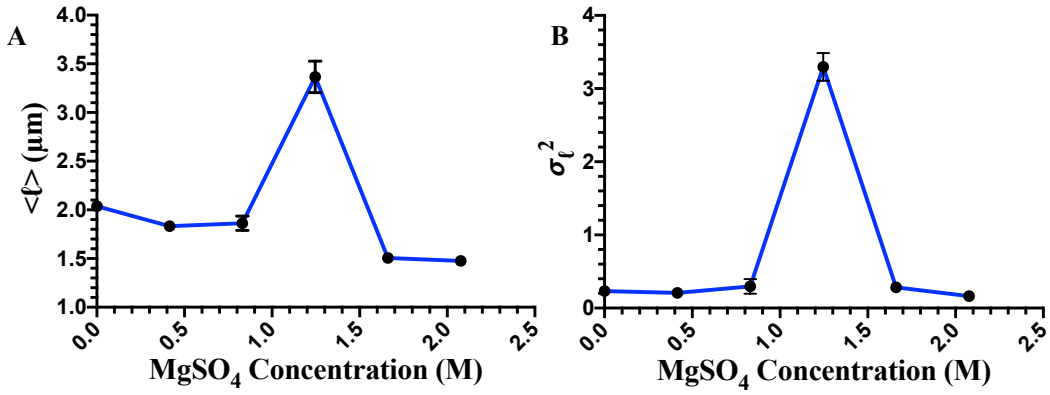


Figure 20: Average and the variance of cell length as a function of $MgSO_4$ concentration.

### 3.3.3 Plasmolysis of Cells

To maintain the shape and size under the high osmotic stress, bacteria actively regulate water to maintain their volume. Cells expel water in a high osmotic medium to balance the turgor pressure in the cell wall from inside and outside of the cell. When the turgor pressure is high, cell walls break resulting in death of the cell. At intermediate turgor pressure, the plasma membranes of cells might detach from the cell wall resulting in a plasmolysis. Previous studies using electron microscopy revealed that the cells plasmolyze at high osmotic pressure caused by 0.35 M of sucrose [229]. The average cell length was decreased on increasing the concentration (Figure 20(A)). To understand the decrease in length, images of the cells were taken using an electron microscope. Figures 21(A–C) are the electron microscopy images of the cells at $MgSO_4$ concentrations of 2 mM (Control), 1.25 M, and 2.07 M, respectively. The scale bar shown in the figure is 500 nm. At high salt concentration, plasmolysis of the cells were clearly observed, and the strength of plasmolysis was found to be increasing with the increase in $MgSO_4$ concentration. Plasmolysis was found to be stronger at the poles. A previous study showed that plasmolysis is dominating around the center of cells [251] which is different compared to the results presented here, while other

studies showed that plasmolysis is stronger at poles and not in the center of the cells [229, 252] which are in agreement with the results obtained here. Previous studies were conducted using sucrose as a osmotic stressor, while, aqueous $MgSO_4$ was used for all the studies performed here.

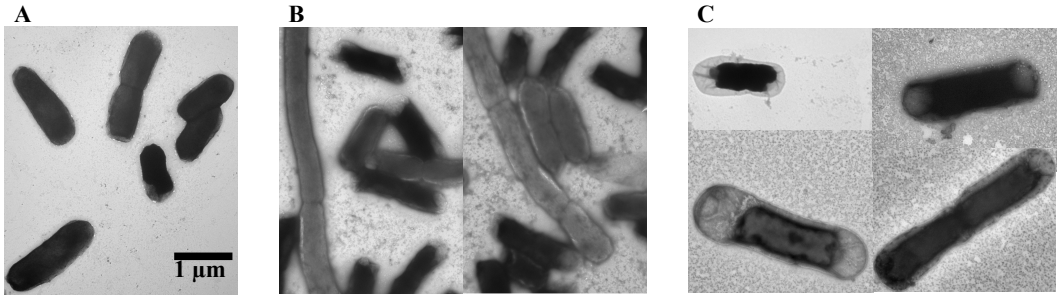


Figure 21: TEM micrograph of *E. coli* at different concentrations of $MgSO_4$.

### 3.3.4 Gene Expression of *aqpZ*, *corA*, *cysP*, and *osmC*

The effect of high salt in growth, cell division, viability, and plasmolysis was presented in previous sections. Next, the effect of $MgSO_4$ on the gene expression level of genes responsible for osmotically driven transport of water (*aqpZ*), transport of magnesium (*corA*), transport of sulfate (*cysP*), and a gene induced by osmotic stress (*osmC*) were studied. The expression level of these genes was compared between the control cells (2 mM) and the cells grown at 1.25 M $MgSO_4$ (high salt). The data and error bars were obtained by averaging over three biological and two technical replicates. Figure 22 is log fold changes in expression, $2^{-\Delta\Delta Ct}$, of genes between control and high salt. The error bars were calculated by estimating the standard errors on $\Delta Ct$. The results showed that there is no significant difference in expression of *aqpZ* and *corA*. The regulation of *aqpZ* on this result is significantly different compared to a previous result in which it was shown that the expression of *aqpZ* decreases in the exponential growth phase in a hyperosmolar media in the presence of NaCl [253]. The later studies suggested that during the growth phase, *aqpZ* does not have a significant role in the transportation of water but it plays an important role in the late growth phase,

stationary phase [254, 255]. The gene expression studies were carried out during the exponential phases and the results obtained here showed similar results as explained by Soupene et al. [254]. Plasmolysis was observed in cells at high salt and it is possible to lose water by pure diffusion of it. The pure diffusion of water is slow and might take a long time because cells appear to show a clear plasmolysis.

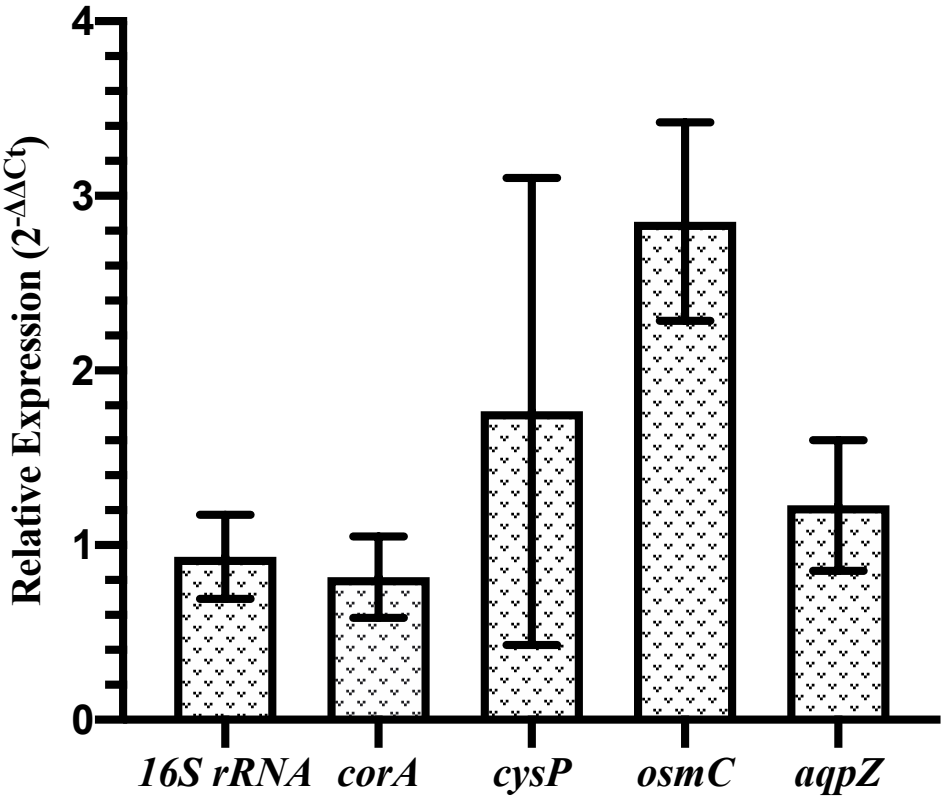


Figure 22: Relative expression of the cells cultivated at mid exponential regime at high and low salt condition.

### 3.3.5 Reversibility of Mass Doubling Time upon Removing the Applied Salinity Stress

Previous studies showed that bacteria grow to filamentous cells under the stress of high pressure [136, 140], antibiotic [256, 257], and temperature [258]. The studies performed here showed similar filamentous cells at 1.25 M $MgSO_4$. The previous chapter discussed the

reversibility of the cells at high pressure. Bacteria reverted back to their normal morphology when the applied pressure was removed. The duration of temporal fluctuation in pressure was important to shape the morphology of cells. When the duration of pressure release was increased, the cell division was unaffected regardless of the history of the cells (long and short exposure to pressure where long exposure increased the fraction of long cells). Here it was shown that the cells showed their phenotypic switching at high salt to new morphological phenotypes (filamentous, short and plasmolyzed). Interesting questions arise here — (i) do cells revert back to normal morphology when applied salt stress is removed? (ii) if cells are able to obtain their original shape when the stress is removed, what will be the time scale for different cells grown at different $MgSO_4$ concentrations? To answer these questions, the reversibility experiments were conducted following the protocol described in the materials and methods section (Section 3.2.5).

Right after the removal of the stress (transferring cells from media with magnesium sulfate to the control media), the first passage, cells experienced a long lag phase, the time in the growth stage of cells before they enter exponential growth, which increased with the increase in $MgSO_4$ concentration(Fig. 23(A)). At every passage, the morphology of the cells was recorded. Cells gain their normal morphology (control cell like morphology) after five generations regardless of the concentration of magnesium sulfate. Figure 23(B) is the reversibility in doubling time, $\tau_d$, after the removal of salt stress. The open bars (1.66 M and 2.07 M) indicates that the cells did not grow, and the mass doubling time is undefined. The mass doubling time, $\tau_d$, is the average mass doubling time over five generations. Cells grown at concentration $\leq 1.25$ M achieve their normal growth rate ($55 \pm 5$ min) within first passage. However, for 1.66 M and 2.07 M $MgSO_4$, the cells regain the original doubling time in the third passage. The morphology of the cells was able to retain normal morphology much faster compared to the growth rate. These results show that the effect of salt can propagate in the cells for several generations (10-15) although the salt stress is removed. Cells that are plasmolyzed and stressed in greater extent took a longer time for the recovery.

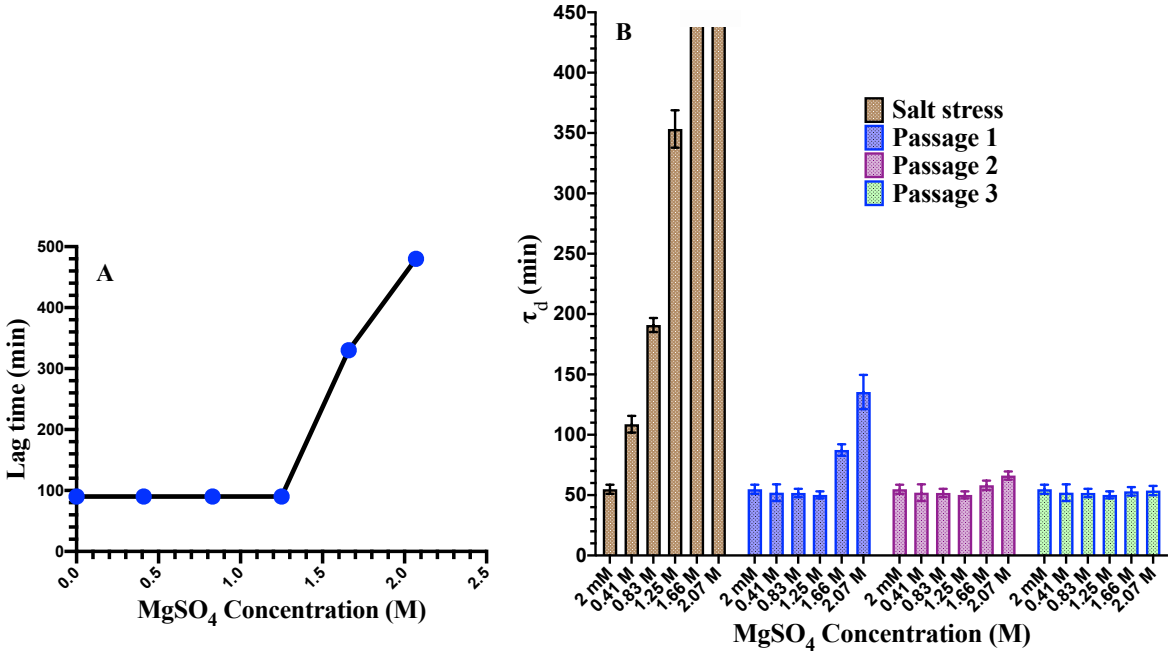


Figure 23: (A) Lag time increases with increasing salt concentration. (B) Mass doubling time, $\tau_d$, of the cells obtained at high salt concentration in control media over different passages.

The error on mass doubling time, $\tau_d$, appeared from the errors on optical density measurements using a spectrophotometer, and it has an error on the order of $\Delta_{\text{OD}} = 0.02$. The errors were assumed to be Gaussian and 1000 values of errors with a fixed standard deviation of 0.2 were generated for each optical density data. Then 1000 optical density curves were obtained for each growth curve and 1000 growth curves were fitted to the optical densities to obtain the same number of doubling time data. The mean of these data provided $\tau_d$. The standard deviations were calculated from 1000 doubling time values to estimate the error on $\tau_d$'s. Error bars were constructed using the standard deviation.

### 3.4 Summary and Discussion

To summarize, the effect of elevated magnesium sulfate concentration, supposedly the most abundant salt on Mars and Europa, on several cellular processes including growth, death, division, and expression of various genes of a mesophilic bacterium, *E. coli*, were

investigated. Firstly, decrease in growth rate was observed up to 1.25 M $MgSO_4$ without any cell death. These results show that *E. coli* can tolerate high salt and can be referred as a halotolerant bacteria. Similar decrease in growth rate was observed as an effect of several other stressors, including high hydrostatic pressure [136, 259], extremes of temperatures [260], and high and low of pH [261]. On the other hand, the growth of cells was suppressed for all the salt concentrations studied here which were greater than 1.25 M and the death rate increased sharply with the increase in salt concnetration. The sharp decrease in viability in case of another salt, sodium chloride, was observed when the concentration was 0.51 M [231]. Similar behavior of cells but at different concentrations signifies that these two salts provide stress to cells differently. One of the strength mechanisms at high salt is retaining a fraction of available water by salts and, hence, decreasing the available water to support life. In the past, it was shown that water activity is a limiting factor for life [262]. Table 6 is the list of water activities in different concentrations of aqueous solutions of $MgSO_4$ [263], and these water activities were compared to that of NaCl at the corresponding concentrations [264, 265]. The water activity at 0.5 M of NaCl is 0.9836 and the water activity of $MgSO_4$ at concentration of 1.25 M is 0.9740. The water activities in both cases are much higher than the minimum water activity to support life (0.61) [227]. The slightly lower value of water activity at the onset of bacterial death shows that *E. coli* is more viable at the ionic strength caused by aqueous solution of $MgSO_4$ compared to the aqueous solution of NaCl. Hence, in this case, the nature of ions is a limiting factor to support the life rather than the water activity.

Cell division and cell morphology at different $MgSO_4$ concentrations were also investigated. The average cell length was decreasing for salt concentrations up to 0.83 M, and for salt concentration greater than 1.25 M, the average length exhibited a discontinuity at 1.25 M. A fraction of the cells were plasmolyzed, cell division was inhibited on another fraction of the cells, and the remaining cells were found to be normal. The plasmolysis of the cell was stronger at the poles. Stronger plasmolysis at the poles (similar to this study) was

Table 6: Water activity of $MgSO_4$ and NaCl at $T = 25$ °C.

| **C**oncentration (M) | Water Activity | |
|---|---|---|
| | $MgSO_4$ | NaCl |
| 0.1 | 0.9970 | 0.9967 |
| 0.2 | 0.9950 | 0.9934 |
| 0.3 | 0.9940 | 0.9901 |
| 0.4 | 0.9920 | 0.9868 |
| 0.5 | 0.9900 | 0.9836 |
| 0.6 | 0.9880 | 0.9803 |
| 0.7 | 0.9870 | 0.9769 |
| 0.8 | 0.9850 | 0.9736 |
| 0.9 | 0.9830 | 0.9702 |
| 1.0 | 0.9810 | 0.9669 |
| 1.2 | 0.9760 | 0.9601 |
| 1.25 | 0.9740 | 0.9552 |
| 1.4 | 0.9710 | 0.9532 |
| 1.6 | 0.9660 | 0.9461 |
| 1.8 | 0.9600 | 0.9389 |
| 2.0 | 0.9530 | 0.9316 |
| 2.5 | 0.9320 | 0.9127 |
| 3.0 | 0.9050 | 0.8932 |

observed in cells grown at high osmolarity using sucrose [229, 252]. Three distinct subpopulations existed at the salt concentration — (i) smaller than the control cells, (ii) comparable to control cells, and (ii) longer than the control cells. A large heterogeneity was observed in cells grown at 1.25 M $MgSO_4$. Cells have underlying stochastic processes including, biochemical networks [266], synthesis and degradation of mRNA [267], gene expression [202], cell growth [190], cell division [268], and interaction between proteins [269] which might have contributed to heterogeneity in cell length and viability. Viable but stressed cells at high osmolarity due to $MgSO_4$ were reversible upon the removal of stress. The cell division process resumed normal after generations. The number of generations was dependent on the strength of the stress applied. The cell division process during the reversibility was studied and is presented in Chapter 4.

The gene expression study revealed that *osmC* and *cysP* upregulated at 1.25 M $MgSO_4$ (high salt). CysP is a part of ABC transporter complex and the increase in gene expression

of *cysP* indicates that the thiosulfate update increases at higher salt concentration. The gene expression of osmotically inducible gene, *osmC*, also increased at high salt. The upregulation of *osmC* at high osmolarity was shown in the past [233]. Two promoters, $osmC_{p1}$ and $osmC_{p2}$, help in the process of transcription of *cysP* [270]. $osmC_{p1}$ needs RpoS for the transcription while $osmC_{p2}$ does not need RpoS for the transcription [233, 270]. The histone-like nucleoid structuring protein, H-NS, and leucine-responsive regulatory protein, LrP, regulate the expression of *osmC* [270, 271]. The upregulation of *osmC* at high salt has two major possibilities — (i) higher synthesis of RpoS at high salt that might have increased the expression of *osmC* and (ii) low synthesis of H-NS and LrP or the decreased binding affinity to *osmC* promoter. Interestingly, the expression of *aqpZ* did not change at high concentration. Previous study found that the level of expression does not change at high salt during the exponential growth phase [254, 255]. The plasmolysis of the cell was observed and the slow diffusion of water is still possible and the loss of water might be significant over a time for the plasmolysis to be observed.

Existence of aqueous $MgSO_4$ solutions is possible at temperature slightly lower than 0 °C in the near surface regions of Mars. The viability of *E. coli* at 1.25 M is important for the perspective of planetary protection for future space missions. The physicochemical condition of planetary bodies has extreme conditions in several aspects. The studies presented here were performed using one physicochemical variable (high salt). To understand the possibility of life on extraterrestrial bodies, the cellular response at several extreme condition variables and a combination of them should be explored.

# 4 Constant Mass Addition and Symmetric Cell Division Drive Size Homeostasis in Filamentous Cells Obtained at High Concentration of Magnesium Sulfate

## 4.1 Introduction

Growth and division are essential characteristics of cells that determine the size of progenies in a population. In nature, size of different cells span over six-fold range, but the size distribution of cells within an organism is usually narrow with a small variability [272, 273]. Inherent stochasticity of molecular activities related to growth and the division of the cells underly small variability in cell size distribution [274, 275, 276]. How different cells achieve cell-size homeostasis is a long standing open question in biology. Several experimental [277, 278, 279, 281, 282] and theoretical studies [283, 284, 285, 287, 288, 289] have been carried out to understand the cell size control and homeostasis [280, 286] in bacteria, yeast, and mammalian cells. The explicit mechanism of size control still remains elusive due to the complexity of the cell division process. There are three prevailing models of cell-size regulation and homeostasis, namely (i) the timer model, (ii) the sizer model, and (iii) the adder model. The timer model assumes that the cells grow for a fixed period of time before they undergo cell division [290]. Therefore, cells must have an underlying mechanism to sense time. The cell size homeostasis is achieved in the timer model if the cells grow linearly for a fixed amount of time. However, no explicit time sensing mechanism is known in bacteria. On the other hand, the sizer model assumes that a cell divides by achieving a threshold size [281, 290, 291, 292, 293]. Cell size homeostasis within the sizer model is achieved within one or more generations. The adder model envisages a constant mass/size addition to cells between divisions. However, experimental studies reveal that size/mass addition to a cell before division, as assumed in the adder model, is noisy [278, 294].

Recent high throughput studies at the single cell level utilizing different bacterial cells find the cell division to be consistent with the adder model with small variability in the mass added between the divisions [278, 279, 295, 296, 297]. However, other studies have found

that the cell division dynamics differ from the adder model. For example, a recent study by Tanouchi et al. on the long-term study of the cell division dynamics of *Escherichia coli* across different strains and growth conditions finds that a small subset of cells in a population exhibits transient oscillations in cell size with periods spanning over many generations [298]. They explain this behavior by assuming a negative feedback on the cell size control assuming that smaller cells divide later than the longer cells [298]. The growth rate of bacteria in a population varies from cell to cell [299]. Many studies have shown an intricate coupling between the growth and the cell division [300, 301, 302]. Therefore, the cell division dynamics may depend on the growth rate of the cells. Indeed, studies show that the fast growing cells follow the adder model and the slow growing cells follow the sizer model to maintain the cell size [303, 304]. In another study, it has been demonstrated that the size homeostasis in bacteria for the fast growing cells are described by a combination of the sizer and the timer models [186].

Cell division is followed by the replication of the DNA, therefore, cell cycle is also affected by the number of DNA replication initiation sites, the duration of the DNA replication, and the time of cell division [305]. Experiments on *Caulobacter crescentus* show that cells follow the timer model during the growth phase before the constriction of the cell wall, and the adder model during the constriction of the cell wall [294]. Usually, replication initiation and cell division are coupled [291, 306]. In order to investigate the effect of replication time on the cell division, Si et al. have used a strain of bacteria where the internal level of thiamine could be controlled. In the thiamine limiting condition, where the amount of nucleotide pool available to the cells is smaller, the replication time increases without affecting the growth [299]. They found that in the thiamine limiting condition, cell division initiation is consistent with the initiator threshold model [292, 307].

Furthermore, the biosynthesis and accumulation of a critical concentration of proteins inside cells is important to maintain the size of cells. Cells must sense this critical accumulation of biomass before they can divide. Production of mRNA is directly related to

the cell size [308] and, hence, the amount of proteins abundance in a cell [309].

The metabolite might have played an important role in sensing the size of the bacteria to initiate the cell division process [277]. Studies have shown that both the replication of chromosomes and division of cells take place after a growth for a constant volume regardless of the media used for the growth and which supports the sizer model for the bacterial cells to control their size [291]. Later, the size control in both budding and fission yeast is described explicitly by the sizer mechanism in which the cell division occurs after reaching a threshold size regardless of the size at the birth [281, 310, 311]. These studies further show that the duration of G1 phase depends on the size of the yeast at birth. However, in bacteria the size control of the cell depends on the growth rate and the cell cycle that inspired the sizer model to describe the cell size homeostasis in bacteria [185, 293, 312]. Recent studies propose that unlike the timer and sizer models, cells add constant volume before a division and is known as an adder/incremental model [278, 279, 295, 313]. The adder model is able to explain the cell size control in mycobacteria that exhibit asymmetric cell division [314].

The majority of the experiments to study size homeostasis mechanism are conducted on the rich growth media where the starting population exhibit a narrow distribution and it is carried over for several generations [277, 278, 281]. These studies lack the study of longer or shorter cells compared to the size of controlled cells. Hence, the study tells us about the propagation of narrow cell size distribution with the generations. Some studies are focused on the longer cells [279, 282], and the studies inform the mechanism of achieving narrow distribution starting from a somewhat heterogeneous distribution. To understand the size control for the smaller cells, models and numerical simulations are employed [278, 279]. Despite several studies, a universal phenomenon of the size homeostasis is unknown, if it exists. The mechanistic description of the size control is still lacking. To obtain a universal phenomenon, experimental study of the small cells and the size control of bacterial cells in a stressed condition where the cells become longer due to lack of cell division is important.

Here, the size control mechanism for the cells cultivated in a stressed condition due to a

high concentration of magnesium sulfate was studied. At 1.25 M $MgSO_4$, a fraction of cells switch to smaller cells due to plasmolysis, a fraction stays the same size, and a fraction of cells are elongated due to lack of cell division. The experimental study was performed for the reversibility of the cell and size control in a highly heterogeneous population upon the removal of applied osmotic stress. Furthermore, the mechanism of size control in bacterial population was studied by investigating the convergence of highly heterogeneous/wide cell length distribution to a relatively homogeneous/narrow distribution. The results are further described by using a model.

## 4.2 Materials and Methods

### 4.2.1 Bacterial Strain and Culture

Wild-type *Escherichia coli* K-12 strain MG1655 was obtained from the Coli Genetic Stock Center located at the Yale University (New Haven, CT, USA). The media to culture cells was prepared using M9 media by adding two carbon sources, 0.4% glucose and 0.4% sodium succinate, and 2 mM $MgSO_4$. 1.25 M $MgSO_4$ was added to the media to observe the effect of osmotic stress. The pH of the media was found to be decreasing with the increase in the concentration of $MgSO_4$, and was 5.3 at 1.25 M of salt. To sterilize the media, it was passed through a 0.22 µm filter (ThermoScientific, Waltham, MA, USA). M9-agar media was prepared by supplementing 1.5% of agar (BD Difco, Franklin Lakes, NJ, USA) in the liquid M9 media. Firstly, 1 µL of bacterial stock was inoculated in solid media prepared in a petri dish and incubated for 16 hours at 37 °C. A single colony was picked using 1 µL inoculating loop (BD Difco, Franklin Lakes, NJ, USA) and dipped in a liquid media, and the sample was cultured in a shaking incubator (VWR, Randor, PA, USA) at 250 rpm at 37 °C. The optical density ($OD_{600}$) was monitored using a spectrophotometer (PerkinElmer, Waltham, MA, USA) and, at $OD_{600} = 0.5 \pm 0.1$, the sample was diluted in a fresh liquid media with the supplement of 1.25 M of $MgSO_4$ to $OD_{600} \approx 0.05$. Then, the bacterial sample was further grown at 37 °C in a shaking incubator at the speed of 250 rpm until the $OD_{600}$ reached one.

### 4.2.2 Imaging and Image Analysis

Immediately after the experiment, the sample was dispensed on multiple glass slides and phase-contrast images were obtained using a SPOT camera (SPOT Imaging Solutions, Sterling Heights, MI, USA) attached to a Nikon EFD-3 (Nikon Instruments, Tokyo, Japan) microscope with a 40X objective (Nikon Instruments, Tokyo, Japan). The images were taken without bias immediately after the experiments to minimize the error. The phase-contrast images were transformed to binary images using ImageJ [247]. The binary images thus obtained were analyzed to obtain cell length data using a custom made MATLAB code. The probability distributions of the cell length were obtained from more than a thousand cells.

### 4.2.3 Time-lapse Imaging of Cell Division Dynamics on Agar Chamber and Analysis

Solid agar LB media was prepared by adding 1.5% agarose to liquid LB media. It was cooled at room temperature and, just before the solidification, 25 µL of the media was transferred into a micro chamber (Thermo scientific, USA) attached to a glass slide (Thermo Fischer, USA). A coverslip (22X50 mm) was used to get rid of excess media and was removed after making the surface smooth by gently sweeping the gel. The micro chamber with the solid media was incubated at room temperature for ten minutes in a biosafety cabinet. After drying the media completely, it was taken out of the cabinet, and 0.6 µL of the cells grown in 1.25 M $MgSO_4$ was dispensed gently on the agar surface. The sample was again incubated in a biosafety cabinet for ten minutes to let the excess liquid evaporate. A coverslip (22X22 mm) was applied on the top of the agar surface and was stuck on it by using the glue provided on the micro chamber. The sample was visualized under a microscope (Nikon Optiphot EFD-3) using a 40X phase-contrast objective. Time-lapse images were obtained using a custom automated focusing system developed for the microscope and integrated with µManager [315]. The reversibility movies obtained were analyzed frame by frame using ImageJ [247] at single-cell scale to extract the cell length as a function of time, $\ell(t)$, their

successive division time, $\tau_{sd}$, the length at birth, $\ell_b$, and the length at division, $\ell_d$, as depicted in Fig. 24. A cell starting with a cell size $l_b$ at birth grows to size $\ell_d = \ell_b + \Delta\ell$ by adding a mass $\Delta\ell$ and divides into two daughter cells at time $\tau_{sd}$. Figure 24(B) is a tree diagram of successive division of a cell and its progenies. A cell starting at $t = 0$ divides into two daughter cells by adding a length, $\Delta\ell$ (color coded), that further grow and divide.

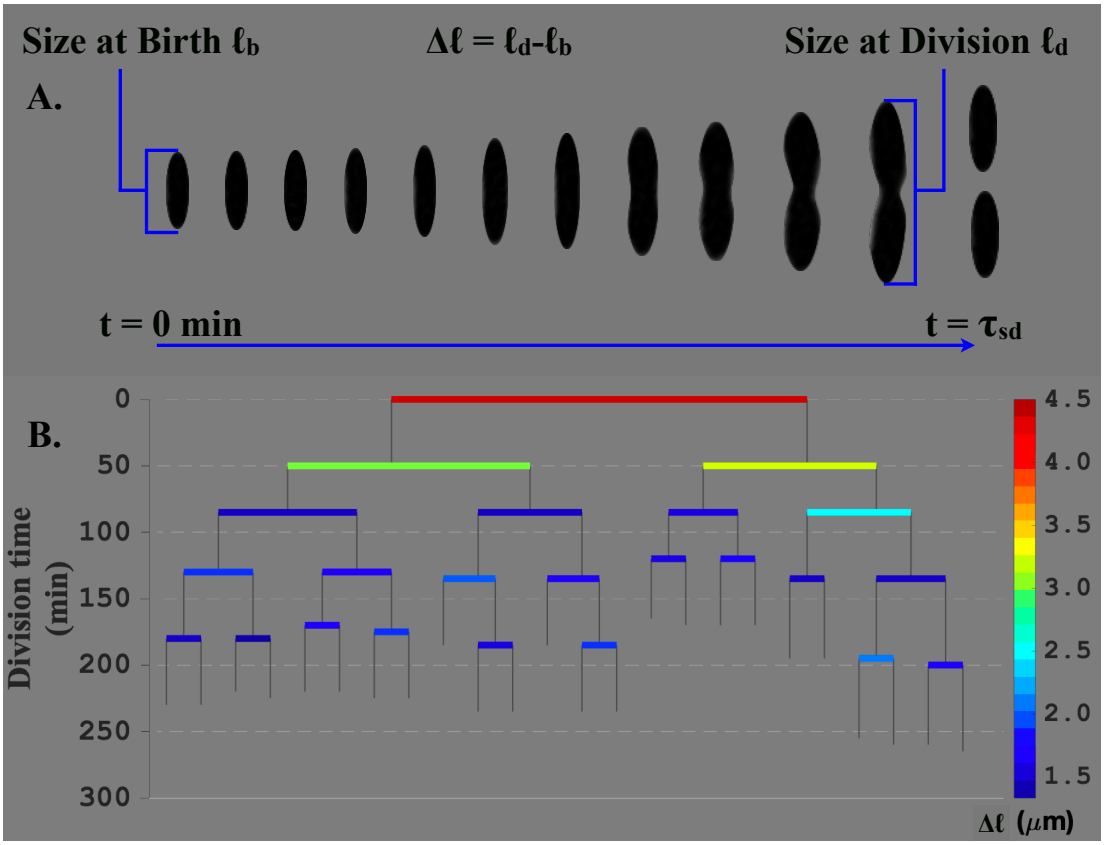


Figure 24: (A) Schematic of cell division of bacterial cells. (B) Tree diagram of successive divisions.

## 4.3 Results

### 4.3.1 Effect of High Concentration of Salt on Cell Morphology

The previous chapter on the effect of high concentration of magnesium sulfate suggested that cells exhibit large heterogeneities in cell length. It was found that cells grown at 1.25 M

salt were both shorter and longer than the cells grown in the control media. The cell-septum sites in longer filamentous cells were visible but the cell division had not taken place. These filamentous cells were counted as one cell. Figure 25 shows the probability distribution, $P(\ell)$, of cell length, $\ell$, for cells cultured in 2 mM and 1.25 M $MgSO_4$, respectively. These probability distributions were obtained from more than a thousand cells. While the probability distribution is narrow with smaller variance at 2 mM, the distribution is long-tailed at 1.25 M $MgSO_4$. Representative images of cells are shown under the distribution plots. At 1.25 M salt concentration, the population of cells is comprised of cells with heterogeneous morphologies as reflected in their cell length. While the distribution is narrow with a smaller mean for 2 mM, the probability distribution is long-tailed with larger variance and mean.

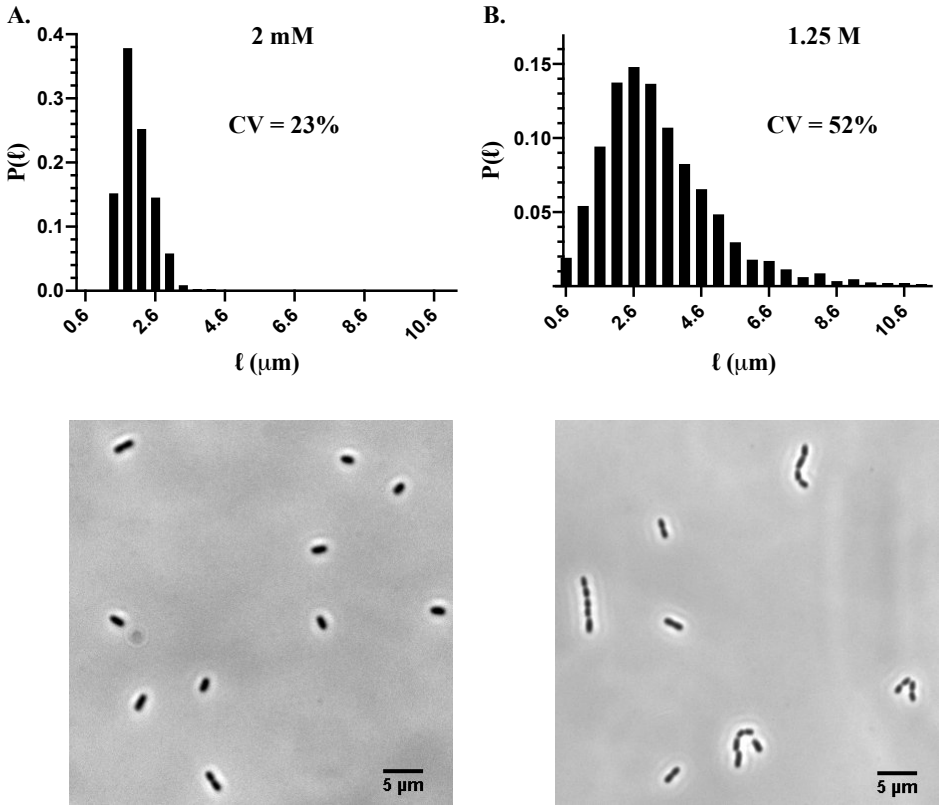


Figure 25: Probability distribution, $P(\ell)$, of cell length, $\ell$, for cells grown in (A) 2 mM $MgSO_4$, and (B) 1.25 mM $MgSO_4$ and the corresponding representative images.

### 4.3.2 Growth and Cell Division of a Heterogeneous Population of Cells

Next, the growth and division of both the control cells (cells grown in 2 mM), and the cells grown at 1.25 M salt, upon removal of the salt stress was studied at the single-cell scale. Real-time dynamics of growth and division of multiple cells and their progenies were tracked. Figure 26, shows cell length as a function of time, $\ell(t)$, the number of cell divisions, $n_d$, and the cell length per unit cell, $\frac{\ell(t)}{2^{n_d}}$, for cells grown in the control media and the media with high salt concentration. Note that the number of cells after $n_d$ division is $2^{n_d}$. The upper panels (Figs. 26(A), 26(B), and 26(C)) show these results for the cells grown in the control media, and the lower panels (Figs. 26D, 26E, and 26F) are the results for the cells grown in high salt concentration. Multiple cells and their daughter cells were tracked to obtain these figures. The exponential fits, $\ell(t) = \ell(0)2^{t/\tau_d}$, to the data points are shown in Figs. 26(A) and 26(D), where $\tau_d$ is the biomass doubling time. Each line represents the corresponding growth, division number, and cell length per unit length for a bacterium.

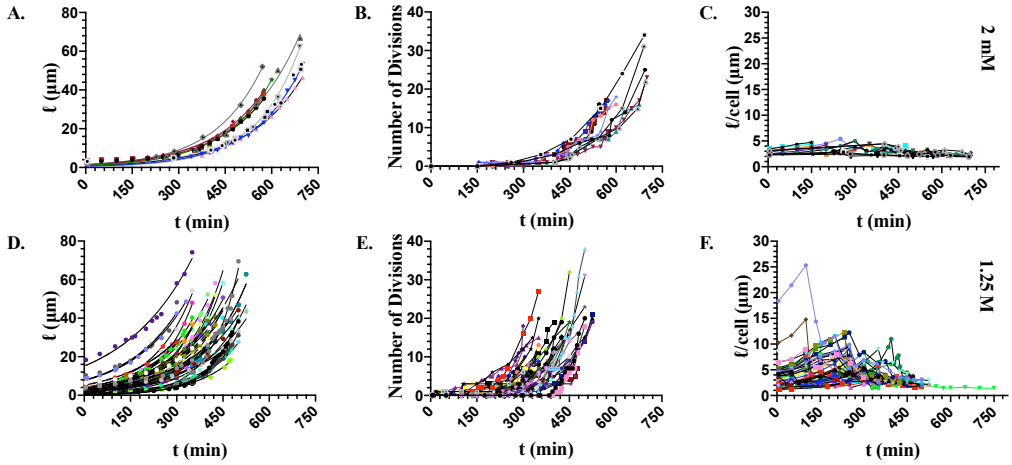


Figure 26: Cell length, $\ell$, number of cell divisions, and mass per unit length of cells as a function of time, $t$, for cells grown at 2 mM and 1.25 M $MgSO_4$.

The diameter of the cells remains a constant and, therefore, length, mass, and size will be used interchangeably throughout the text. The initial length of the cells grown in 2 mM were distributed between 1.6 µm and 4.5 µm, while the cells grown at high salt concentration

ranged between 0.6 and 16 µm. The length per unit cell as a function of time for 2 mM concentration remained uniform around 2.5 µm. The length per unit cell for high salt concentration decreased with time and converged to 2.5 µm in about 8 hrs.

### 4.3.3 Correlation Between the Size of the Mother and the Daughter Cells

In Figs. 27(A), and 27(B), the probability distribution of the length at birth of the cells grown in 2 mM and 1.25 M $MgSO_4$ are shown. The probability distributions of the length at division for these salt concentrations are shown in Figs. 27(C) and 27(D). Statistical measures of these distributions are summarized in Table 7.

Table 7: Statistical measures of the cell length at the birth and the division for control and stressed cells.

| Concentrations | Events | Mean (µm) | Standard Deviation (µm) | Median (µm) |
|---|---|---|---|---|
| 2 mM | Birth | 2.23 | 0.42 | 2.16 |
| | Division | 4.44 | 0.70 | 4.26 |
| 1.25 M | Birth | 3.37 | 1.64 | 2.96 |
| | Division | 6.27 | 2.87 | 5.45 |

The average length, standard deviation, and the median at the birth and division are higher for the cells grown in high salt concentration because the statistics are gathered over both small and filamentous cells. Next, the relation between the size of the mother and the daughter cells was explored. For the adder model with a constant mass addition, $\Delta$, the length of the two daughter cells upon division, $\ell_{D_1}$ and $\ell_{D_2}$, are related to the length of the cell at birth (or the length of the mother cell) by

$$\ell_{D1} = r(\ell_b + \Delta) \text{ and } \ell_{D2} = (1 - r)(\ell_b + \Delta) \qquad \text{(Equation 2)}$$

where $r$ is the division ratio. A value of $r = 0.5$ means symmetrical division. For symmetric division, both the daughter cells upon division have the same cell length, hence,

$$\ell_{D1} = \ell_{D2} = \ell_D = \frac{1}{2}(\ell_b + \Delta) \qquad \text{(Equation 3)}$$

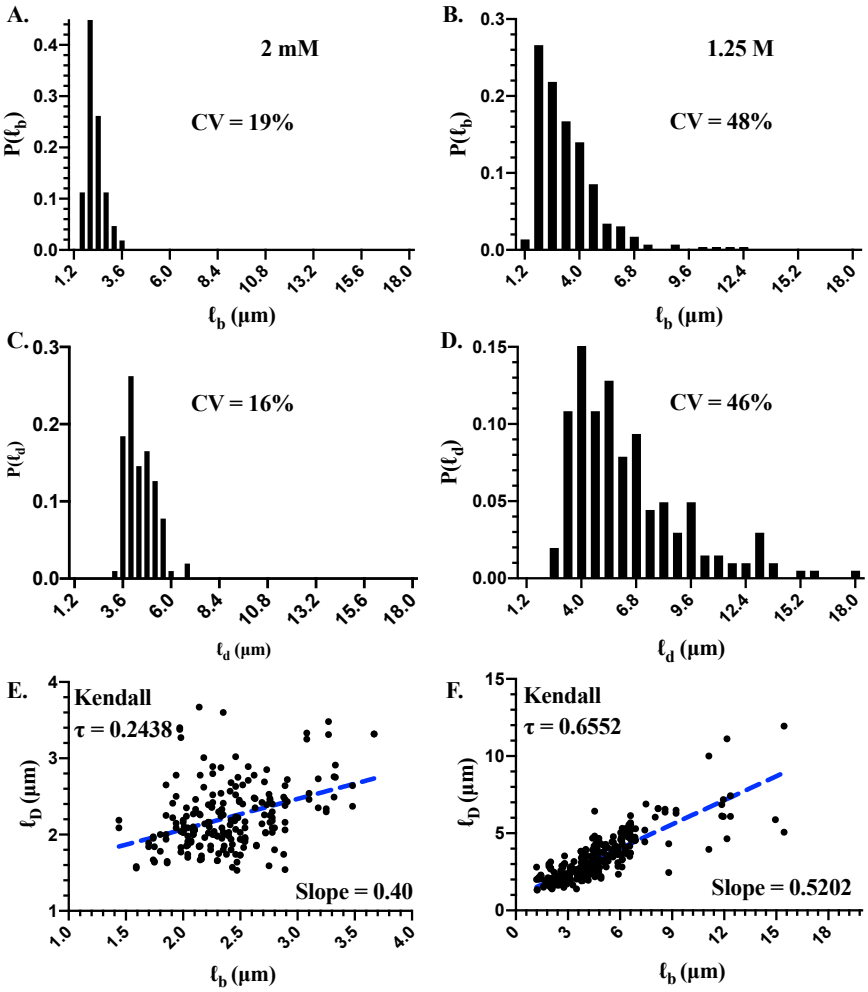


Figure 27: $P(\ell)$ at birth and at division, and the correlation between $\ell_{\rm b}$ and $\ell_{\rm d}$ for the cells cultivated at 2 mM and 1.25 M $MgSO_4$.

For a fixed value of $\ell_b$, the mean lengths of the daughter cells are given by

$$\bar{\ell_D} = \frac{1}{2}\left(\ell_b + \bar{\Delta}\right) \qquad \text{(Equation 4)}$$

Figures 27(E) and 27(F) show the correlation between the length of the daughter cells and the length at birth for the two salt concentrations. In both cases, there is a positive correlation between the lengths of the mother and the daughter cells. The slopes of the linear regression for the control and stressed cells are 0.40 and 0.52, respectively. The Kendall-$\tau$ correlation coefficients for the control (2 mM $MgSO_4$) and the salt stressed cells (1.25 M

$MgSO_4$) are 0.213 and 0.6552, respectively. A slope close to 0.5 in Figs. 27(C) and 27(D) implies that the cells divide symmetrically for all the cells grown in both low and high salt concentrations.

### 4.3.4 Size Extension and Symmetric Cell Division

To find the nature of the distribution of added mass during successive divisions, the probability distributions were constructed as shown in Figs. 28(A) and 28(B). The solid blue lines are Gaussian fits through the experimental points. The width of the distribution was smaller for control cell compared to the cells grown in 1.25 M $MgSO_4$. In order to investigate if there is any correlation between the size extension between successive cell division events and the size of the cell at the birth, the scatter plot $\Delta\ell$ against $\ell_b$ is shown in Figs. 28(C) and 28(D) for the cells grown in 2 mM and 1.25 M $MgSO_4$, respectively. There was no correlation between $\Delta\ell$ and $\ell_b$ for both the salt concentrations as reflected in values of the slope of the linear regression as the values of the Kendall-$\tau$ correlation coefficient were close to zero in both the cases. To look more closely, the symmetry in cell division, the division ratio, $r$, is defined as

$$r = \frac{\ell_D}{\ell_b + \Delta\ell} = \frac{\ell_D}{\ell_d} \qquad \text{(Equation 5)}$$

where $\ell_D$ is the length of either of the daughter cells and $\ell_b + \Delta\ell = \ell_d$ is the total length at the division. In Fig. 28, the length extension, $\Delta\ell$, during successive division events as a function of the length at the birth, $\ell_b$, for the cells grown in (C) 2 mM, and (D) 1.25 M magnesium sulfate is presented. Small values of the slope, as well Kendall's $\tau$ correlation coefficient, suggest negligible correlation between $\ell_b$ and $\Delta\ell$. Figures 28 (E) and 28 (F) are the probability distributions, P($r$), of the division ratio, $r$, for the cells grown in $MgSO_4$ concentrations of 2 mM and 1.25 M, respectively. The solid blue lines are the Gaussian fits to P($r$). For both the salt concentrations, P($r$) is centered at 0.5 with standard deviations 0.021 and 0.027, respectively, suggesting the cells divide symmetrically with a small variability.

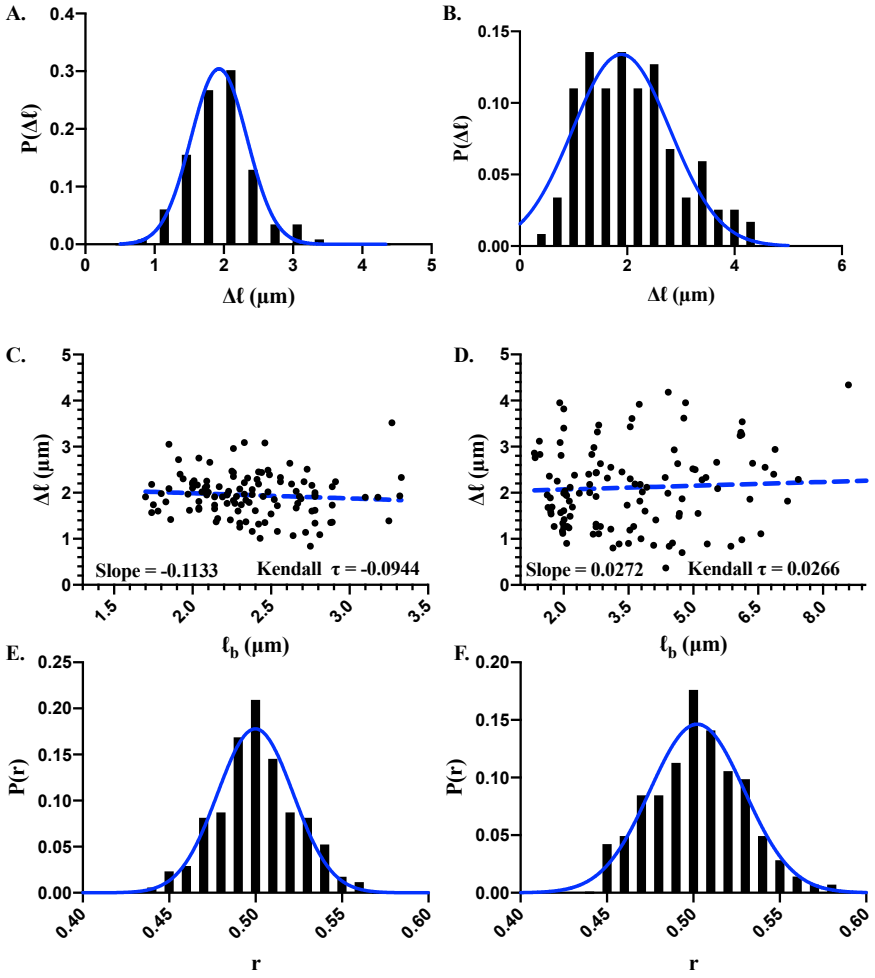


Figure 28: Scatter plots and probability distributions of mass addition and probability distributions of division ratio for the cells grown in control and in high salt media.

While overall no correlation between $\Delta\ell$ and $\ell_b$ was found, next, determining if there is a temporal correlation between the size extension in the same lineage of cells starting with a mother cell was examined. Figures 28(C) and 28(D) are the generation dependent biomass addition for the control and the stressed cells, respectively. The cells add constant mass regardless of the generations in case of the control cells (Figure 28(C)). The mass added has slight negative correlation in case of the stressed cells. The biomass added is slightly smaller for the higher generations compared to the second generation. The cells might have memory of the stress for the first couple of generations. Beyond the fifth generation, the mass

addition is comparable to the control cells. The results further prove that the cells add constant mass for the cell length homeostasis.

Next, the heterogeneity in growth and division of both control and stressed cells was studied by quantifying the initial length dependent mass doubling time and successive division time. Figures 29(A) and 29(B) show the probability distribution of $\tau_d$ and $\tau_{\rm sd}$. Both $\tau_d$ and $\tau_{\rm sd}$ exhibit a broad distribution with variance 1 and 2, respectively. Next, the question of whether is variability in $\tau_d$ and $\tau_{\rm sd}$ depend on the length of the cells was considered. In Figs. 29(C) and 29(D), the mass doubling time (solid black circles), $\tau_d$, and successive division time (solid pink circles), $\tau_{\rm sd}$, as a function of initial length, $\ell_i$, and the length at birth, $\ell_b$, are shown. It is found that $\tau_d$ increases linearly with the initial length of the cells with a slope 7.85, while $\tau_{\rm sd}$ decreases with $\ell_b$. The variability in $\tau_{\rm sd}$ for a given length at birth, $\tau_{\ell_b}$, arises from the variability in $\Delta\ell$, $r$, and the length dependence of the mass doubling time. The variability was considered in all these quantities with the constant mass addition model to test if it can explain the variability observed in the $\ell_b$-dependence of $\tau_{\rm sd}$. For the following analysis, only the length dependence of $\tau_d$ was considered, and the variability in the length dependence of $\tau_d$ was ignored. Since, the distribution of $r$ is very narrow, and the variability in $r$ was also ignored. For an exponentially growing cell with initial length $\ell_0$, the cell divides after a time $\tau_{\rm sd}$ by adding a length $\Delta\ell$ and, hence, $\tau_{\rm sd}$ and $\Delta\ell$ are related by

$$\tau_{\rm sd} = \frac{1}{\lambda}\log\left(1+\frac{\Delta\ell}{\ell_0}\right) \qquad \text{(Equation 6)}$$

where $\lambda = \frac{\log 2}{\tau_d}$ is the growth rate of the cell. The normalized probability distribution $P(\tau_{\rm sd};\ell_0)$ for a given length of cell, $\ell_0$, is given by

$$P(\tau_{\rm sd};\ell_0) = \frac{1}{\sqrt{2\pi}\sigma_{\Delta\ell}}\lambda\ell_0 e^{\lambda\tau_{\rm sd}} e^{-\frac{\left(\ell_0(e^{\lambda\tau_{\rm sd}}-1)-\Delta_0\right)^2}{2\sigma^2_{\Delta\ell}}} \qquad \text{(Equation 7)}$$

where $\Delta_0$ and $\sigma^2_{\Delta\ell}$ are the mean and the variance of $\Delta\ell$, respectively. The mean value,

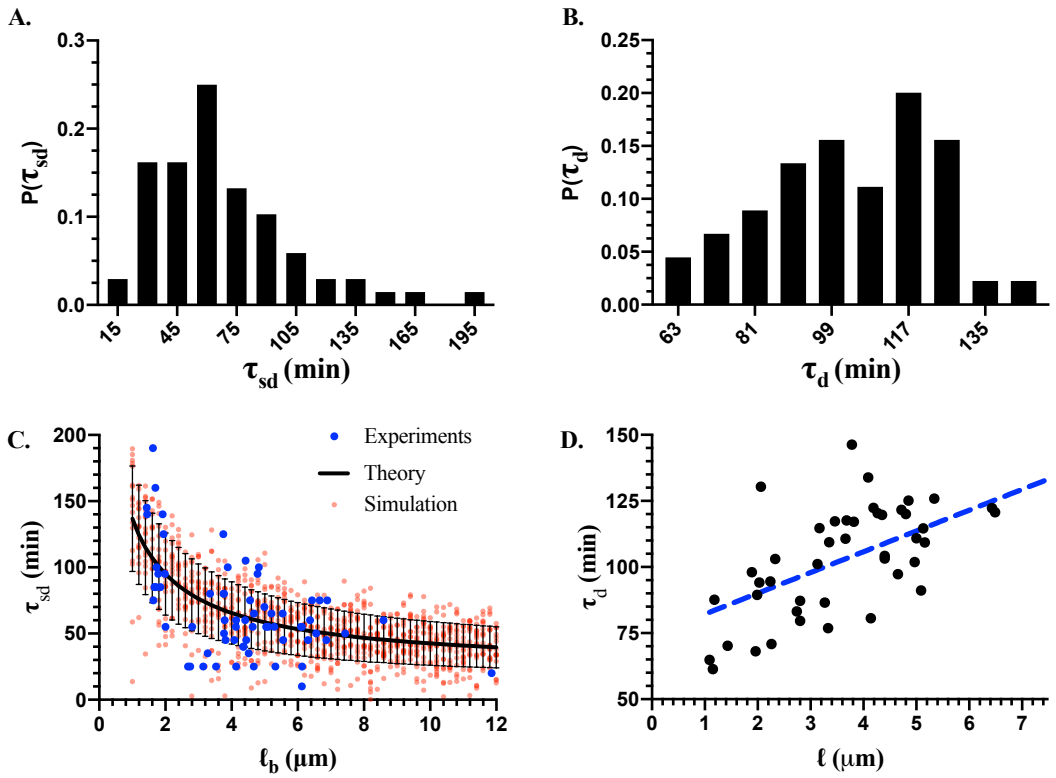


Figure 29: Probability distributions and scatter plot of the mass doubling time, $\tau_d$, as a function of the initial length and length at birth of the cells grown in 1.25 M magnesium sulfate.

$\langle \tau_{\rm sd}(\ell_0) \rangle$, is given by

$$\langle \tau_{\rm sd}(\ell_0) \rangle = \frac{1}{\sqrt{2\pi}\sigma_{\Delta\ell}} \lambda \ell_0 \int_0^\infty \tau_{\rm sd} e^{\lambda \tau_{\rm sd}} e^{-\frac{\left(\ell_0(e^{\lambda\tau_{\rm sd}}-1)-\Delta_0\right)^2}{2\sigma^2_{\Delta\ell}}} d\tau_{\rm sd}, \qquad \text{(Equation 8)}$$

and the second moment, $\langle \tau^2_{\rm sd}(\ell_0) \rangle$, is given by

$$\left\langle \tau^2_{\rm sd}(\ell_0) \right\rangle = \frac{1}{\sqrt{2\pi}\sigma_{\Delta\ell}} \lambda \ell_0 \int_0^\infty \tau^2_{\rm sd} e^{\lambda \tau_{\rm sd}} e^{-\frac{\left(\ell_0(e^{\lambda\tau_{\rm sd}}-1)-\Delta_0\right)^2}{2\sigma^2_{\Delta\ell}}} d\tau_{\rm sd}, \qquad \text{(Equation 9)}$$

The dependence of the above quantities on $\ell_b$ is introduced in $\lambda(\ell_b)$. The integral of the above equation was computed numerically to find the mean and the variance, $\sigma^2_{\tau_{\rm sd}} = \langle \tau^2_{\rm sd}(\ell_0) \rangle - (\langle \tau_{\rm sd}(\ell_0) \rangle)^2$, of $\tau_{\rm sd}$ as a function of $\ell_b$. Figure 29(C) shows the computed values of the mean of $\tau_{\rm sd}$ with the standard deviation as the error bar of the solid black

curve. A stochastic simulations was also performed considering a Gaussian distribution of $\Delta\ell$ with the mean and the variance of $\Delta\ell$ found in experiments (see Fig. 28), and taking the initial length dependence of $\lambda_d(\ell_b)$. The simulation data are presented as solid red circles in Fig. 29(C). The theoretical and simulation data are in a good agreement with the experimental data.

### 4.4 Summary and Discussion

How bacteria maintain a near constant size amidst underlying stochasticity is a longstanding open question. Various models of growth and division have been proposed to explain cell size homeostasis in bacteria. High concentration of $MgSO_4$ leads to heterogeneities in cell length of *Escherichia coli* — a small fraction of cells become smaller than the control cells while a large number of cells become elongated due to a lack of cell division. The dynamics of division of these cells with heterogeneous morphology upon removal of the salt stress were studied. Two key ingredients of the cell division — (i) constant mass addition, and (ii) symmetrical division, are required to explain the dynamics of cell division. Figure 30 shows the gist of the findings. A cell starting with length at birth, $\ell_b$, grew and reached a length, $\ell_d$, by adding a constant mass, $\Delta\ell$, and divided symmetrically into two daughter cells with a small variability in length. Figure 30 is a pictorial representation of the conclusion. Both long and short cells in this study exhibited cell division dynamics in accordance with the adder model, albeit with the added mass with variability. The average lengths at birth as a function of generations for cells with different initial lengths are shown in Fig. 30 (D).

All the cells approach normal length of cells, $\approx 2$ µm, after a few generations. Symbols are the experimental data and the lines are the fit assuming the adder model with symmetric cell division and mass addition with variability. This was true regardless of the morphology of the cells *i.e.* for both short and long (filamentous) cells as depicted in Fig. 30. Furthermore, the mass added, $\Delta\ell$, between successive divisions was uncorrelated with the

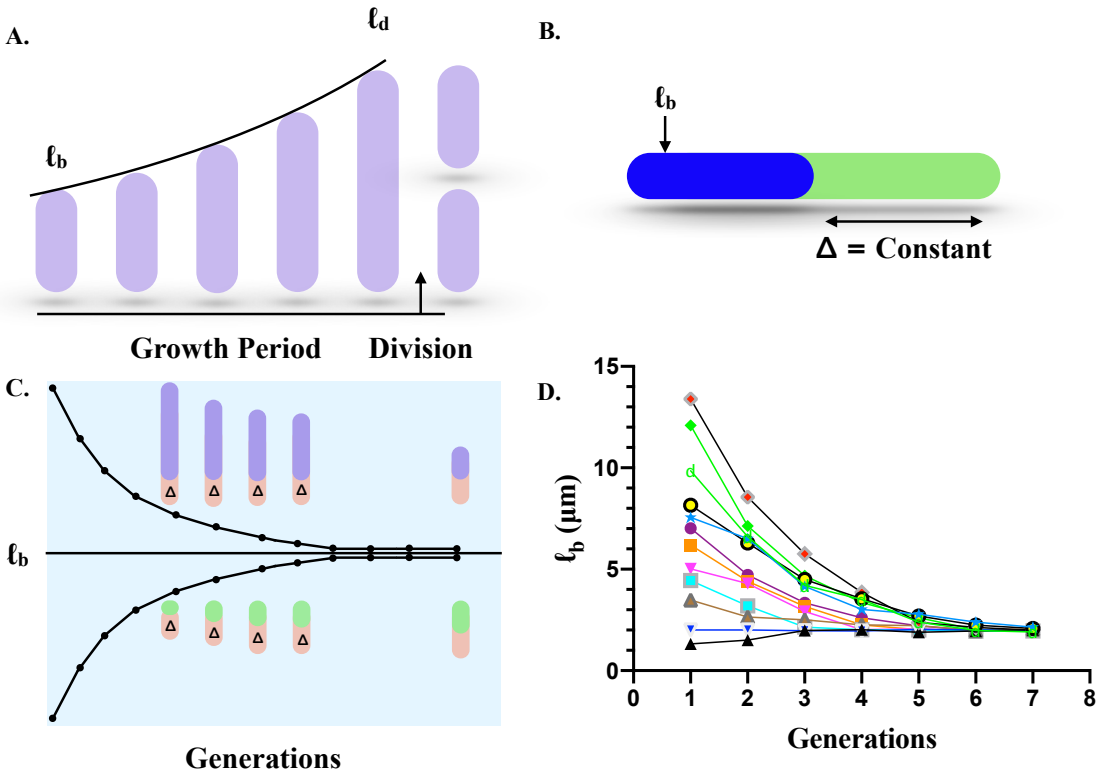


Figure 30: A pictorial depiction of the size control and homeosatsis for bacterial cells grown at 1.25 M $MgSO_4$.

length of the cells at birth. Both short and long cells approached nearly constant size in a few generations. These results are consistent with a class of cell division models, called an adder model [278, 279, 295, 296, 297].

In addition, it was found that the cell doubling time and division time depended on the length of the cells. These experimental results were explained using theory and simulations. While these confirm few earlier studies [278], there are subtle differences between results of this work and prior studies of the cell size homeostasis in bacteria. Specifically, only few studies have considered the dependence of cell doubling time and division time on the length of the cells at birth. This research found that both the cell doubling time and the cell division time are correlated with length of the cells at birth as shown in Fig. 29.

# 5 Temperature Dependence of Multistability of the Lactose Utilization Network of *Escherichia coli*

## 5.1 Introduction

Gene expression in an isogenic population is different due to intrinsic stochasticity present in the translation and transcription process as well as due to extrinsic stochasticity present in repressor proteins [316] and gene expression can be taken as a stochastic process containing both intrinsic and extrinsic noise [316]. The stochasticity in gene expression might lead to different distinct phenotypes. The gene expression of *Escherichia coli* (*E. coli*) is determined by surrounding physicochemical conditions and change in morphology of cells is related to gene expression. To decide the amount of gene expression and turning the gene on or off, bacteria sense the environmental condition around them [317, 318]. The environment dependence of change in gene expression and/or morphology of cells is termed as phenotypic switching.

One of the early studies on phenotypic switching was performed on *Candida albicans* in which the difference on colony morphology of isogenic population was discernible [319]. The color of the colony appeared to be white and opaque and the genotoxic and oxidative stress might have caused cells to change the colony color [320]. Later, several investigations were performed on phenotypic variations of isogenic populations in different bacterial species at different conditions [321, 322, 323, 324, 325]. Deviations in optimal growth conditions of bacteria pose challenges on them. Bacteria switch to new phenotypes under extreme conditions that might be beneficial for the survival strategy [184]. One example of phenotypic switching at a stressed condition is the effect of high pressure on cell length and morphology. At high pressure, bacteria switch to a new phenotype with a fraction of elongated cells [136]. A fraction of bacteria acquire temporary phenotypic switching and survive the stress of antibiotic [326].

*Escherichia coli* has a preference of a particular carbon source over another. In a mixture of glucose and lactose, *E. coli* utilizes glucose in the first growth phase and it

consumes lactose in the second phase of growth shortly after a pause in growth [327]. The duration of these two growth phases can be controlled by changing the proportion of lactose and glucose in the media [328]. The pause in growth is the time required to transcribe the necessary enzymes to digest lactose in bacteria. Jacob and Monod describe conceptually the phenomenon by concluding some genes in bacteria are in an off state and they need a chemical cue before turning on some genes [329]. The structural genes encode together according to the requirement of metabolite and the regulation of such genes required for one or more mechanism of regulation. The repressor proteins fulfill the requirement of regulation mechanism.

The *lac* operon consists of three encoding regions formed by three genes (*lacZYA*) [328]. *lacY* encodes lactose permease, an enzyme involved in lactose uptake; *lacZ* encodes for $\beta$-galactosidase, an enzyme responsible for the cleavage of lactose; and, *lacA* encodes for transacetylase whose function related to lactose digestion is still unknown [330]. However, the dynamics of the *lac* operon is well studied by controllable synthetic gratuitous lactose inducers like isopropyl-$\beta$-D-1-thiogalactopyranoside (IPTG) and methyl-$\beta$-D-thiogalactoside (TMG). In the absence of lactose, the *lac* operon is tightly controlled by *lac* repressor (LacI). When lactose is present, it binds with LacI repressor and allows RNA polymerase to bind with *lac* promoter. Presence of catabolic activator proteins (CAP) increases the binding affinity of RNA polymerase. Cyclic adenosine monophosphate (cAMP) senses the presence of glucose in a media and it does bind with CAP protein and the operon is in an off state. Absence of glucose and presence of lactose turns the gene to an on state and the transcription of the *lac* operon occurs and, by the process of translation, lactose permease and $\beta$-galactosidase are formed. The presence of lactose permease acts as a positive feedback for the process on gene expression giving rise to bistability on the *lac* operon with two distinct phenotypes in an isogenic population [331]. Furthermore, the dynamicity of the growth of bacteria causes diminution of the amount of lactose available for bacteria giving rise to negative feedback on the *lac* operon expression level. This negative feedback weakens

the positive feedback created by lactose polemerase [332]. Synthetic and non-metabolized lactose like IPTG [333, 334] and TMG [335, 336] have been used to induce the *lac* operon which prevents the reduction of the lactose amount in the media.

Three bistable systems in bacteria — (i) the *lac* operon, (ii) the *trp* operon, and (iii) the phase-$\lambda$ switch are well studied [337, 338, 339]. The *lac* operon exhibits bistability due to positive feedback [332] and the *trp* operon exhibits bistability due to negative feedback [340] in the presence of non-metabolized lactose. Bistability in the *lac* operon was first observed by Jacob and Monod over 60 years ago [341]. Novik and Weiner explained the bistability of the *lac* operon for the first time in 1957 [335]. Since then, several studies have been carried out both experimentally [335, 336, 342, 343] and theoretically [332, 337, 344, 345, 346, 347, 348]. Ozbudak et al. in 2004 showed the phase diagram of the *lac* operon bistability at different concentrations of glucose and lactose at 37 °C [336]. Temperature changes the synthesis and degradation rate of biomolecules [349]. How the temperature affects the glucose and lactose metabolism in *E. coli* and the bistable behavior of the *lac* operon remains unknown. In this chapter, the temperature dependence of the phase diagram on the bistability is discussed. Furthermore, the disappearance of bistability at low temperature is explained using the maximum possible range of gene expression.

## 5.2 Materials and Methods

### 5.2.1 Bacterial Strains

Wild-type MG1655 strain of *Escherichia coli* was obtained from coli genetic stock center located at the Yale University (New Haven, CT, USA). A plasmid DNA cloned wild-type MG1655 containing a green fluorescence protein (GFP) gene under the control of the *lac* promoter was obtained from GE Dharmacon (Chicago, IL, USA). The average copy number of the plasmid is reported to be five [350, 351].

### 5.2.2 Cell Culture and Media

For the culture media, 52 g of M9 salt (BD Difco, Franklin Lakes, NJ, USA) was dissolved in one liter of water and autoclaved at 121 °C for 15 minutes. Supplements of 0.4% of glucose (Alfa Aesar, Haverhill, MA, USA), 0.4% succinate (Alfa Aesar, Haverhill, MA, USA), and 0.05% of magnesium sulfate ($MgSO_4.7H_2O$) (Amresco, Framingham, MA, USA) were added in the media. For cells cloned with a plasmid, 50 µg/mL of kanamycin (Amresco, Framingham, MA, USA) was added to the media. The media was then filter sterilized passing through a 2 µm filter (Thermo Scientific, Waltham, MA, USA). The pH of the media was maintained at 7.0. Solid media in Petri dishes containing $\approx 25$ mL were prepared by adding 1.5% agar to the liquid media. The bacterial stock was first inoculated in a solid media and incubated at 37 °C for about 16 hours. A single colony was picked from the petri dish and inoculated in liquid media. The sample was then grown at 37 °C in a shaker incubator shaking at 250 rpm. To obtain a master culture [336], cells were grown to $OD_{600} = 0.6 - 0.8$ and diluted to $OD_{600} \approx 0.001$. The process of cell culture and successive dilution was repeated four times. The master culture was continuously transferred to a new media and maintained at 37 °C for all the experiments. The master culture was diluted with supplements of different levels of TMG and cultivated at different temperatures until the $OD_{600}$ reached one. The culture was then diluted $OD_{600} \approx 0.01$, and the fluorescence intensities were obtained for each cell using a flow cytometer (BD Facsaria Fusion, BD Biosciences, Franklin Lakes, NJ, USA).

### 5.2.3 Data Analysis

The fluorescence intensities of about $100,000$ cells were acquired for each sample by maintaining the same voltage and the same gating parameters for all the experiments. A custom made MATLAB program was used to analyze the flow cytometry data by gating FSC, SSC, and FITC. The post-gated data were then used to create probability distributions.

### 5.2.4 Repression Factor Measurement

The repression factor, $\rho$, is defined as the ratio of fully induced fluorescence intensity of cells to the intensity of non-induced cells [336]

$$\rho = \frac{F_I - F_B}{F_{UI} - F_B} \qquad \text{(Equation 10)}$$

where $F_I$ is the normalized fluorescence intensity of fully induced cells, $F_B$ is the normalized background intensity, and $F_{UI}$ is the normalized fluorescence intensity of the master culture. TMG concentration of 1 mM was used to obtain full induction of cells. The background intensity was measured using wild type (no plasmid cloned) cells in the respective media.

## 5.3 Results

### 5.3.1 Gene Expression of the *lac* Operon

At the end of the experiments, phase contrast and fluorescence images of cells grown at different temperatures with a varying supplement of TMG were acquired. Figures 31(A) and 31(B) are the representative phase contrast and fluorescence images of the bacterial sample, respectively. The expression of cells indicates the *lac* operon is turned on. The plasmid is under the control of the *lac* promoter. The three genes in *lac* operon, *lacZYA*, express together with the GPF fused on the plasmid under the *lac* promoter in the presence of lactose (TMG) in the media. The expression of cells was observed to be all in or nothing. Bacteria did not express at TMG concentrations less than three µM, and beyond it, cells start expressing. The fraction of expressed cells increased with the increase in TMG concentration and all cells were expressed at 30 µM. These results agree with the induction shown in a previous study [336]. With further increase of the TMG concentration, the fluorescence intensity increased and saturated at 100 µM. The saturation on the expression level was observed to be dependent on the temperature. The intensity data for each cell at different temperatures and TMG concentrations were employed to explore the temperature dependence multistability of the lactose utilization network.

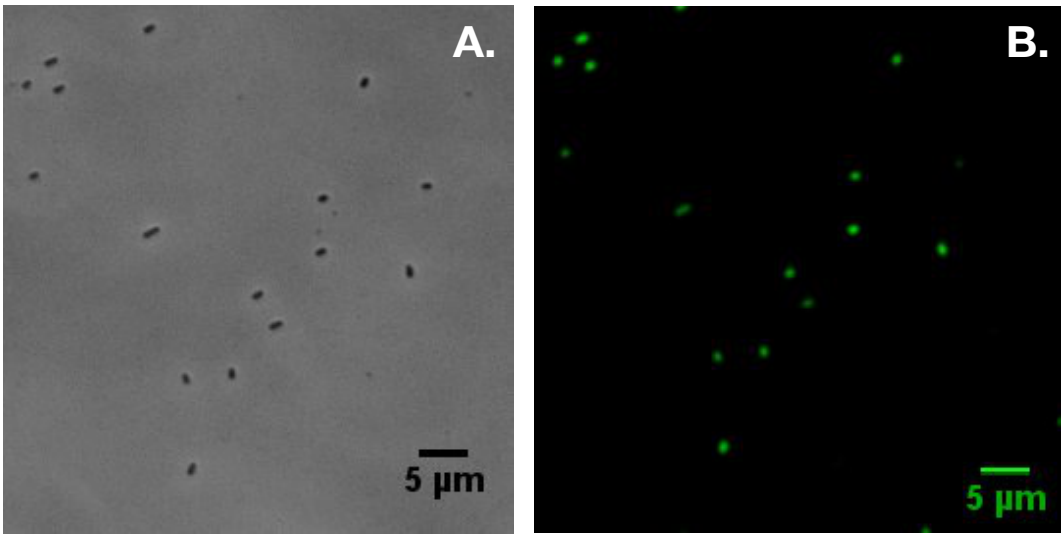


Figure 31: Phase contrast and fluorescence images of bacterial cells cloned with plasmid under the control of the *lac* promoter.

### 5.3.2 Graded and Bistable Response

The fluorescent intensity data obtained from the flow cytometer were gated and the post-gated data were plotted to obtain the probability distribution. Figure 32 represents the probability distribution of the intensities at different levels of TMG at several temperatures. The upper, middle, and lower panels represent the distributions at 25 °C, 37 °C, and 40 °C, respectively. The *lac* operon network exhibited a monostable response at 20 °C, and the peak intensity remained the same regardless of the TMG concentration (data not shown). The lactose utilization network exhibited monostable response when the amount of TMG was $\geq 100$ µM. Bistability arose at 25 °C and persisted for the TMG concentrations between $10 - 30$ µM. The peak of the distribution shifted to higher intensity when the amount of TMG in the media was increased. The network was found to be at a monostable stage at lower TMG concentration. It further expanded to bistable regions at intermediate concentrations and the monostable distribution appeared again at high TMG concentration. The monostable peak at high TMG concentration had overall higher intensity indicating that the production of $\beta$-galactosidase increased with the increase in the amount of lactose

present in the media. Next, the area under the curve was calculated to find the proportion of cells with higher and the lower expression in the *lac* operon.

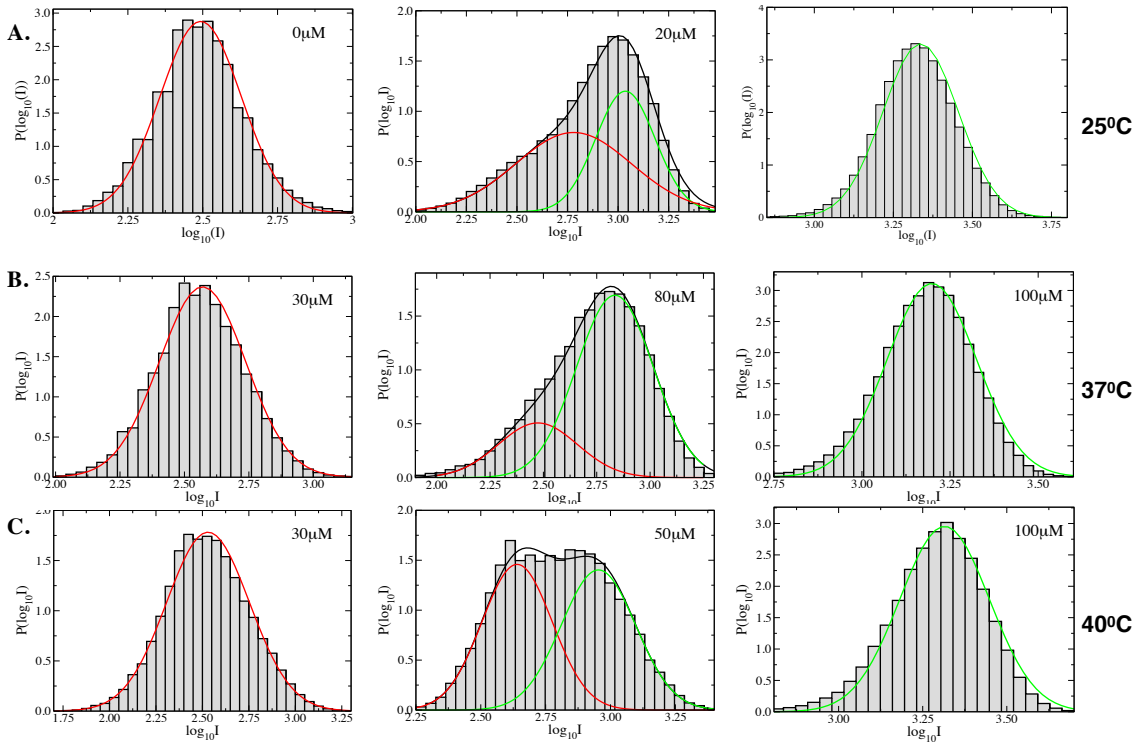


Figure 32: Probability distributions of the intensities of the *lac* activity at different temperatures and TMG concentrations.

### 5.3.3 Determination of Bistability

Figure 33 is the plot of the fractions of the population corresponding to low fluorescence intensity (green) and high fluorescence intensity (red) for four different temperatures (A) 25 °C, (B) 32 °C, (C) 37 °C, and (D) 40 °C. $f_L$ and $f_H$ are the areas obtained from the Gaussian curves with the peak at lower intensity (red Gaussian curve in Fig. 32) and the peak with the higher intensity (green Gaussian curve in Fig. 32), respectively. The sum of $f_L$ and $f_H$ is unity. At low TMG levels, all the bacterial cells follow the low fluorescent intensity distribution, and at high TMG concentrations, all the bacterial cells follow the high fluorescent intensity distribution. At both low and high regions, the *lac* operon has graded behavior and at the intermediate concentration the operon shows hysteretic behavior.

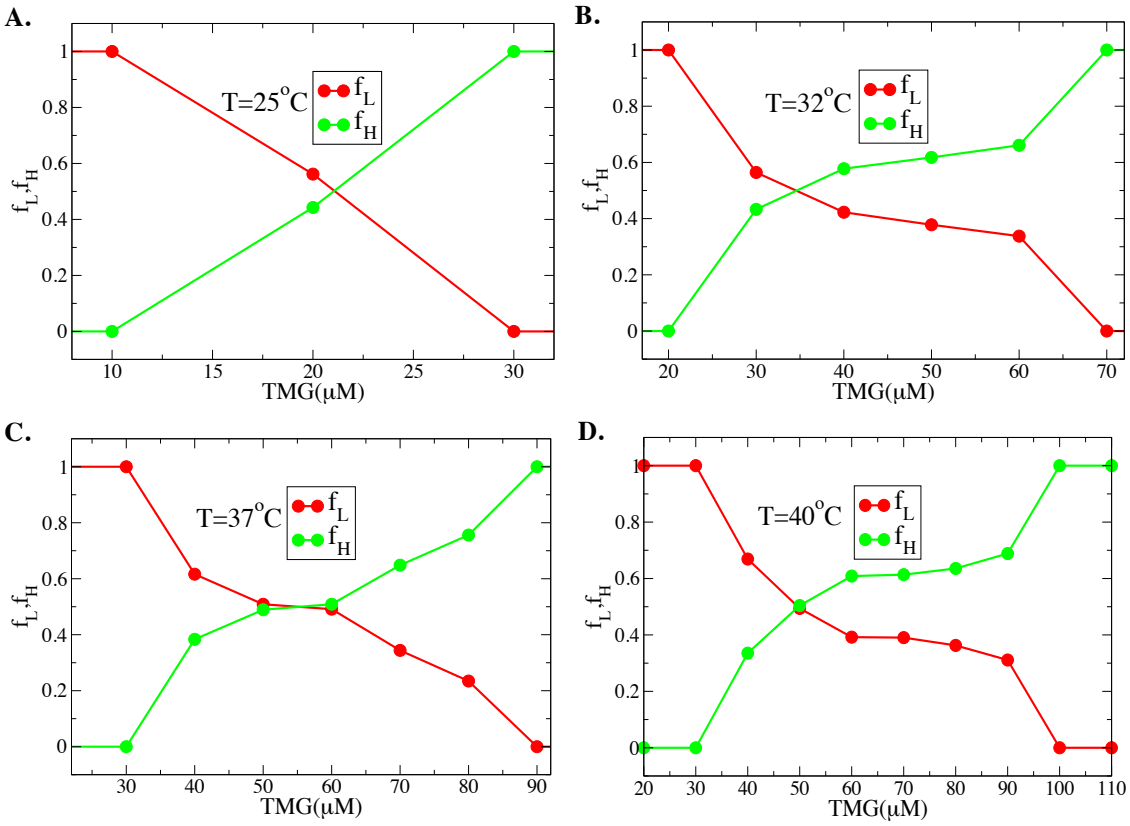


Figure 33: Fractions of the populations having the peaks at a low and a high intensity at different TMG concentrations.

### 5.3.4 Temperature and TMG Concentration Dependence Phase Diagram

To understand the effect of temperature and TMG concentration on bistability, a phase diagram was constructed using the parameters obtained from Figs. 32. and 33. Figure 34 is the temperature dependent phase diagram showing bistable and graded regions on the TMG space. The gray region (between the red and the blue lines) represents the hysteretic response and the white region represents the graded response of the *lac* operon. The region below the red curve represents the monostable region, and the *lac* operon was uninduced, whereas, the region above the blue curve the *lac* operon was induced and monostable. The black circles are extracted from the intersection of $f_L$ and $f_H$ in Fig. 33. The black line represents the temperature dependence of the TMG concentration at which the area of $f_L$ and $f_H$ is equal. In other words, along the black line, the fraction of the population

metabolizing glucose and lactose is equal.

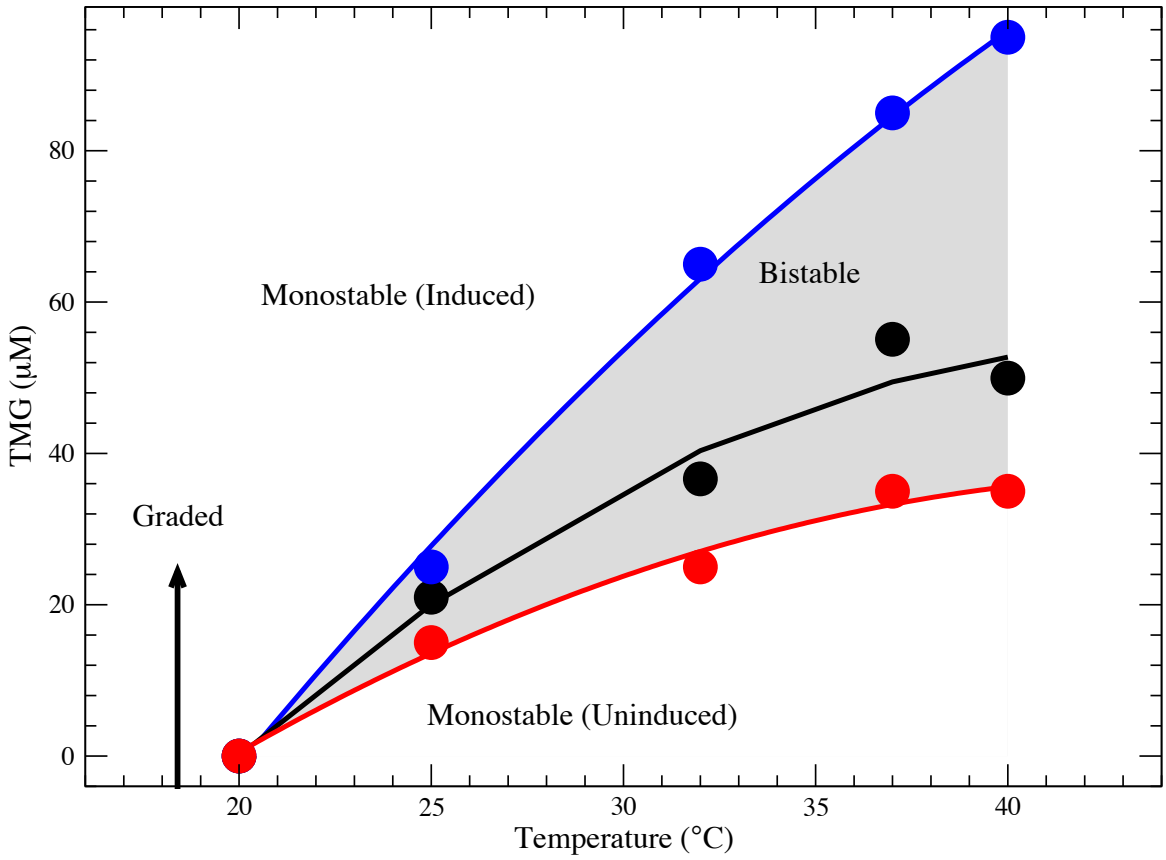


Figure 34: Temperature and lactose concentration dependent phase diagram of *lac* activity.

In the region between the red and black lines, bacteria prefer to metabolize glucose, and the population of bacteria metabolizing glucose is higher than the population metabolizing lactose. Similarly, in the region between the back and blue lines, bacteria prefer to metabolize lactose, and the population of bacteria metabolizing lactose is higher. These results suggest that bacteria switch from a glucose preferring population to a lactose preferring population with increasing lactose availability at high temperature. The phenotypic switching was obtained by varying the amount of lactose and temperature for a constant amount of glucose supplemented in the media. Furthermore, the results are helpful for the construction of the temperature dependence biological switches. Temperature is a crucial factor in determining the bistability of the network.

### 5.3.5 Repression Factor and the Bistability

The lactose utilization network being monostable at temperatures less than 20 °C, regardless of the lactose concentration in a media, suggests that the entire bacterial population utilizes glucose. At TMG concentrations greater than 10 µM, the *lac* operon was expressed, and the level of expression remained the same when increasing the TMG concentration. The saturated expression at 20 °C was ten-fold smaller than the saturated expression at 37 °C. The bistability on the *lac* operon did not appear at 20 °C. When the temperature was 25 °C, the bistable region appeared and it was narrow. The bistable region increased monotonically with the increase in temperature. The result signifies that the lactose metabolism process at 20 °C is slower and smaller than the lactose metabolism at higher temperatures. The bistable region increases with increasing temperature. The lactose and glucose metabolism in *E. coli* depends on the temperature.

Figure 35 is the repression factor, the ratio of maximum expression to a basal level expression, at different temperatures. The repression factor ($\rho$) significantly decreased with a decrease in temperature. It was $\approx$ 20 at 37 °C and $\approx$ 8 at 20 °C. The plot of repression factor and temperature follows a sigmoidal curve. A temperature derivative of the curve was taken to determine the peak of the curve. The peak point on the sigmoidal curve was found to be where temperature was 23.3 °C and the repression factor was 10.3. Ozbudak et al. in 2004 showed that a repression factor of nine or greater is necessary for the system to exhibit a bistable behavior [336]. The results show a small variation of the repression factor with past theoretical results. The experiments and the repression factor measurement agree with the experimental results obtained in Figure 32.

## 5.4 Summary and Discussion

Glucose and lactose are monosaccharide and disaccharide sugars, respectively. Lactose metabolism takes one more step to break it into two monosaccharides. Due to fewer steps and the efficiency in digestion, bacteria prefer glucose metabolism over lactose metabolism.

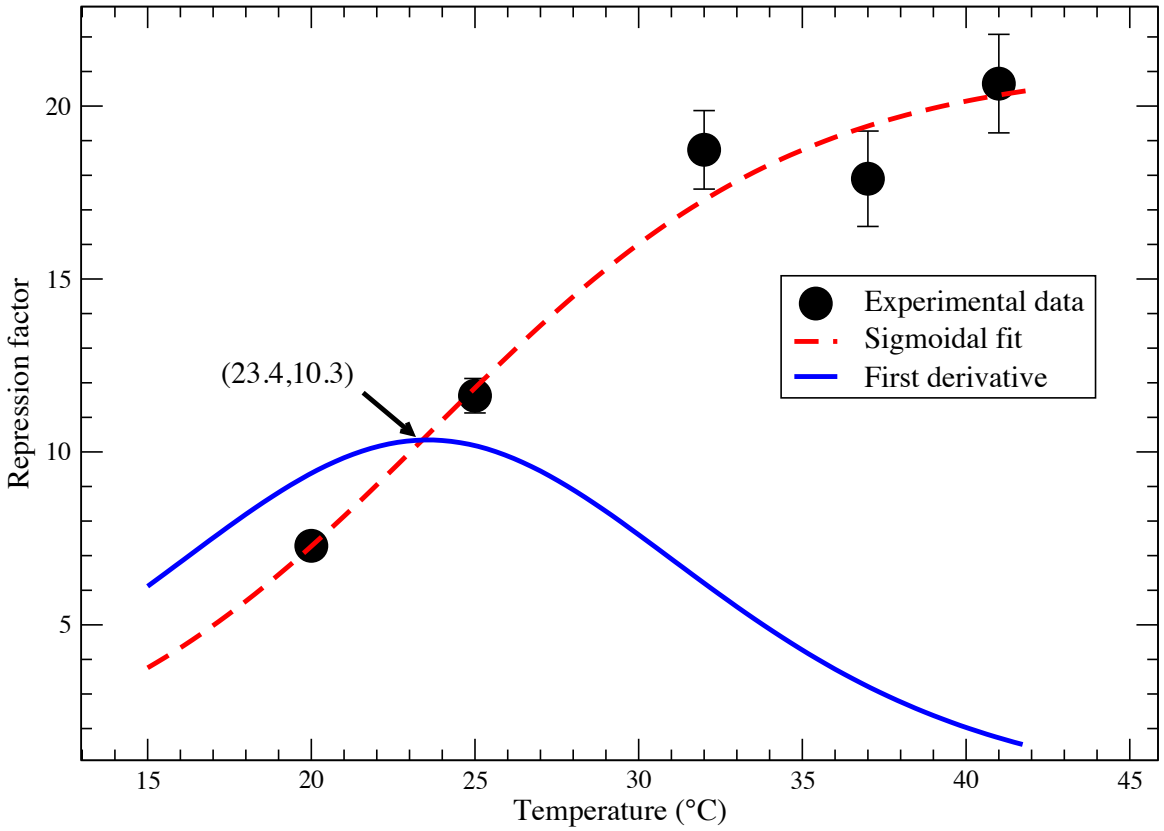


Figure 35: Repression factor, $\rho$, at different temperatures.

In a mixture of two sugars, *E. coli* metabolizes both sugars with a maximum efficiency [352]. Lactose metabolism is active when the genes related to uptake and digestion of lactose are turned on. The *lac* operon becomes functional when the media contains a high amount of lactose and an absence of glucose. Bistability of the *lac* operon in a mixture of glucose and lactose is known at optimal growth temperature (OGT) of *E. coli* [336, 353]. Temperature alters several biological processes including the transcriptional activity of RNA polymerase [354, 355], mRNA synthesis rate [356], and metabolism and biomass production rate [349]. The effect of temperature on the bistability is still elusive. In this chapter, the effect of temperature on bistability of the *lac* operon was studied.

At high temperature, the region of bistability on the *lac* operon in glucose and lactose concentration space is well studied [336]. This chapter investigates the regions of bistability at high and low temperatures compared to OGT of *E. coli*. Specifically, the dynamics of

lactose utilization network at the temperature range of $20 - 40$ °C was studied. The bistable region defined by temperature and lactose concentration decreases with the decrease in temperature, and at 23.4 °C, the bistable behavior disappears irrespective of lactose concentration. The repression factor, the ratio of maximum to basal level promoter activity, dictates the bistable regions. The system is bistable when the repression factor, $\rho$, is greater than 10.3. The repression factor decreases with the temperature and at 23.4 °C, the measured repression factor was 10.3 (Figure 35). The results are in close agreement with a theoretical calculation of repression factor [336].

The study of the *lac* operon bistability at different temperature transcends the operon system. The alternating metabolisms are present outside of the *lac* operon in the genetic system of different species. Glucose or tryptophan metabolism in *E. coli* [357], glucose + galactose in *Saccharomyces cerevisiae* [358], and nucleotide metabolism or polymer synthesis in *Pseudomonas fluorescens* [359] have similar coexisting phenotypes with two types of metabolism. The metabolic networks in other species, where the transport and metabolism are coupled in a gene giving rise to positive or negative feedback, should be considered. A complete understanding of *lac* operon system unveils the understanding of several genes present with similar architecture. The studies performed here are important to elucidate the temperature dependent biological switches. The study investigated the effect of bistability as a function of temperature and lactose concentration. The temperature related dynamics on the stability of the *lac* operon in concentrations of varying mixtures of lactose and glucose is still unknown and will be the subject of a future study.

# 6 Conclusion

## 6.1 Phenotypic Switching at Temporal Oscillation at High Pressures

High pressure is a stress for mesophyllic bacterium, *E. coli*, that inhibits growth and cell division resulting in an elongated cell. The cells at normal morphology switch stochastically to high pressure morphology on the application of high pressure and switch back to the normal morphology when the applied pressure is removed. The experimental results of phenotypic switching can be explained by a two state model. The rate at which cells switch from one state to another define the morphology and the distribution of the cell length. The study did not provide evidence of phenotypic memory for the time period of pressure applied in this study.

## 6.2 Dynamics of Cell Growth, Division, Death, and Phenotypic Switching in an Elevated Salt Concentration

*Escherichia coli* grow at low salt concentrations optimally. Increase in the salt concentration in the media pose several changes in cellular response. The growth rate decreases with an elevated salt concentrations, and the cells do not grow at concentration $\geq$ 2.07 M $MgSO_4$. The cell length decreases at high salt concentrations (except 1.25 M) due to plasmolysis. The plasmolysis increases with the strength of osmotic stress and it is stronger at the poles of the cells. Cells exhibit maximum heterogeinity at 1.25 M salt with the population containing short, average, and filamentous cells. The expression of *aqpZ*, aquaporin channel, and *cysP*, thiosulfate binding protein precursor increases at high salt condition.

## 6.3 Constant Mass Addition and Symmetric Cell Division Drive Size Homeostasis in Filamentous Cells Obtained at High Concentration of Magnesium Sulfate

Cell length is a fundamental characteristic of the living organism. The control over the growth and the length is necessary for the optimal functionality. The heterogeneous

population at high salt becomes a homogeneous population upon removal of high salt stress. For cells grown both in control and high salt condition, the added mass is constant with a variability. The cells divide from the middle with some uncertainty. Longer cells grow slower than short cells and take a longer time to divide.

## 6.4 Temperature Dependence of the Multistability of the Lactose Utilization Network of *Escherichia coli*

Lactose utilization network exhibits bistability. The bistability is temperature sensitive. At low temperatures, the bistable behavior of *lac* operon disappears. With increasing temperature, the range of bistability increases with an increase in TMG, a synthetic lactose. One of the measurements of the protein synthesis is a repression factor which decreases with the decrease in temperature. Below the repression factor of 10.3, the bistability disappears and the corresponding temperature is found to be 22.5 °C.

# 7 Future Work

This study shows that *Escherichia coli*, a mesophyllic bacterium, can tolerate high hydrostatic pressure and high salt stresses. There are several harsh conditions on the Earth like highly acidic rivers, cold and freezing environments, hypersaline lakes, and arid places, where extremophiles can live and grow optimally. *Escherichia coli* does not grow optimally in these environmental conditions. Since mixed environmental conditions are prevalent in nature, the study of bacterial responses at the such environments is highly important to uncover the adaptational mechanisms and the possibility of existence of life on extraterrestrial bodies.

This work discusses cell division of bacteria at different stresses. Despite several studies, the fundamental rule of cell division is still elusive. The study of cell division at stresses other than those studied here might help to find the fundamental rule of cell division in bacteria and higher organisms.

In this dissertation, the short term stress responses and reversibility of bacterial cells at high hydrostatic pressure and at high salinity were discussed. It would be good to investigate the phenotypic and genetic response of *E. coli* at continuous stresses for a long time. The gene expression study of several genes is necessary to understand the genetic pathway and to have a better picture of response of bacteria to a stress.

## References


[1] Stanley L Miller and Antonio Lazcano. The origin of life—did it occur at high temperatures? *Journal of Molecular Evolution*, 41(6):689–692, 1995.

[2] Matthew Levy and Stanley L Miller. The stability of the RNA bases: implications for the origin of life. *Proceedings of the National Academy of Sciences*, 95(14):7933–7938, 1998.

[3] Norman R Pace. Origin of life-facing up to the physical setting. *Cell*, 65(4):531–533, 1991.

[4] Isabelle Daniel, Philippe Oger, and Roland Winter. Origins of life and biochemistry under high-pressure conditions. *Chemical Society Reviews*, 35(10):858–875, 2006.

[5] Robert M Hazen, Nabil Boctor, Jay A Brandes, George D Cody, Russell J Hemley, Anurag Sharma, and Hatten S Yoder Jr. High pressure and the origin of life. *Journal of Physics: Condensed Matter*, 14(44):11489, 2002.

[6] James H Cleaves and John H Chalmers. Extremophiles may be irrelevant to the origin of life. *Astrobiology*, 4(1):1–9, 2004.

[7] Yinon M Bar-On, Rob Phillips, and Ron Milo. The biomass distribution on earth. *Proceedings of the National Academy of Sciences*, 115(25):6506–6511, 2018.

[8] Philip Hugenholtz, Christian Pitulle, Karen L Hershberger, and Norman R Pace. Novel division level bacterial diversity in a Yellowstone hot spring. *Journal of Bacteriology*, 180(2):366–376, 1998.

[9] Barrie D Johnson, Naoko Okibe, and Francisco F Roberto. Novel thermo-acidophilic bacteria isolated from geothermal sites in Yellowstone National Park: physiological and phylogenetic characteristics. *Archives of Microbiology*, 180(1):60–68, 2003.

[10] Zazil D Alvarado-Cuevas, Angel M L'opez-Hidalgo, Leandro G Ordoñez, Ed'en Oceguera-Contreras, Jos'e T Ornelas-Salas, and Antonio De Le'on-Rodr'ıguez. Biohydrogen production using psychrophilic bacteria isolated from Antarctica. *International Journal of Hydrogen Energy*, 40(24):7586–7592, 2015.

[11] Anna-Louise Reysenbach, Krista Longnecker, and Julie Kirshtein. Novel bacterial and archaeal lineages from an in situ growth chamber deployed at a mid-atlantic ridge hydrothermal vent. *Appl. Environ. Microbiol.*, 66(9):3798–3806, 2000.

[12] James K Fredrickson and Tullis C Onstott. Microbes deep inside the Earth. *Scientific American*, 275(4):68–73, 1996.

[13] John A Baross and Jody W Deming. Growth of "black smoker" bacteria at temperatures of at least 250 °C. *Nature*, 303(5916):423, 1983.

[14] Birgit Sattler, Hans Puxbaum, and Roland Psenner. Bacterial growth in supercooled cloud droplets. *Geophysical Research Letters*, 28(2):239–242, 2001.

[15] Muriel Joly, El'eonore Attard, Martine Sancelme, Laurent Deguillaume, Caroline Guilbaud, Cindy E Morris, Pierre Amato, and Anne-Marie Delort. Ice nucleation activity of bacteria isolated from cloud water. *Atmospheric Environment*, 70:392–400, 2013.

[16] Koki Horikoshi, Garabed Antranikian, Alan T Bull, Frank T Robb, and Karl O Stetter. *Extremophiles handbook*. Springer Science & Business Media, 2010.

[17] Ricardo Cavicchioli. Extremophiles and the search for extraterrestrial life. *Astrobiology*, 2(3):281–292, 2002.

[18] Claude E Zobell and Richard Y Morita. Barophilic bacteria in some deep sea sediments. *Journal of Bacteriology*, 73(4):563, 1957.

[19] Douglas Bartlett, Miriam Wright, Aristides A Yayanos, and Michael Silverman. Isolation of a gene regulated by hydrostatic pressure in a deep-sea bacterium. *Nature*, 342(6249):572, 1989.

[20] Chiaki Kato, Lina Li, Yuichi Nogi, Yuka Nakamura, Jin Tamaoka, and Koki Horikoshi. Extremely barophilic bacteria isolated from the Mariana Trench, Challenger Deep, at a depth of 11,000 meters. *Appl. Environ. Microbiol.*, 64(4):1510–1513, 1998.

[21] Yuichi Nogi and Chiaki Kato. Taxonomic studies of extremely barophilic bacteria isolated from the Mariana Trench and description of *Moritella yayanosii sp. nov.*, a new barophilic bacterial isolate. *Extremophiles*, 3(1):71–77, 1999.

[22] Hideto Takami, Akira Inoue, Fumie Fuji, and Koki Horikoshi. Microbial flora in the deepest sea mud of the Mariana Trench. *FEMS Microbiology Letters*, 152(2):279–285, 1997.

[23] Sjöfn Sigurg'ıslad'ottir, Malta Konr'aòsd'ottir, 'Asbjörn J'onsson, Jakob K Kristj'ansson, and Einar Matthiasson. Lipase activity of thermophilic bacteria from Icelandic hot springs. *Biotechnology Letters*, 15(4):361–366, 1993.

[24] Robert Folk. Interaction between bacteria, nannobacteria, and mineral precipitation in hot springs of central Italy. *G'eographie Physique et Quaternaire*, 48(3):233–246, 1994.

[25] Guus Roeselers, Tracy B Norris, Richard W Castenholz, Søren Rysgaard, Ronnie N Glud, Michael Kühl, and Gerard Muyzer. Diversity of phototrophic bacteria in microbial mats from arctic hot springs (Greenland). *Environmental Microbiology*, 9(1):26–38, 2007.

[26] Thomas M Wahlund, Carl R Woese, Richard W Castenholz, and Michael T Madigan. A thermophilic green sulfur bacterium from New Zealand hot springs, *Chlorobium tepidum sp. nov. Archives of Microbiology*, 156(2):81–90, 1991.

[27] Ahmet Adiguzel, Hakan Ozkan, Ozlem Baris, Kadriye Inan, Medine Gulluce, and Fikrettin Sahin. Identification and characterization of thermophilic bacteria isolated from hot springs in Turkey. *Journal of Microbiological Methods*, 79(3):321–328, 2009.

[28] Christopher T Lefevre, Fernanda Abreu, Marian L Schmidt, Ulysses Lins, Richard B Frankel, Brian P Hedlund, and Dennis A Bazylinski. Moderately thermophilic magnetotactic bacteria from hot springs in Nevada. *Appl. Environ. Microbiol.*, 76(11):3740–3743, 2010.

[29] Roald Hoffmann. Marginalia: Thermophiles in Kamchatka. *American Scientist*, 89(1):20–23, 2001.

[30] Andrew A Tronin, Pier F Biagi, Oleg A Molchanov, Yu M Khatkevich, and Evgeniy I Gordeev. Temperature variations related to earthquakes from simultaneous observation at the ground stations and by satellites in Kamchatka area. *Physics and Chemistry of the Earth, Parts A/B/C*, 29(4-9):501–506, 2004.

[31] Svetlana B Bortnikova, Gregory M Gavrilenko, Ye P Bessonova, and Alexander S Lapukhov. The hydrogeochemistry of thermal springs on Mutnovskii Volcano, southern Kamchatka. *Journal of Volcanology and Seismology*, 3(6):388–404, 2009.

[32] Ken Takai, Kentaro Nakamura, Tomohiro Toki, Urumu Tsunogai, Masayuki Miyazaki, Junichi Miyazaki, Hisako Hirayama, Satoshi Nakagawa, Takuro Nunoura, and Koki Horikoshi. Cell proliferation at 122 °C and isotopically heavy $CH_4$ production by a hyperthermophilic methanogen under high-pressure cultivation. *Proceedings of the National Academy of Sciences*, 105(31):10949–10954, 2008.

[33] Richard W Castenholz and Ferran Garcia-Pichel. Cyanobacterial responses to uv radiation. In *Ecology of Cyanobacteria II*, pages 481–499. Springer, 2012.

[34] Linda L Jahnke, Tsegereda Embaye, Janet Hope, Kendra A Turk, Mark V Zuilen, David J Marais, Jack D Farmer, and Roger E Summons. Lipid biomarker and carbon isotopic signatures for stromatolite-forming, microbial mat communities and phormidium cultures from Yellowstone National Park. *Geobiology*, 2(1):31–47, 2004.

[35] Hiroki Hirabayashi, Takasada Ishii, Shinichi Takaichi, Kazuhito Inoue, and Kaku Uehara. The role of the carotenoids in the photoadaptation of the brown-colored sulfur bacterium chlorobium phaerobacteroides. *Photochemistry and Photobiology*, 79(3):280–285, 2004.

[36] Thomas D Brock. Life at high temperatures. *Science*, 230(4722):132–138, 1985.

[37] Beverly K Pierson and Richard W Castenholz. A phototrophic gliding filamentous bacterium of hot springs, chloroflexus aurantiacus, gen. and sp. nov. *Archives of Microbiology*, 100(1):5–24, 1974.

[38] Roger Y Stanier and Germaine Cohen-Bazire. Phototrophic prokaryotes: the cyanobacteria. *Annual Review of Microbiology*, 31(1):225–274, 1977.

[39] Kathy B Sheehan and Brett L Dicks. *Seen and unseen: discovering the microbes of Yellowstone*. Globe Pequot, $1^st$ edition, 2005.

[40] Chester A Darling and Paul A Siple. Bacteria of Antarctica. *Journal of Bacteriology*, 42(1):83, 1941.

[41] Robert P Straka and Jeffery L Stokes. Psychrophilic bacteria from Antarctica. *Journal of Bacteriology*, 80(5):622, 1960.

[42] Jemma L Wadham, Sandra Arndt, Slawek Tulaczyk, Marek Stibal, Martyn Tranter, Jon Telling, Grzegorz P Lis, Melissa AE Lawson, Andy Ridgwell, Ashley Dubnick, Martin J Sharp, Alexandre M Anesio, and Catriona EH Butler. Potential methane reservoirs beneath Antarctica. *Nature*, 488(7413):633, 2012.

[43] Hilary A Dugan, Peter T Doran, Slawek Tulaczyk, Jill A Mikucki, Steven A Arcone, Esben Auken, Cyril Schamper, and Ross A Virginia. Subsurface imaging reveals a confined aquifer beneath an ice-sealed Antarctic lake. *Geophysical Research Letters*, 42(1):96–103, 2015.

[44] Owen F Rowe, Javier S'anchez-España, Kevin B Hallberg, and Barrie D Johnson. Microbial communities and geochemical dynamics in an extremely acidic, metal-rich stream at an abandoned sulfide mine (Huelva, Spain) underpinned by two functional primary production systems. *Environmental Microbiology*, 9(7):1761–1771, 2007.

[45] Barrie D Johnson and Kevin B Hallberg. Carbon, iron and sulfur metabolism in acidophilic micro-organisms. *Advances in Microbial Physiology*, 54:201–255, 2008.

[46] Craig Baker-Austin and Mark Dopson. Life in acid: pH homeostasis in acidophiles. *Trends in Microbiology*, 15(4):165–171, 2007.

[47] Irene S'anchez-Andrea, Nuria Rodr'ıguez, Ricardo Amils, and Jos'e Luis Sanz. Microbial diversity in anaerobic sediments at rio tinto, a naturally acidic environment with a high heavy metal content. *Appl. Environ. Microbiol.*, 77(17):6085–6093, 2011.

[48] Elena V Pikuta, Richard B Hoover, and Jane Tang. Microbial extremophiles at the limits of life. *Critical Reviews in Microbiology*, 33(3):183–209, 2007.

[49] Donn J Kushner. Lysis and dissolution of cells and envelopes of an extremely halophilic bacterium. *Journal of Bacteriology*, 87(5):1147–1156, 1964.

[50] Aharon Oren. Diversity of halophilic microorganisms: environments, phylogeny, physiology, and applications. *Journal of Industrial Microbiology and Biotechnology*, 28(1):56–63, 2002.

[51] Arlette Danon and Walther Stoeckenius. Photophosphorylation in halobacterium halobium. *Proceedings of the National Academy of Sciences*, 71(4):1234–1238, 1974.

[52] Beth N Orcutt, Jason B Sylvan, Nina J Knab, and Katrina J Edwards. Microbial ecology of the dark ocean above, at, and below the seafloor. *Microbiol. Mol. Biol. Rev.*, 75(2):361–422, 2011.

[53] Anna-Louise Reysenbach, Amy B Banta, David R Boone, Stephen C Cary, and George W Luther. Biogeochemistry: microbial essentials at hydrothermal vents. *Nature*, 404(6780):835, 2000.

[54] Kenneth S Johnson, James J Childress, Robert R Hessler, Carole M Sakamoto-Arnold, and Carl L Beehler. Chemical and biological interactions in the rose garden hydrothermal vent field, galapagos spreading center. *Deep Sea Research Part A. Oceanographic Research Papers*, 35(10-11):1723–1744, 1988.

[55] Karen L Von Damm and James L Bischoff. Chemistry of hydrothermal solutions from the southern Juan de Fuca Ridge. *Journal of Geophysical Research: Solid Earth*, 92(B11):11334–11346, 1987.

[56] Daniel S Scheirer, Timothy M Shank, and Daniel J Fornari. Temperature variations at diffuse and focused flow hydrothermal vent sites along the northern East Pacific Rise. *Geochemistry, Geophysics, Geosystems*, 7(3), 2006.

[57] Gerard Muyzer and Alfons JM Stams. The ecology and biotechnology of sulphate-reducing bacteria. *Nature Reviews Microbiology*, 6(6):441, 2008.

[58] Bo B Jørgensen, Mai F Isaksen, and Holger W Jannasch. Bacterial sulfate reduction above 100 °C in deep-sea hydrothermal vent sediments. *Science*, 258(5089):1756–1757, 1992.

[59] Bo B Jørgensen. Mineralization of organic matter in the sea bed? The role of sulphate reduction. *Nature*, 296(5858):643, 1982.

[60] Huiluo Cao, Yong Wang, On O Lee, Xiang Zeng, Zongze Shao, and Pei-Yuan Qian. Microbial sulfur cycle in two hydrothermal chimneys on the Southwest Indian Ridge. *MBio*, 5(1):e00980–13, 2014.

[61] Dean G Ellis, Richard W Bizzoco, and Scott T Kelley. Halophilic archaea determined from geothermal steam vent aerosols. *Environmental Microbiology*, 10(6):1582–1590, 2008.

[62] Stuart P Donachie, Shaobin Hou, Todd S Gregory, Alexander Malahoff, and Maqsudul Alam. *Idiomarina loihiensis sp. nov.*, a halophilic $\gamma$-proteobacterium from the Lō'ihi submarine volcano, Hawai'i. *International Journal of Systematic and Evolutionary Microbiology*, 53(6):1873–1879, 2003.

[63] Jonathan Z Kaye, Carmen M Marquez, Antonio Ventosa, and John A Baross. *Halomonas neptunia sp. nov.*, *Halomonas sulfidaeris sp. nov.*, *Halomonas axialensis sp. nov.* and *Halomonas hydrothermalis sp. nov.*: halophilic bacteria isolated from deep-sea hydrothermal-vent environments. *International Journal of Systematic and Evolutionary Microbiology*, 54(2):499–511, 2004.

[64] Jim T Enright, William A Newman, Robert R Hessler, and John A McGowan. Deep-ocean hydrothermal vent communities. *Nature*, 289(5795):219, 1981.

[65] Monika Bright, Julia Klose, and Andrea D Nussbaumer. Giant tubeworms. *Current Biology*, 23(6):R224–R225, 2013.

[66] Julie C Robidart, Shellie R Bench, Robert A Feldman, Alexey Novoradovsky, Sheila B Podell, Terry Gaasterland, Eric E Allen, and Horst Felbeck. Metabolic versatility of the *Riftia pachyptila* endosymbiont revealed through metagenomics. *Environmental Microbiology*, 10(3):727–737, 2008.

[67] Colleen M Cavanaugh, Stephen L Gardiner, Meredith L Jones, Holger W Jannasch, and John B Waterbury. Prokaryotic cells in the hydrothermal vent tube worm *Riftia pachyptila* jones: possible chemoautotrophic symbionts. *Science*, 213(4505):340–342, 1981.

[68] Daniel L Distel, Henri K-W Lee, and Colleen M Cavanaugh. Intracellular coexistence of methano-and thioautotrophic bacteria in a hydrothermal vent mussel. *Proceedings of the National Academy of Sciences*, 92(21):9598–9602, 1995.

[69] Rhiana M Daniel. *Primitive coenzymes and metabolites in archaeal/thermophilic metabolic pathways*. CRC Press, 1998.

[70] Mark Van de Casteele, Marc Demarez, Christiane Legrain, Nicolas Glansdorff, and Andr'e Pi'erard. Pathways of arginine biosynthesis in extreme thermophilic archaeo-and eubacteria. *Microbiology*, 136(7):1177–1183, 1990.

[71] Reinhard Sterner, Anke Dahm, Beatrice Darimont, Andreas Ivens, Wolfgang Liebl, and Kasper Kirschner. (beta alpha) 8-barrel proteins of tryptophan biosynthesis in the hyperthermophile *Thermotoga maritima*. *The EMBO Journal*, 14(18):4395–4402, 1995.

[72] Montserrat Tetas and John M Lowenstein. The effect of bivalent metal ions on the hydrolysis of adenosine di-and triphosphate. *Biochemistry*, 2(2):350–357, 1963.

[73] Claire Vieille and Gregory J Zeikus. Hyperthermophilic enzymes: sources, uses, and molecular mechanisms for thermostability. *Microbiol. Mol. Biol. Rev.*, 65(1):1–43, 2001.

[74] Tim Coolbear, Rhian M Daniel, and Hugh W Morgan. The enzymes from extreme thermophiles: bacterial sources, thermostabilities and industrial relevance. In *Enzymes and Products from Bacteria Fungi and Plant Cells*, pages 57–98. Springer, 1992.

[75] James R Lepock. Measurement of protein stability and protein denaturation in cells using differential scanning calorimetry. *Methods*, 35(2):117–125, 2005.

[76] Yuji GoTo, Linda J Calciano, and Anthony L Fink. Acid-induced folding of proteins. *Proceedings of the National Academy of Sciences*, 87(2):573–577, 1990.

[77] Michele A Kelly, Martha M Vestling, Catherine C Fenselau, and Philip B Smith. Electrospray analysis of proteins: A comparison of positive-ion and negative-ion mass spectra at high and low pH. *Organic Mass Spectrometry*, 27(10):1143–1147, 1992.

[78] Yuji Goto and Anthony L Fink. Conformational states in. beta.-lactamase: molten-globule states at acidic and alkaline pH with high salt. *Biochemistry*, 28(3):945–952, 1989.

[79] Robert L Baldwin. Temperature dependence of the hydrophobic interaction in protein folding. *Proceedings of the National Academy of Sciences*, 83(21):8069–8072, 1986.

[80] Vadim V Mozhaev, Karel Heremans, Johannes Frank, Patrick Masson, and Claude Balny. High pressure effects on protein structure and function. *Proteins: Structure, Function, and Bioinformatics*, 24(1):81–91, 1996.

[81] Andrew D Robertson and Kenneth P Murphy. Protein structure and the energetics of protein stability. *Chemical Reviews*, 97(5):1251–1268, 1997.

[82] Rainer Jaenicke. Protein stability and molecular adaptation to extreme conditons. *European Journal of Biochemistry*, 202(3):715–728, 1991.

[83] Ken A Dill, Kingshuk Ghosh, and Jeremy D Schmit. Physical limits of cells and proteomes. *Proceedings of the National Academy of Sciences*, 108(44):17876–17882, 2011.

[84] Roy M Daniel, Mark Dines, and Helen H Petach. The denaturation and degradation of stable enzymes at high temperatures. *Biochemical Journal*, 317(Pt 1):1, 1996.

[85] Hanne C Bertram, Mette Kristensen, and Henrik J Andersen. Functionality of myofibrillar proteins as affected by pH, ionic strength and heat treatment–a low-field NMR study. *Meat Science*, 68(2):249–256, 2004.

[86] Sergi Garcia-Manyes, Lorna Dougan, and Julio M Fern'andez. Osmolyte-induced separation of the mechanical folding phases of ubiquitin. *Proceedings of the National Academy of Sciences*, 106(26):10540–10545, 2009.

[87] Yi Cao and Hongbin Li. How do chemical denaturants affect the mechanical folding and unfolding of proteins? *Journal of Molecular Biology*, 375(1):316–324, 2008.

[88] David H Clyne, Amadeo J Pesce, and Richard E Thompson. Nephrotoxicity of bence jones proteins in the rat: importance of protein isoelectric point. *Kidney International*, 16(3):345–352, 1979.

[89] Winy Messens, John V Camp, and Andr'e Huyghebaert. The use of high pressure to modify the functionality of food proteins. *Trends in Food Science & Technology*, 8(4):107–112, 1997.

[90] Frederick Sanger, Steven Nicklen, and Alan R Coulson. DNA sequencing with chain-terminating inhibitors. *Proceedings of the National Academy of Sciences*, 74(12):5463–5467, 1977.

[91] Frederick Sanger, Gilian M Air, Bart G Barrell, Nigel L Brown, Alan R Coulson, John C Fiddes, Clyde A Hutchison, Patrick M Slocombe, and Mo Smith. Nucleotide sequence of bacteriophage $\varphi$x174 DNA. *Nature*, 265(5596):687, 1977.

[92] Elaine R Mardis. A decade's perspective on DNA sequencing technology. *Nature*, 470(7333):198, 2011.

[93] John E McCormack, Sarah M Hird, Amanda J Zellmer, Bryan C Carstens, and Robb T Brumfield. Applications of next-generation sequencing to phylogeography and phylogenetics. *Molecular Phylogenetics and Evolution*, 66(2):526–538, 2013.

[94] Daniel G Gibson, Gwynedd A Benders, Cynthia Andrews-Pfannkoch, Evgeniya A Denisova, Holly Baden-Tillson, Jayshree Zaveri, Timothy B Stockwell, Anushka Brownley, David W Thomas, Mikkel A Algire, , and C. Merryman. Complete chemical synthesis, assembly, and cloning of a mycoplasma genitalium genome. *science*, 319(5867):1215–1220, 2008.

[95] Jaume Pellicer, Michael F Fay, and Ilia J Leitch. The largest eukaryotic genome of them all? *Botanical Journal of the Linnean Society*, 164(1):10–15, 2010.

[96] Scott M Shell, Banu S Ozkan, Vincent Voelz, Albert G Wu, and Ken A Dill. Blind test of physics-based prediction of protein structures. *Biophysical Journal*, 96(3):917–924, 2009.

[97] James D Watson and Francis HC Crick. The structure of DNA. In *Cold Spring Harbor symposia on quantitative biology*, volume 18, pages 123–131. Cold Spring Harbor Laboratory Press, 1953.

[98] Akiyoshi Wada and Akira Suyama. Local stability of DNA and RNA secondary structure and its relation to biological functions. *Progress in Biophysics and Molecular Biology*, 47(2):113–157, 1986.

[99] Yu S Lazurkin, Maxim D Frank-Kamenetskii, and Edward N Trifonov. Perspectives report: Melting of DNA: Its study and application as a research method. *Biopolymers: Original Research on Biomolecules*, 9(11):1253–1306, 1970.

[100] Thomas D Brock, Katherine M Brock, Robert T Belly, and Richard L Weiss. Sulfolobus: a new genus of sulfur-oxidizing bacteria living at low pH and high temperature. *Archiv für Mikrobiologie*, 84(1):54–68, 1972.

[101] Tairo Oshima and Kazutomo Imahori. Description of thermus thermophilus (yoshida and oshima) comb. nov., a nonsporulating thermophilic bacterium from a japanese thermal spa. *International Journal of Systematic and Evolutionary Microbiology*, 24(1):102–112, 1974.

[102] Yasuo Kagawa, Hiroshi Nojima, Noriko Nukiwa, Morio Ishizuka, Takahiro Nakajima, Tadashi Yasuhara, Teruo Tanaka, and Tairo Oshima. High guanine plus cytosine content in the third letter of codons of an extreme thermophile. DNA sequence of the isopropylmalate dehydrogenase of thermus thermophilus. *Journal of Biological Chemistry*, 259(5):2956–2960, 1984.

[103] Hao Zheng and Hongwei Wu. Gene-centric association analysis for the correlation between the guanine-cytosine content levels and temperature range conditions of prokaryotic species. *BMC Bioinformatics*, 11(11):S7, 2010.

[104] Oksana Lukjancenko, Trudy M Wassenaar, and David W Ussery. Comparison of 61 sequenced *Escherichia coli* genomes. *Microbial Ecology*, 60(4):708–720, 2010.

[105] Andrey Karshikoff and Rudolf Ladenstein. Ion pairs and the thermotolerance of proteins from hyperthermophiles: a "traffic rule" for hot roads. *Trends in Biochemical Sciences*, 26(9):550–557, 2001.

[106] Benjamin D Greenbaum, Pradeep Kumar, and Albert Libchaber. Using first passage statistics to extract environmentally dependent amino acid correlations. *PloS One*, 9(7), 2014.

[107] Arnab Nayek, Parth S Gupta, Shyamashree Banerjee, Buddhadev Mondal, and Amal K Bandyopadhyay. Salt-bridge energetics in halophilic proteins. *Plos One*, 9(4):e93862, 2014.

[108] Colin Raeside, Joël Gaff'e, Daniel E Deatherage, Olivier Tenaillon, Adam M Briska, Ryan N Ptashkin, St'ephane Cruveiller, Claudine M'edigue, Richard E Lenski, Jeffrey E Barrick, and Dominique Schneider. Large chromosomal rearrangements during a long-term evolution experiment with *Escherichia coli*. *MBio*, 5(5):e01377–14, 2014.

[109] Michelle M Riehle, Albert F Bennett, Richard E Lenski, and Anthony D Long. Evolutionary changes in heat-inducible gene expression in lines of *Escherichia coli* adapted to high temperature. *Physiological Genomics*, 14(1):47–58, 2003.

[110] David Alc'antara-D'ıaz, Matilde Breña-Valle, and Jorge Serment-Guerrero. Divergent adaptation of *Escherichia coli* to cyclic ultraviolet light exposures. *Mutagenesis*, 19(5):349–354, 2004.

[111] Sean C Sleight and Richard E Lenski. Evolutionary adaptation to freeze-thaw-growth cycles in *Escherichia coli*. *Physiological and Biochemical Zoology*, 80(4):370–385, 2007.

[112] Daniel M Stoebel, Karsten Hokamp, Michael S Last, and Charles J Dorman. Compensatory evolution of gene regulation in response to stress by *Escherichia coli* lacking RpoS. *PLoS Genetics*, 5(10):e1000671, 2009.

[113] Birgit Rudolph, Katharina M Gebendorfer, Johannes Buchner, and Jeannette Winter. Evolution of *Escherichia coli* for growth at high temperatures. *Journal of Biological Chemistry*, 285(25):19029–19034, 2010.

[114] Hani Goodarzi, Bryson D Bennett, Sasan Amini, Marshall L Reaves, Alison K Hottes, Joshua D Rabinowitz, and Saeed Tavazoie. Regulatory and metabolic rewiring during laboratory evolution of ethanol tolerance in *E. coli*. *Molecular Systems Biology*, 6(1):378, 2010.

[115] Takaaki Horinouchi, Kuniyasu Tamaoka, Chikara Furusawa, Naoaki Ono, Shingo Suzuki, Takashi Hirasawa, Tetsuya Yomo, and Hiroshi Shimizu. Transcriptome analysis of parallel-evolved *Escherichia coli* strains under ethanol stress. *BMC Genomics*, 11(1):579, 2010.

[116] Ian Dundas. Was the environment for primordial life hypersaline? *Extremophiles*, 2(3):375–377, 1998.

[117] Christopher T Russell. The magnetic field of Mars: Mars 3 evidence reexamined. *Geophysical Research Letters*, 5(1):81–84, 1978.

[118] John R Spreiter, Audrey L Summers, and Arthur W Rizzi. Solar wind flow past nonmagnetic planets? Venus and Mars. *Planetary and Space Science*, 18(9):1281–1299, 1970.

[119] Michael H Carr. Water on mars. *Nature*, 326(6108):30–35, 1987.

[120] Daria Morozova, Diedrich Möhlmann, and Dirk Wagner. Survival of methanogenic archaea from siberian permafrost under simulated Martian thermal conditions. *Origins of Life and Evolution of Biospheres*, 37(2):189–200, 2007.

[121] Navita Sinha, Sudip Nepal, Timothy Kral, and Pradeep Kumar. Survivability and growth kinetics of methanogenic archaea at various pHs and pressures: Implications for deep subsurface life on Mars. *Planetary and Space Science*, 136:15–24, 2017.

[122] Navita Sinha, Sudip Nepal, Timothy Kral, and Pradeep Kumar. Effects of temperatures and high pressures on the growth and survivability of methanogens and stable carbon isotope fractionation: Implications for deep subsurface life on Mars. *International Journal of Astrobiology*, pages 1–7, 2018.

[123] patrick Cassen, Ray T Reynolds, and Stanton J Peale. Is there liquid water on Europa? *Geophysical Research Letters*, 6(9):731–734, 1979.

[124] Steven W Squyres, Ray T Reynolds, Patrick M Cassen, and Stanton J Peale. Liquid water and active resurfacing on Europa. *Nature*, 301(5897):225, 1983.

[125] Bruno E Schmidt, Donald D Blankenship, George W Patterson, and Peer M Schenk. Active formation of 'chaos terrain' over shallow subsurface water on Europa. *Nature*, 479(7374):502, 2011.

[126] Eric J Gaidos and Francis Nimmo. Planetary science: tectonics and water on Europa. *Nature*, 405(6787):637, 2000.

[127] Michael Manga and Chi-Yuen Wang. Pressurized oceans and the eruption of liquid water on Europa and Enceladus. *Geophysical Research Letters*, 34(7), 2007.

[128] Mathew H Burger, Edward C Sittler Jr, Robert E Johnson, Todd H Smith, Orenthal J Tucker, and Valerie I Shematovich. Understanding the escape of water from Enceladus. *Journal of Geophysical Research: Space Physics*, 112(A6):1–10, 2007.

[129] William B Sparks, Kevin P Hand, Mellisa A McGrath, Gorham E Bergeron, Misty Cracraft, and Susana E Deustua. Probing for evidence of plumes on Europa with HST/STIS. *The Astrophysical Journal*, 829(2):121, 2016.

[130] William B McKinnon and Michael E Zolensky. Sulfate content of Europa's ocean and shell: Evolutionary considerations and some geological and astrobiological implications. *Astrobiology*, 3(4):879–897, 2003.

[131] Jeffrey S Kargel, Jonathan Z Kaye, James W Head III, Giles M Marion, Roger Sassen, James K Crowley, Olga Prieto Ballesteros, Steven A Grant, and David L Hogenboom. Europa's crust and ocean: origin, composition, and the prospects for life. *Icarus*, 148(1):226–265, 2000.

[132] James B Dalton III. Spectral behavior of hydrated sulfate salts: Implications for Europa mission spectrometer design. *Astrobiology*, 3(4):771–784, 2003.

[133] Michael E Brown and Kevin P Hand. Salts and radiation products on the surface of Europa. *The Astronomical Journal*, 145(4):110, 2013.

[134] Anna M Giuliodori, Claudio O Gualerzi, Sara Soto, Jordi Vila, and Mar'Ia M Tav'Io. Review on bacterial stress topics. *Annals of the New York Academy of Sciences*, 1113(1):95–104, 2007.

[135] Michael Gänzle and Yang Liu. Mechanisms of pressure-mediated cell death and injury in *Escherichia coli*: from fundamentals to food applications. *Frontiers in Microbiology*, 6:599, 2015.

[136] Pradeep Kumar and Albert Libchaber. Pressure and temperature dependence of growth and morphology of *Escherichia coli*: experiments and stochastic model. *Biophysical Journal*, 105(3):783–793, 2013.

[137] Adriana Molina-Höppner, Takako Sato, Chiaki Kato, Michael G Gänzle, and Rudi F Vogel. Effects of pressure on cell morphology and cell division of lactic acid bacteria. *Extremophiles*, 7(6):511–516, 2003.

[138] Claude E ZoBell and Frank H Johnson. The influence of hydrostatic pressure on the growth and viability of terrestrial and marine bacteria. *Journal of Bacteriology*, 57(2):179, 1949.

[139] Claude E Zobell and Carl H Oppenheimer. Some effects of hydrostatic pressure on the multiplication and morphology of marine bacteria. *Journal of Bacteriology*, 60(6):771, 1950.

[140] Claude E ZoBell. Pressure effects on morphology and life processes of bacteria. *High Pressure Effects on Cellular Processes*, 1970.

[141] Akihiro Ishii, Takako Sato, Masaaki Wachi, Kazuo Nagai, and Chiaki Kato. Effects of high hydrostatic pressure on bacterial cytoskeleton FtsZ polymers in vivo and in vitro. *Microbiology*, 150(6):1965–1972, 2004.

[142] Pradeep Kumar and Albert Libchaber. Cell fates and reversibility of *Escherichia coli* at high hydrostatic pressure. *Preprint*.

[143] Masayoshi Nishiyama and Yoshiyuki Sowa. Microscopic analysis of bacterial motility at high pressure. *Biophysical Journal*, 102(8):1872–1880, 2012.

[144] R Meganathan and Robert E Marquis. Loss of bacterial motility under pressure. *Nature*, 246(5434):525, 1973.

[145] Jan M Smelt. Recent advances in the microbiology of high pressure processing. *Trends in Food Science & Technology*, 9(4):152–158, 1998.

[146] Ferreris E Torres, Martin G Gonz'alez, Bernadette Klotz, and Daniel Rodrigo. Effects of high hydrostatic pressure and temperature increase on *Escherichia coli* spp. and pectin methyl esterase inactivation in orange juice. *Food Science and Technology International*, 22(2):173–180, 2016.

[147] Gregorio Weber and Harry G Drickamer. The effect of high pressure upon proteins and other biomolecules. *Quarterly Reviews of Biophysics*, 16(1):89–112, 1983.

[148] St'ephanie Follonier, Sven Panke, and Manfred Zinn. Pressure to kill or pressure to boost: a review on the various effects and applications of hydrostatic pressure in bacterial biotechnology. *Applied Microbiology and Biotechnology*, 93(5):1805–1815, 2012.

[149] Ute Neugebauer, Ulrike Schmid, Knut Baumann, Holder Simon, Michael Schmitt, and Juergen Popp. DNA tertiary structure and changes in DNA supercoiling upon interaction with ethidium bromide and gyrase monitored by UV resonance Raman spectroscopy. *Journal of Raman Spectroscopy: An International Journal for Original Work in all Aspects of Raman Spectroscopy, Including Higher Order Processes, and also Brillouin and Rayleigh Scattering*, 38(10):1246–1258, 2007.

[150] Karel Heremans and L Smeller. Protein structure and dynamics at high pressure. *Biochimica et Biophysica Acta (BBA)-Protein Structure and Molecular Enzymology*, 1386(2):353–370, 1998.

[151] Jack Merrin, Pradeep Kumar, and Albert Libchaber. Effects of pressure and temperature on the binding of reca protein to single-stranded DNA. *Proceedings of the National Academy of Sciences*, 108(50):19913–19918, 2011.

[152] Robert B Macoregor Jr, John Q Wu, and Reza Najaf-Zadeh. Stability of DNA at high pressure. *High Pressure Effects in Molecular Biophysics and Enzymology*, page 149, 1996.

[153] Dmitri P Kharakoz. Partial volumes and compressibilities of extended polypeptide chains in aqueous solution: additivity scheme and implication of protein unfolding at normal and high pressure. *Biochemistry*, 36(33):10276–10285, 1997.

[154] Claude Balny and Patrick Masson. Effects of high pressure on proteins. *Food Reviews International*, 9(4):611–628, 1993.

[155] Huahua Jian, Lei Xiong, Guanpeng Xu, Xiang Xiao, and Fengping Wang. Long 5' untranslated regions regulate the RNA stability of the deep-sea filamentous phage SW1. *Scientific Reports*, 6(21908):1–9, 2016.

[156] Ronald Winter. DNA supercoiling under high pressure. In *Advances in High Pressure Bioscience and Biotechnology*, pages 315–318. Springer, 1999.

[157] Claude E Zobell and Andre B Cobet. Effects of hydrostatic pressure on *E. coli*. *Journal of Bacteriology*, 84(6):1228–1236, 1962.

[158] Claude E Zobell and Andre B Cobet. Filament formation by *Escherichia coli* at increased hydrostatic pressures. *Journal of Bacteriology*, 84(6):710–719, 1964.

[159] Filip Meersman and Karel Heremans. High hydrostatic pressure effects in the biosphere: from molecules to microbiology. In *High-pressure Microbiology*, pages 1–17. American Society of Microbiology, 2008.

[160] Aaron S Malone, Yoon-Kyung Chung, and Ahmed E Yousef. Genes of *Escherichia coli* o157: H7 that are involved in high-pressure resistance. *Appl. Environ. Microbiol.*, 72(4):2661–2671, 2006.

[161] Timothy J Welch, Anne Farewell, Frederick C Neidhardt, and Douglas H Bartlett. Stress response of *Escherichia coli* to elevated hydrostatic pressure. *Journal of Bacteriology*, 175(22):7170–7177, 1993.

[162] Abram Aertsen, Rob V Houdt, Kristof Vanoirbeek, and Chris W Michiels. An sos response induced by high pressure in *Escherichia coli*. *Journal of Bacteriology*, 186(18):6133–6141, 2004.

[163] Aurelie Guyet, Martyn Dade-Robertson, Anil Wipat, John Casement, Wendy Smith, Helen Mitrani, and Meng Zhang. Mild hydrostatic pressure triggers oxidative responses in *Escherichia coli*. *PloS One*, 13(7):e0200660, 2018.

[164] Abram Aertsen, Philipp De Spiegeleer, Kristof Vanoirbeek, Maria Lavilla, and Chris W Michiels. Induction of oxidative stress by high hydrostatic pressure in *Escherichia coli*. *Appl. Environ. Microbiol.*, 71(5):2226–2231, 2005.

[165] Zonglin Hu and Joe Lutkenhaus. Topological regulation of cell division in *Escherichia coli* involves rapid pole to pole oscillation of the division inhibitor minc under the control of mind and mine. *Molecular Microbiology*, 34(1):82–90, 1999.

[166] John N Reeve, Neil H Mendelson, Sheila I Coyne, and Linda L Hallock. Minicells of *Bacillus subtilis*. *Journal of Bacteriology*, 114(2):860–873, 1973.

[167] Erfei Bi and Joe Lutkenhaus. FtsZ ring structure associated with division in *Escherichia coli*. *Nature*, 354(6349):161, 1991.

[168] William Martin, John Baross, Deborah Kelley, and Michael J Russell. Hydrothermal vents and the origin of life. *Nature Reviews Microbiology*, 6(11):805, 2008.

[169] John A Baross and Sarah E Hoffman. Submarine hydrothermal vents and associated gradient environments as sites for the origin and evolution of life. *Origins of Life and Evolution of the Biosphere*, 15(4):327–345, 1985.

[170] Barry Herschy, Alexandra Whicher, Eloi Camprubi, Cameron Watson, Lewis Dartnell, John Ward, Julian R Evans, and Nick Lane. An origin-of-life reactor to simulate alkaline hydrothermal vents. *Journal of Molecular Evolution*, 79(5-6):213–227, 2014.

[171] Bernice Slutsky, Jeffrey Buffo, and David R Soll. High-frequency switching of colony morphology in *Candida albicans*. *Science*, 230(4726):666–669, 1985.

[172] Ana M Sousa, Idalina Machado, and Maria O Pereira. Phenotypic switching: an opportunity to bacteria thrive. *Science Against Microbial Pathogens: Communicating Current Research and Technological Advances*, 1:252–262, 2012.

[173] Oliver J Rando and Kevin J Verstrepen. Timescales of genetic and epigenetic inheritance. *Cell*, 128(4):655–668, 2007.

[174] Avraham Be'er, E-L Florin, Carolyn R Fisher, Harry L Swinney, and Shelley M Payne. Surviving bacterial sibling rivalry: inducible and reversible phenotypic switching in *Paenibacillus dendritiformis*. *MBio*, 2(3):e00069–11, 2011.

[175] Hubertus J Beaumont, Jenna Gallie, Christian Kost, Gayle C Ferguson, and Paul B Rainey. Experimental evolution of bet hedging. *Nature*, 462(7269):90, 2009.

[176] Abram Aertsen and Chris W Michiels. Diversify or die: generation of diversity in response to stress. *Critical Reviews in Microbiology*, 31(2):69–78, 2005.

[177] Guillaume Lambert and Edo Kussell. Memory and fitness optimization of bacteria under fluctuating environments. *PLoS Genetics*, 10(9):e1004556, 2014.

[178] Joseph E Peters, Timothy E Thate, and Nancy L Craig. Definition of the *Escherichia coli* MC4100 genome by use of a DNA array. *Journal of Bacteriology*, 185(6):2017–2021, 2003.

[179] Michael D Abràmoff, Paulo J Magalhães, and Sunanda J Ram. Image processing with ImageJ. *Biophotonics International*, 11(7):36–42, 2004.

[180] Galina Reshes, Sharon Vanounou, Itzhak Fishov, and Mario Feingold. Cell shape dynamics in *Escherichia coli*. *Biophysical Journal*, 94(1):251–264, 2008.

[181] Manasi S Gangan and Chaitanya A Athale. Threshold effect of growth rate on population variability of *Escherichia coli* cell lengths. *Royal Society open science*, 4(2):160417, 2017.

[182] Edo Kussell and Stanislas Leibler. Phenotypic diversity, population growth, and information in fluctuating environments. *Science*, 309(5743):2075–2078, 2005.

[183] Edo Kussell, Roy Kishony, Nathalie Q Balaban, and Stanislas Leibler. Bacterial persistence: a model of survival in changing environments. *Genetics*, 169(4):1807–1814, 2005.

[184] Murat Acar, Jerome T Mettetal, and Alexander V Oudenaarden. Stochastic switching as a survival strategy in fluctuating environments. *Nature Genetics*, 40(4):471, 2008.

[185] Lydia Robert, Marc Hoffmann, Nathalie Krell, St'ephane Aymerich, J'erôme Robert, and Marie Doumic. Division in *Escherichia coli* is triggered by a size-sensing rather than a timing mechanism. *BMC Biology*, 12(1):17, 2014.

[186] Matteo Osella, Eileen Nugent, and Marco Cosentino Lagomarsino. Concerted control of *Escherichia coli* cell division. *Proceedings of the National Academy of Sciences*, 111(9):3431–3435, 2014.

[187] Masaaki Wachi and Michio Matsuhashi. Negative control of cell division by *mreB*, a gene that functions in determining the rod shape of *Escherichia coli* cells. *Journal of Bacteriology*, 171(6):3123–3127, 1989.

[188] Henrik Strahl, Frank Bürmann, and Leendert W Hamoen. The actin homologue MreB organizes the bacterial cell membrane. *Nature Communications*, 5:3442, 2014.

[189] Andrew K Fenton and Kenn Gerdes. Direct interaction of FtsZ and MreB is required for septum synthesis and cell division in *Escherichia coli*. *The EMBO Journal*, 32(13):1953–1965, 2013.

[190] Srividya Iyer-Biswas, Charles S Wright, Jonathan T Henry, Klevin Lo, Stanislav Burov, Yihan Lin, Gavin E Crooks, Sean Crosson, Aaron R Dinner, and Norbert F Scherer. Scaling laws governing stochastic growth and division of single bacterial cells. *Proceedings of the National Academy of Sciences*, 111(45):15912–15917, 2014.

[191] Kang Dai, Yifan Xu, and Joe Lutkenhaus. Topological characterization of the essential *Escherichia coli* cell division protein FtsN. *Journal of Bacteriology*, 178(5):1328–1334, 1996.

[192] Nienke Buddelmeijer, Mirjam E Aarsman, Arend H Kolk, Miguel Vicente, and Nanne Nanninga. Localization of cell division protein FtsQ by immunofluorescence microscopy in dividing and nondividing cells of *Escherichia coli*. *Journal of Bacteriology*, 180(23):6107–6116, 1998.

[193] Xuan-chuan Yu, Anthony H Tran, Qin Sun, and William Margolin. Localization of cell division protein FtsK to the *Escherichia coli* septum and identification of a potential n-terminal targeting domain. *Journal of Bacteriology*, 180(5):1296–1304, 1998.

[194] Jean-Marc Ghigo, David S Weiss, Joseph C Chen, Justin C Yarrow, and Jon Beckwith. Localization of ftsl to the *Escherichia coli* septal ring. *Molecular Microbiology*, 31(2):725–737, 1999.

[195] Luz-Maria Guzman, James J Barondess, and Jon Beckwith. Ftsl, an essential cytoplasmic membrane protein involved in cell division in *Escherichia coli*. *Journal of Bacteriology*, 174(23):7717–7728, 1992.

[196] Xiaolan Ma, David W Ehrhardt, and William Margolin. Colocalization of cell division proteins FtsZ and FtsA to cytoskeletal structures in living *Escherichia coli* cells by using green fluorescent protein. *Proceedings of the National Academy of Sciences*, 93(23):12998–13003, 1996.

[197] Eugenia Mileykovskaya, Qin Sun, William Margolin, and William Dowhan. Localization and function of early cell division proteins in filamentous *Escherichia coli* cells lacking phosphatidylethanolamine. *Journal of Bacteriology*, 180(16):4252–4257, 1998.

[198] Purva Vats and Lawrence Rothfield. Duplication and segregation of the actin (MreB) cytoskeleton during the prokaryotic cell cycle. *Proceedings of the National Academy of Sciences*, 104(45):17795–17800, 2007.

[199] Erfei Bi and Joe Lutkenhaus. Cell division inhibitors SulA and MinCD prevent formation of the FtsZ ring. *Journal of Bacteriology*, 175(4):1118–1125, 1993.

[200] Ganhui Lan, Alex Dajkovic, Denis Wirtz, and Sean X Sun. Polymerization and bundling kinetics of FtsZ filaments. *Biophysical Journal*, 95(8):4045–4056, 2008.

[201] David Popp, Akihiro Narita, Kayo Maeda, Tetsuro Fujisawa, Umesh Ghoshdastider, Mitsusada Iwasa, Yuichiro Ma'eda, and Robert C Robinson. Filament structure, organization, and dynamics in MreB sheets. *Journal of Biological Chemistry*, 285(21):15858–15865, 2010.

[202] Michael B Elowitz, Arnold J Levine, Eric D Siggia, and Peter S Swain. Stochastic gene expression in a single cell. *Science*, 297(5584):1183–1186, 2002.

[203] Takeshi Naganuma and Hirohiko Uematsu. Dive [Europa]: a search-for-life initiative. *Biological Sciences in Space*, 12(2):126–130, 1998.

[204] Giles M Marion. A molal-based model for strong acid chemistry at low temperatures ($< 200$ to 298 k). *Geochimica et Cosmochimica Acta*, 66(14):2499–2516, 2002.

[205] Paul V Johnson, Robert Hodyss, Tuan H Vu, and Mathieu Choukroun. Insights into Europa's ocean composition derived from its surface expression. *Icarus*, 321:857–865, 2019.

[206] Benton C Clark. Implications of abundant hygroscopic minerals in the Martian regolith. *Icarus*, 34(3):645–665, 1978.

[207] Heinrich Wänke, Johannes Brückner, Gerlind Dreibus, Rudolf Rieder, and Igor D Ryabchikov. Chemical composition of rocks and soils at the Pathfinder site. In *Chronology and Evolution of Mars*, pages 317–330. Springer, 2001.

[208] Benton C Clark, Richard V Morris, Scott M McLennan, Ralf Gellert, Bradley L Jolliff, Andrew H Knoll, Steven W Squyres, Tim K Lowenstein, Douglas W Ming, Nicholas J Tosca, Albert Yen, Philip R Christensen, Stephen Gorevan, Johanas Bruckner, Wendy Calvin, Gerlind Dreibus, Wetwitoo Farrand, Goestar Klingelhoefer, Heinrich Waenke, Jutta Zipfel, James F Bell III, John Grotzinger, Harry Y McSween, and Rudolf Rieder. Chemistry and mineralogy of outcrops at Meridiani Planum. *Earth and Planetary Science Letters*, 240(1):73–94, 2005.

[209] Aline Gendrin, Nicolas Mangold, Jean-Pierre Bibring, Yves Langevin, Brigitte Gondet, François Poulet, Guillaume Bonello, Cathy Quantin, John Mustard, Ray Arvidson, and Stephane LeMouelic. Sulfates in Martian layered terrains: the OMEGA/Mars Express view. *Science*, 307(5715):1587–1591, 2005.

[210] Travis Altheide, Vincent Chevrier, Christine Nicholson, and Jackie Denson. Experimental investigation of the stability and evaporation of sulfate and chloride brines on mars. *Earth and Planetary Science Letters*, 282(1-4):69–78, 2009.

[211] David T Vaniman, David L Bish, Steve J Chipera, Claire I Fialips, J William Carey, and William C Feldman. Magnesium sulphate salts and the history of water on Mars. *Nature*, 431(7009):663–665, 2004.

[212] Shiladitya DasSarma and Priya DasSarma. Halophiles. *eLS*, pages 1–13, 2001.

[213] Adrienne L Huston, Barbara B Krieger-Brockett, and Jody W Deming. Remarkably low temperature optima for extracellular enzyme activity from arctic bacteria and sea ice. *Environmental Microbiology*, 2(4):383–388, 2000.

[214] Giles M Marion, Christian H Fritsen, Hajo Eicken, and Meredith C Payne. The search for life on Europa: limiting environmental factors, potential habitats, and Earth analogues. *Astrobiology*, 3(4):785–811, 2003.

[215] Louisa J Preston and Lewis R Dartnell. Planetary habitability: lessons learned from terrestrial analogues. *International Journal of Astrobiology*, 13(1):81–98, 2014.

[216] Olaf P Jenkins. Spotted lakes of epsomite in Washington and British Columbia. *American Journal of Science*, 46(275):638–644, 1918.

[217] Ian S Foster, Penelope L King, Brendt C Hyde, and Gordon Southam. Characterization of halophiles in natural $MgSO_4$ salts and laboratory enrichment samples: astrobiological implications for Mars. *Planetary and Space Science*, 58(4):599–615, 2010.

[218] Rui Xing, Qing-bo Gao, Fa-qi Zhang, Jiu-li Wang, and Shi-long Chen. Large-scale distribution of bacterial communities in the Qaidam Basin of the Qinghai–Tibet Plateau. *MicrobiologyOpen*, 8(10):e909, 2019.

[219] Alexandra Pontefract, Ting F Zhu, Virginia K Walker, Holli Hepburn, Clarissa Lui, Maria T Zuber, Gary Ruvkun, and Christopher E Carr. Microbial diversity in a

hypersaline sulfate lake: a terrestrial analog of ancient mars. *Frontiers in Microbiology*, 8:1819, 2017.

[220] James D Crisler, Trista M Newville, Fei Chen, Benton C Clark, and Mark A Schneegurt. Bacterial growth at the high concentrations of magnesium sulfate found in Martian soils. *Astrobiology*, 12(2):98–106, 2012.

[221] Brian R Kilmer, Timothy C Eberl, Brent Cunderla, Fei Chen, Benton C Clark, and Mark A Schneegurt. Molecular and phenetic characterization of the bacterial assemblage of Hot Lake, WA, an environment with high concentrations of magnesium sulphate, and its relevance to Mars. *International Journal of Astrobiology*, 13(1):69–80, 2014.

[222] Mark G Fox-Powell and Charles S Cockell. Building a geochemical view of microbial salt tolerance: halophilic adaptation of marinococcus in a natural magnesium sulfate brine. *Frontiers in Microbiology*, 9:739, 2018.

[223] Jonathan M Wilks, Fei Chen, Benton C Clark, and Mark A Schneegurt. Bacterial growth in saturated and eutectic solutions of magnesium sulphate and potassium chlorate with relevance to Mars and the ocean worlds. *International Journal of Astrobiology*, 18(6):502–509, 2019.

[224] Neeti Sinha and Sandra J Smith-Gill. Electrostatics in protein binding and function. *Current Protein and Peptide Science*, 3(6):601–614, 2002.

[225] Kim A Sharp and Barry Honig. Salt effects on nucleic acids. *Current Opinion in Structural Biology*, 5(3):323–328, 1995.

[226] Laszlo N Csonka. Physiological and genetic responses of bacteria to osmotic stress. *Microbiology and Molecular Biology Reviews*, 53(1):121–147, 1989.

[227] Andrew Stevenson, Jonathan A Cray, Jim P Williams, Ricardo Santos, Richa Sahay, Nils Neuenkirchen, Colin D McClure, Irene R Grant, Jonathan DR Houghton, John P Quinn, David J Timson, Satish V Patil, Rekha S Singhal, Josepha Anton, Aharon Oren, Kenneth N Timmis, Terry J McGenity, and John E Hallsworth. Is there a common water-activity limit for the three domains of life? *The ISME Journal*, 9(6):1333, 2015.

[228] Thomas M Record Jr, Elizabeth S Courtenay, D Scott Cayley, and Harry J Guttman. Responses of *E. coli* to osmotic stress: large changes in amounts of cytoplasmic solutes and water. *Trends in Biochemical Sciences*, 23(4):143–148, 1998.

[229] Eugene H Cota-Robles. Electron microscopy of plasmolysis in *Escherichia coli*. *Journal of Bacteriology*, 85(3):499–503, 1963.

[230] Enrique Rojas, Julie A Theriot, and Kerwyn C Huang. Response of *Escherichia coli* growth rate to osmotic shock. *Proceedings of the National Academy of Sciences*, 111(21):7807–7812, 2014.

[231] Michael Doudoroff. Experiments on the adaptation of *Escherichia coli* to sodium chloride. *The Journal of General Physiology*, 23(5):585–611, 1940.

[232] Peter C Loewen, Bei Hu, Jeanna Strutinsky, and Richard Sparling. Regulation in the *rpoS* regulon of *Escherichia coli*. *Canadian Journal of Microbiology*, 44(8):707–717, 1998.

[233] Claude Gutierrez and Jean C Devedjian. Osmotic induction of gene osmc expression in *Escherichia coli* k12. *Journal of Molecular Biology*, 220(4):959–973, 1991.

[234] Christian Delamarche, Daniel Thomas, Jean-Paul Rolland, Alexandrine Froger, Jean Gouranton, Maria Svelto, Peter Agre, and Giuseppe Calamita. Visualization of AqpZ-mediated water permeability in *Escherichia coli* by cryoelectron microscopy. *Journal of Bacteriology*, 181(14):4193–4197, 1999.

[235] Giuseppe Calamita. The *Escherichia coli* Aquaporin-Z water channel: Microreview. *Molecular Microbiology*, 37(2):254–262, 2000.

[236] Namrata V Rao, Ravindranath Shashidhar, and Jayant R Bandekar. Comparative analysis of induction of osmotic-stress-dependent genes in vibrio vulnificus exposed to hyper-and hypo-osmotic stress. *Canadian Journal of Microbiology*, 59(5):333–338, 2013.

[237] Ronald L Smith and Michael E Maguire. Microbial magnesium transport: unusual transporters searching for identity. *Molecular Microbiology*, 28(2):217–226, 1998.

[238] Jian Payandeh, Roland Pfoh, and Emil F Pai. The structure and regulation of magnesium selective ion channels. *Biochimica et Biophysica Acta (BBA)-Biomembranes*, 1828(11):2778–2792, 2013.

[239] Paul S Hmiel, Marshal D Snavely, Charles G Miller, and Michael E Maguire. Magnesium transport in *Salmonella typhimurium*: characterization of magnesium influx and cloning of a transport gene. *Journal of Bacteriology*, 168(3):1444–1450, 1986.

[240] Halina Karbonowska, Alina Wiater, and D Hulanicka. Sulphate permease of *Escherichia coli* k12. *Acta Biochimica Polonica*, 24(4):329–334, 1977.

[241] Monika Hryniewicz, Agnieszka Sirko, A Pałucha, A Böck, and Danuta M Hulanicka. Sulfate and thiosulfate transport in *Escherichia coli* k-12: identification of a gene encoding a novel protein involved in thiosulfate binding. *Journal of Bacteriology*, 172(6):3358–3366, 1990.

[242] Nancy G Nossal and Leon A Heppel. The release of enzymes by osmotic shock from *Escherichia coli* in exponential phase. *Journal of Biological Chemistry*, 241(13):3055–3062, 1966.

[243] Darren D Sledjeski and Susan Gottesman. Osmotic shock induction of capsule synthesis in *Escherichia coli* k-12. *Journal of Bacteriology*, 178(4):1204–1206, 1996.

[244] Yasuhiro Anraku. The reduction and restoration of galactose transport in osmotically shocked cells of *Escherichia coli*. *Journal of Biological Chemistry*, 242(5):793–800, 1967.

[245] Tatyana Romantsov, Ziqiang Guan, and Janet M Wood. Cardiolipin and the osmotic stress responses of bacteria. *Biochimica et Biophysica Acta (BBA)-Biomembranes*, 1788(10):2092–2100, 2009.

[246] Roy D Sleator and Colin Hill. Bacterial osmoadaptation: the role of osmolytes in bacterial stress and virulence. *FEMS Microbiology Reviews*, 26(1):49–71, 2002.

[247] Caroline A Schneider, Wayne S Rasband, and Kevin W Eliceiri. NIH Image to ImageJ: 25 years of image analysis. *Nature Methods*, 9(7):671, 2012.

[248] Xiayu Rao, Xuelin Huang, Zhicheng Zhou, and Xin Lin. An improvement of the 2ˆ (-delta delta CT) method for quantitative real-time polymerase chain reaction data analysis. *Biostatistics, Bioinformatics and Biomathematics*, 3(3):71, 2013.

[249] Basanta R Wagle, Abhinav Upadhyay, Komala Arsi, Sandip Shrestha, Kumar Venkitanarayanan, Annie M Donoghue, and Dan J Donoghue. Application of $\beta$-resorcylic acid as potential antimicrobial feed additive to reduce campylobacter colonization in broiler chickens. *Frontiers in Microbiology*, 8:599, 2017.

[250] Joseba Bikandi, Rosario S Mill'an, Aitor Rementeria, and Javier Garaizar. In silico analysis of complete bacterial genomes: PCR, AFLP–PCR and endonuclease restriction. *Bioinformatics*, 20(5):798–799, 2004.

[251] Tom Olijhoek, Corbert G Van Eden, Frank J Trueba, Evelien Pas, and Nanne Nanninga. Plasmolysis during the division cycle of *Escherichia coli*. *Journal of Bacteriology*, 152(1):479–484, 1982.

[252] Conrad L Woldringh and Woutera V Iterson. Effects of treatment with sodium dodecyl sulfate on the ultrastructure of *Escherichia coli*. *Journal of Bacteriology*, 111(3):801–813, 1972.

[253] Giuseppe Calamita, Bettina Kempf, M'elanie Bonhivers, William R Bishai, Erhard Bremer, and Peter Agre. Regulation of the *Escherichia coli* water channel gene *aqpZ*. *Proceedings of the National Academy of Sciences*, 95(7):3627–3631, 1998.

[254] Eric Soupene, Natalie King, Haidy Lee, and Sydney Kustu. Aquaporin-Z of *Escherichia coli*: reassessment of its regulation and physiological role. *Journal of Bacteriology*, 184(15):4304–4307, 2002.

[255] Rachael C Mallo and Michael T Ashby. AqpZ-mediated water permeability in *Escherichia coli* measured by stopped-flow spectroscopy. *Journal of Bacteriology*, 188(2):820–822, 2006.

[256] Hiromi Suzuki, Jack Pangborn, and Wendell W Kilgore. Filamentous cells of *Escherichia coli* formed in the presence of mitomycin. *Journal of Bacteriology*, 93(2):683–688, 1967.

[257] George N Rolinson. Effect of $\beta$-lactam antibiotics on bacterial cell growth rate. *Microbiology*, 120(2):317–323, 1980.

[258] Tineke Jones, Thomas Gill, and Lynn M McMullen. The behaviour of log phase *Escherichia coli* at temperatures that fluctuate about the minimum for growth. *Letters in Applied Microbiology*, 39(3):296–300, 2004.

[259] Chad M Nelson, Michael R Schuppenhauer, and Douglas S Clark. High-pressure, high-temperature bioreactor for comparing effects of hyperbaric and hydrostatic pressure on bacterial growth. *Appl. Environ. Microbiol.*, 58(5):1789–1793, 1992.

[260] Marcel H Zwietering, Koos JT De, Birgit E Hasenack, Jamie C De Witt, and Klass V Riet. Modeling of bacterial growth as a function of temperature. *Appl. Environ. Microbiol.*, 57(4):1094–1101, 1991.

[261] Erland Bååth and Kristina Arnebrant. Growth rate and response of bacterial communities to pH in limed and ash treated forest soils. *Soil Biology and Biochemistry*, 26(8):995–1001, 1994.

[262] William D Grant. Life at low water activity. *Philosophical Transactions of the Royal Society of London. Series B: Biological Sciences*, 359(1448):1249–1267, 2004.

[263] Joseph A Rard and Donald G Miller. Isopiestic determination of the osmotic coefficients of aqueous sodium sulfate, magnesium sulfate, and sodium sulfate-magnesium sulfate at 25. degree. c. *Journal of Chemical and Engineering Data*, 26(1):33–38, 1981.

[264] Jorge Chirife and Silvia L Resnik. Unsaturated solutions of sodium chloride as reference sources of water activity at various temperatures. *Journal of Food Science*, 49(6):1486–1488, 1984.

[265] Robert A Robinson and Robert H Stokes. *Electrolyte solutions*. Courier Corporation, 2002.

[266] Vahid Shahrezaei and Peter S Swain. The stochastic nature of biochemical networks. *Current Opinion in Biotechnology*, 19(4):369–374, 2008.

[267] Arjun Raj, Charles S Peskin, Daniel Tranchina, Diana Y Vargas, and Sanjay Tyagi. Stochastic mRNA synthesis in mammalian cells. *PLoS Biology*, 4(10):e309, 2006.

[268] Rex A Kerr, Herbert Levine, Terrence J Sejnowski, and Wouter-Jan Rappel. Division accuracy in a stochastic model of Min oscillations in *Escherichia coli*. *Proceedings of the National Academy of Sciences*, 103(2):347–352, 2006.

[269] Nizar N Batada, Larry A Shepp, and David O Siegmund. Stochastic model of protein–protein interaction: Why signaling proteins need to be colocalized. *Proceedings of the National Academy of Sciences*, 101(17):6445–6449, 2004.

[270] Jean Bouvier, Sylvie Gordia, Gabriele Kampmann, Roland Lange, Regine Hengge-Aronis, and Claude Gutierrez. Interplay between global regulators of *Escherichia coli*: effect of RpoS, Lrp and H-NS on transcription of the gene *osmC*. *Molecular Microbiology*, 28(5):971–980, 1998.

[271] Ch Ueguchi and Takeshi Mizuno. The *Escherichia coli* nucleoid protein H-NS functions directly as a transcriptional repressor. *The EMBO Journal*, 12(3):1039–1046, 1993.

[272] Arthur Koch. *Bacterial growth and form*. Springer Science & Business Media, 2001.

[273] Jaan Männik, Fabai Wu, Felix JH Hol, Paola Bisicchia, David J Sherratt, Juan E Keymer, and Cees Dekker. Robustness and accuracy of cell division in *Escherichia coli* in diverse cell shapes. *Proceedings of the National Academy of Sciences*, 109(18):6957–6962, 2012.

[274] Daniel J Kiviet, Philippe Nghe, Noreen Walker, Sarah Boulineau, Vanda Sunderlikova, and Sander J Tans. Stochasticity of metabolism and growth at the single-cell level. *Nature*, 514(7522):376–379, 2014.

[275] Arjun Raj and Alexander V Oudenaarden. Nature, nurture, or chance: stochastic gene expression and its consequences. *Cell*, 135(2):216–226, 2008.

[276] Dann Huh and Johan Paulsson. Random partitioning of molecules at cell division. *Proceedings of the National Academy of Sciences*, 108(36):15004–15009, 2011.

[277] Mikael Björklund. Cell size homeostasis: Metabolic control of growth and cell division. *Biochimica et Biophysica Acta (BBA)-Molecular Cell Research*, 1866(3):409–417, 2019.

[278] Manuel Campos, Ivan V Surovtsev, Setsu Kato, Ahmad Paintdakhi, Bruno Beltran, Sarah E Ebmeier, and Christine Jacobs-Wagner. A constant size extension drives bacterial cell size homeostasis. *Cell*, 159(6):1433–1446, 2014.

[279] Sattar Taheri-Araghi, Serena Bradde, John T Sauls, Norbert S Hill, Petra A Levin, Johan Paulsson, Massimo Vergassola, and Suckjoon Jun. Cell-size control and homeostasis in bacteria. *Current Biology*, 25(3):385–391, 2015.

[280] Alison C Lloyd. The regulation of cell size. *Cell*, 154(6):1194–1205, 2013.

[281] Jonathan J Turner, Jennifer C Ewald, and Jan M Skotheim. Cell size control in yeast. *Current Biology*, 22(9):R350–R359, 2012.

[282] Fangwei Si, Guillaume Le Treut, John T Sauls, Stephen Vadia, Petra A Levin, and Suckjoon Jun. Mechanistic origin of cell-size control and homeostasis in bacteria. *Current Biology*, 29(11):1760–1770, 2019.

[283] Ariel Amir. Point of view: Is cell size a spandrel? *eLife*, 6:e22186, 2017.

[284] Philipp Thomas. Analysis of cell size homeostasis at the single-cell and population level. *Frontiers in Physics*, 6:64, 2018.

[285] Bo Li, Bin Shao, Chenlu Yu, Qi Ouyang, and Hongli Wang. A mathematical model for cell size control in fission yeast. *Journal of Theoretical Biology*, 264(3):771–781, 2010.

[286] Stephen Cooper. Control and maintenance of mammalian cell size. *BMC Cell Biology*, 5(1):35, 2004.

[287] Frederick R Cross, Vincent Archambault, Mary Miller, and Martha Klovstad. Testing a mathematical model of the yeast cell cycle. *Molecular Biology of the Cell*, 13(1):52–70, 2002.

[288] Clotilde Cadart, Sylvain Monnier, Jacopo Grilli, Pablo J S'aez, Nishit Srivastava, Rafaele Attia, Emmanuel Terriac, Buzz Baum, Marco Cosentino-Lagomarsino, and Matthieu Piel. Size control in mammalian cells involves modulation of both growth rate and cell cycle duration. *Nature communications*, 9(1):1–15, 2018.

[289] Marek Kimmel and David E Axelrod. Unequal cell division, growth regulation and colony size of mammalian cells: a mathematical model and analysis of experimental data. *Journal of Theoretical Biology*, 153(2):157–180, 1991.

[290] Peter A Fantes and Paul Nurse. Division timing: controls, models and mechanisms. *The Cell Cycle*, pages 11–33, 1981.

[291] William D Donachie. Relationship between cell size and time of initiation of DNA replication. *Nature*, 219(5158):1077–1079, 1968.

[292] Peter A Fantes, William D Grant, Robert H Pritchard, Peter E Sudbery, and Alan E Wheals. The regulation of cell size and the control of mitosis. *Journal of Theoretical Biology*, 50(1):213–244, 1975.

[293] Ariel Amir. Cell size regulation in bacteria. *Physical Review Letters*, 112(20):208102, 2014.

[294] Shiladitya Banerjee, Klevin Lo, Matthew K Daddysman, Alan Selewa, Thomas Kuntz, Aaron R Dinner, and Norbert F Scherer. Biphasic growth dynamics control cell division in caulobacter crescentus. *Nature Microbiology*, 2(9):17116, 2017.

[295] Maxime Deforet, Dave V Ditmarsch, and Joao B Xavier. Cell-size homeostasis and the incremental rule in a bacterial pathogen. *Biophysical Journal*, 109(3):521–528, 2015.

[296] Yanyan Chen, Rosa Baños, and Javier Buceta. A markovian approach towards bacterial size control and homeostasis in anomalous growth processes. *Scientific Reports*, 8(9612):1–13, 2018.

[297] Khem R Ghusinga, Cesar A Vargas-Garcia, and Abhyudai Singh. A mechanistic stochastic framework for regulating bacterial cell division. *Scientific Reports*, 6(30229):1–9, 2016.

[298] Yu Tanouchi, Anand Pai, Heungwon Park, Shuqiang Huang, Rumen Stamatov, Nicolas E Buchler, and Lingchong You. A noisy linear map underlies oscillations in cell size and gene expression in bacteria. *Nature*, 523(7560):357–360, 2015.

[299] Fangwei Si, Dongyang Li, Sarah E Cox, John T Sauls, Omid Azizi, Cindy Sou, Amy B Schwartz, Michael J Erickstad, Yonggun Jun, Xintian Li, and Suckjoon Jun. Invariance of initiation mass and predictability of cell size in *Escherichia coli*. *Current Biology*, 27(9):1278–1287, 2017.

[300] Douglas E Dix and Charles E Helmstetter. Coupling between chromosome completion and cell division in *Escherichia coli*. *Journal of Bacteriology*, 115(3):786–795, 1973.

[301] Po-Yi Ho and Ariel Amir. Simultaneous regulation of cell size and chromosome replication in bacteria. *Frontiers in Microbiology*, 6:662, 2015.

[302] Daniel P Haeusser and Petra A Levin. The great divide: coordinating cell cycle events during bacterial growth and division. *Current Opinion in Microbiology*, 11(2):94–99, 2008.

[303] Mats Wallden, David Fange, Ebba G Lundius, Özden Baltekin, and Johan Elf. The synchronization of replication and division cycles in individual *E. coli* cells. *Cell*, 166(3):729–739, 2016.

[304] Seoungjun Lee, Ling J Wu, and Jeff Errington. Microfluidic time-lapse analysis and reevaluation of the *Bacillus subtilis* cell cycle. *MicrobiologyOpen*, 8(10):e876, 2019.

[305] Lisa Willis and Kerwyn C Huang. Sizing up the bacterial cell cycle. *Nature Reviews Microbiology*, 15(10):606, 2017.

[306] William D Donachie and Garry W Blakely. Coupling the initiation of chromosome replication to cell size in *Escherichia coli*. *Current Opinion in Microbiology*, 6(2):146–150, 2003.

[307] Charles E Helmstetter and Stephen Cooper. DNA synthesis during the division cycle of rapidly growing *Escherichia coli Br*. *Journal of Molecular Biology*, 31(3):507–518, 1968.

[308] Olivia Padovan-Merhar, Gautham P Nair, Andrew G Biaesch, Andreas Mayer, Steven Scarfone, Shawn W Foley, Angela R Wu, L Stirling Churchman, Abhyudai Singh, and Arjun Raj. Single mammalian cells compensate for differences in cellular volume and DNA copy number through independent global transcriptional mechanisms. *Molecular Cell*, 58(2):339–352, 2015.

[309] Samuel Marguerat, Alexander Schmidt, Sandra Codlin, Wei Chen, Ruedi Aebersold, and Jürg Bähler. Quantitative analysis of fission yeast transcriptomes and proteomes in proliferating and quiescent cells. *Cell*, 151(3):671–683, 2012.

[310] Gerald C Johnston, John R Pringle, and Leland H Hartwell. Coordination of growth with cell division in the yeast *Saccharomyces cerevisiae*. *Experimental Cell Research*, 105(1):79–98, 1977.

[311] Peter A Fantes. Control of cell size and cycle time in *Schizosaccharomyces pombe*. *Journal of Cell Science*, 24(1):51–67, 1977.

[312] Giuseppe Facchetti, Fred Chang, and Martin Howard. Controlling cell size through sizer mechanisms. *Current Opinion in Systems Biology*, 5:86–92, 2017.

[313] Suckjoon Jun and Sattar Taheri-Araghi. Cell-size maintenance: universal strategy revealed. *Trends in Microbiology*, 23(1):4–6, 2015.

[314] Michelle M Logsdon, Po-Yi Ho, Kadamba Papavinasasundaram, Kirill Richardson, Murat Cokol, Christopher M Sassetti, Ariel Amir, and Bree B Aldridge. A parallel adder coordinates mycobacterial cell-cycle progression and cell-size homeostasis in the context of asymmetric growth and organization. *Current Biology*, 27(21):3367–3374, 2017.

[315] Arthur D Edelstein, Mark A Tsuchida, Nenad Amodaj, Henry Pinkard, Ronald D Vale, and Nico Stuurman. Advanced methods of microscope control using μmanager software. *Journal of Biological Methods*, 1(2), 2014.

[316] Peter S Swain, Michael B Elowitz, and Eric D Siggia. Intrinsic and extrinsic contributions to stochasticity in gene expression. *Proceedings of the National Academy of Sciences*, 99(20):12795–12800, 2002.

[317] Sara Via and Russell Lande. Genotype-environment interaction and the evolution of phenotypic plasticity. *Evolution*, 39(3):505–522, 1985.

[318] Bo Hu, David A Kessler, Wouter-Jan Rappel, and Herbert Levine. How input fluctuations reshape the dynamics of a biological switching system. *Physical Review E*, 86(6):061910, 2012.

[319] David R Soll. High-frequency switching in *Candida albicans*. *Clinical Microbiology Reviews*, 5(2):183–203, 1992.

[320] Kevin Alby and Richard J Bennett. Stress-induced phenotypic switching in *Candida albicans*. *Molecular Biology of the Cell*, 20(14):3178–3191, 2009.

[321] Ana M Sousa, Idalina Machado, and Maria O Pereira. Phenotypic switching: an opportunity to bacteria thrive. *Science Against Microbial Pathogens: Communicating Current Research and Technological Advances*, 1:252–262, 2012.

[322] Magee Allegrucci and Karin Sauer. Characterization of colony morphology variants isolated from *Streptococcus pneumoniae* biofilms. *Journal of Bacteriology*, 189(5):2030–2038, 2007.

[323] Susanne Häußler, Isabell Ziegler, Alexandra Löttel, Franz v Götz, Manfred Rohde, Dirk Wehmhöhner, Selvan Saravanamuthu, Burkhard Tümmler, and Ivo Steinmetz. Highly adherent small-colony variants of *Pseudomonas aeruginosa* in cystic fibrosis lung infection. *Journal of Medical Microbiology*, 52(4):295–301, 2003.

[324] Nele Wellinghausen, Indranil Chatterjee, Anja Berger, Andrea Niederfuehr, Richard A Proctor, and Barbara C Kahl. Characterization of clinical enterococcus faecalis small-colony variants. *Journal of Clinical Microbiology*, 47(9):2802–2811, 2009.

[325] John R Roche and Richard E Moxon. Phenotypic variation in haemophilus influenzae: the interrelationship of colony opacity, capsule and lipopolysaccharide. *Microbial Pathogenesis*, 18(2):129–140, 1995.

[326] Nathalie Q Balaban, Jack Merrin, Remy Chait, Lukasz Kowalik, and Stanislas Leibler. Bacterial persistence as a phenotypic switch. *Science*, 305(5690):1622–1625, 2004.

[327] Jacques Monod. Recherches sur la croissance des cultures bacteriennes. hermann et cie, paris (1942). *Ann. Inst. Pasteur*, 69:179, 1943.

[328] Benno Müller-Hill and Stefan Oehler. *The* lac *operon*. Walter de Gruyter New York:, 1996.

[329] Francois Jacob, Agnes Ullmann, and Jacques Monod. D'el'etions fusionnant l'op'eron lactose et un op'eron purine chez *Escherichia coli*. *Journal of Molecular Biology*, 13(3):704–719, 1965.

[330] Sankar Adhya. The *lac*and gal operons today. In *Regulation of gene expression in* Escherichia coli, pages 181–200. Springer, 1996.

[331] Sol Spiegelman. Differentiation as the controlled production of unique enzymatic patterns. In *Symp. Soc. Exp. Biol*, volume 2, pages 286–325, 1948.

[332] Atul Narang and Sergei S Pilyugin. Bistability of the *lac* operon during growth of *Escherichia coli* on lactose and lactose+ glucose. *Bulletin of mathematical biology*, 70(4):1032–1064, 2008.

[333] Anja Marbach and Katja Bettenbrock. *lac* operon induction in *Escherichia coli*: systematic comparison of iptg and tmg induction and influence of the transacetylase laca. *Journal of Biotechnology*, 157(1):82–88, 2012.

[334] Peter C Maloney and Boris Rotman. Distribution of suboptimally induced $\beta$-d-galactosidase in *Escherichia coli*: the enzyme content of individual cells. *Journal of Molecular Biology*, 73(1):77–91, 1973.

[335] Aaron Novick and Milton Weiner. Enzyme induction as an all-or-none phenomenon. *Proceedings of the National Academy of Sciences of the United States of America*, 43(7):553, 1957.

[336] Ertugrul M Ozbudak, Mukund Thattai, Han N Lim, Boris I Shraiman, and Alexander V Oudenaarden. Multistability in the lactose utilization network of *Escherichia coli*. *Nature*, 427(6976):737, 2004.

[337] Mois'es Santill'an, Michael C Mackey, and Eduardo S Zeron. Origin of bistability in the *lac* operon. *Biophysical Journal*, 92(11):3830–3842, 2007.

[338] David I Orozco-G'omez, Juan E Sosa-Hern'andez, 'Oscar A Gallardo-Navarro, Jes'us Santana-Solano, and Mois'es Santill'an. Bistable behaviour and medium-dependent post-translational regulation of the tryptophanase operon regulatory pathway in *Echerichia coli*. *Scientific Reports*, 9(5451):1–13, 2019.

[339] Xiaona Fang, Qiong Liu, Christopher Bohrer, Zach Hensel, Wei Han, Jin Wang, and Jie Xiao. Cell fate potentials and switching kinetics uncovered in a classic bistable genetic switch. *Nature Communications*, 9(1):1–9, 2018.

[340] Richard W Schevitz, Zdzislaw Otwinowski, Andrzej Joachimiak, Catherine L Lawson, and Paul B Sigler. The three-dimensional structure of trp repressor. *Nature*, 317(6040):782–786, 1985.

[341] Harvey Lodish, Arnold Berk, S Lawrence Zipursky, Paul Matsudaira, David Baltimore, and James Darnell. Bacterial gene control: The Jacob-Monod model. In *Molecular Cell Biology. 4th edition*. WH Freeman, 2000.

[342] Melvin Cohn and Kengo Horibata. Analysis of the differentiation and of the heterogeneity within a population of *Escherichia coli* undergoing induced $\beta$-galactosidase synthesis. *Journal of Bacteriology*, 78(5):613, 1959.

[343] Bidisha Banerjee, Sivashankaran Balasubramanian, Garani Ananthakrishna, Tamilthiruvalluvar V Ramakrishnan, and GV Shivashankar. Tracking operator state fluctuations in gene expression in single cells. *Biophysical Journal*, 86(5):3052–3059, 2004.

[344] Janith S Griffith. Mathematics of cellular control processes. I. Negative feedback to one gene. *Journal of Theoretical Biology*, 20(2):202–208, 1968.

[345] Necmettin Yildirim, Moises Santillan, Daisuke Horike, and Michael C Mackey. Dynamics and bistability in a reduced model of the *lac* operon. *Chaos: An Interdisciplinary Journal of Nonlinear Science*, 14(2):279–292, 2004.

[346] Orlando D'ıaz-Hern'andez and Mois'es Santill'an. Bistable behavior of the *lac* operon in *E. coli* when induced with a mixture of lactose and TMG. *Frontiers in Physiology*, 1:158, 2010.

[347] Alan Veliz-Cuba and Brandilyn Stigler. Boolean models can explain bistability in the *lac* operon. *Journal of Computational Biology*, 18(6):783–794, 2011.

[348] Dominique Zander, Daniel Samaga, Ronny Straube, and Katja Bettenbrock. Bistability and nonmonotonic induction of the *lac* operon in the natural lactose uptake system. *Biophysical Journal*, 112(9):1984–1996, 2017.

[349] Buford P Price and Todd Sowers. Temperature dependence of metabolic rates for microbial growth, maintenance, and survival. *Proceedings of the National Academy of Sciences*, 101(13):4631–4636, 2004.

[350] Michal Ronen, Revital Rosenberg, Boris I Shraiman, and Uri Alon. Assigning numbers to the arrows: parameterizing a gene regulation network by using accurate expression kinetics. *Proceedings of the National Academy of Sciences*, 99(16):10555–10560, 2002.

[351] Yaakov Setty, Avraham E Mayo, Michael G Surette, and Uri Alon. Detailed map of a cis-regulatory input function. *Proceedings of the National Academy of Sciences*, 100(13):7702–7707, 2003.

[352] David L Nelson, Albert L Lehninger, and Michael M Cox. *Lehninger Principles of Biochemistry*. Macmillan, 2008.

[353] David W Dreisigmeyer, Jelena Stajic, Ilya Nemenman, William S Hlavacek, and Michael E Wall. Determinants of bistability in induction of the *Escherichia coli lac* operon. *IET Systems Biology*, 2(5):293–303, 2008.

[354] Jesse Stricker, Scott Cookson, Matthew R Bennett, William H Mather, Lev S Tsimring, and Jeff Hasty. A fast, robust and tunable synthetic gene oscillator. *Nature*, 456(7221):516–519, 2008.

[355] Jerome G Chandraseelan, Samuel MD Oliveira, Antti Häkkinen, Huy Tran, Ilya Potapov, Adrien Sala, Meenakshisundaram Kandhavelu, and Andre S Ribeiro. Effects of temperature on the dynamics of the LacI-TetR-CI repressilator. *Molecular BioSystems*, 9(12):3117–3123, 2013.

[356] John Ryals, Roderick Little, and Hans Bremer. Temperature dependence of RNA synthesis parameters in *Escherichia coli*. *Journal of Bacteriology*, 151(2):879–887, 1982.

[357] Feng Gong, Koichi Ito, Yoshikazu Nakamura, and Charles Yanofsky. The mechanism of tryptophan induction of tryptophanase operon expression: tryptophan inhibits release factor-mediated cleavage of TnaC-peptidyl-tRNAPro. *Proceedings of the National Academy of Sciences*, 98(16):8997–9001, 2001.

[358] Johan H van Heerden, Meike T Wortel, Frank J Bruggeman, Joseph J Heijnen, Yves JM Bollen, Robert Planqu'e, Josephus Hulshof, Tom G O'Toole, Aljoscha S Wahl, and Bas Teusink. Lost in transition: start-up of glycolysis yields subpopulations of nongrowing cells. *Science*, 343(6174):1245114, 2014.

[359] Jenna Gallie, Eric Libby, Frederic Bertels, Philippe Remigi, Christian B Jendresen, Gayle C Ferguson, Nicolas Desprat, Marieke F Buffing, Uwe Sauer, Hubertus JE Beaumont, Jan Martinuseen, Mogens Kilstrup, and Paul B. Rainey. Bistability in a metabolic network underpins the de novo evolution of colony switching in *Pseudomonas fluorescens*. *PLoS Biol*, 13(3):e1002109, 2015.

# Appendix A

## Description of Research for Popular Publication

### A1 Study of Bacterial Response in Fluctuating Environments

Environmental fluctuations are inevitable. Bacteria experience stress when they are grown in an unfamiliar environment. Organisms adapt with time in the surrounding environments they live. If the environmental stress is very high, cells may either adapt to the new environment or become extinct. The selective pressure caused by the environment might lead to the evolution on the organisms. Origin and evolution of life are fundamental and exciting questions, and to find the solution is extremely challenging. Significant progress has been made toward the techniques and the methods to study the fundamental mechanism cellular processes, but a satisfactory answer regarding origin of life is still elusive. Therefore, to understand and contribute to the field, Sudip Nepal joined a research team dedicated to addressing these questions using experimental, theoretical, numerical, and biological techniques. During his research, he worked on several projects that involved various techniques and experiments that required a long time. The studies carried out contribute to understanding the response of bacteria in steady and fluctuating environments. The study might help to understand the origin of life and explore the possibility of life on the extraterrestrial planets.

The first part of the project was to explore the growth and morphology of anaerobic thermophilic methanogen at different temperatures, pH, and pressures. *Methanothermobacter wolfeii*, an anaerobic archaea, survives in a wide range of temperature, pressure, and pH. The growth rate of the cells increases with the increase in pressure in acidic medium and, cells tolerate a pH of $5 - 9$ at 55 °C. Cell morphology remains intact at high pressures. The production of methane is maximum at the pressure and temperature of 800 atm and 65 °C, respectively. Geochemical models show the possibility of similar conditions on the martian subsurfaces and might help to understand the possibility of life in such places.

The second part of the project was to study the phenotypic switching of bacterial cells

at high pressure. *Escherichia coli*, mesophilic bacterium, has an optimal growth rate at atmospheric pressure and temperature of 37 °C. Cells elongate at high pressure and become filamented due to a lack of cell division and revert to normal length upon removing the pressure in temporal relaxation. Using a stochastic model of cell growth and division, it is observed that the experimental data on the switching of the cells from low-pressure morphology to high-pressure morphology and vice versa can be accounted by the growth, division, and the switching rates of the cells. The stress experienced by the cell is smaller at the oscillatory pressure compared to continuous pressures. When the pressure release time is 10 minutes, bacteria do not experience the stress in morphological perspective.

The third part of the research was to observe the growth, cell division, morphology, plasmolysis, gene expression, and reversibility of bacteria in an elevated concentration of magnesium sulfate. The project deals with the effect of high concentration of magnesium sulfate, presumably the most prevalent salt on one of the icy bodies in our solar system, Europa, one of the Galilean moons of Jupiter. High salt stress causes the cells to plasmolyze, decrease in growth rate, and cell death. The average length of cells is a non-monotonic function of salt concentration. The survival fraction of the cells is not affected at the concentration range of $0 - 1.25$ M of salt. Beyond 1.25 M of salt, the survival fraction decreases monotonically. At concentration $\geq 2.07$ M, the cells do not survive in the time period of the experiments. These results helped characterize the range of salt concentrations for the long-term evolution of *E. coli* to extreme physicochemical conditions.

The fourth part of the project was to study the cell-size homeostasis in bacteria under high concentration of $MgSO_4$ stress. Cell-size control and homeostasis are the fundamental characteristics of organisms. A nearly uniform size of bacterial cells is maintained by growth and division regardless of the size at the birth and the stochastic processes underlying it. Any of the three proposed models can describe cell-size homeostasis for the cells grown under normal conditions — (i) timer, (ii) sizer, and (iii) the adder. In this project, the mechanistic view of cell-size homeostasis for the cells grown in a media containing a high concentration of

magnesium sulfate was studied. The cells exhibited heterogeneity in cell lengths at the concentration of 1.25 M $MgSO_4$. A small fraction of cells became smaller than the control cells, while a large number of cells became elongated due to a lack of cell division. The heterogeneity in the cell length decreased upon removing the high salt stress over a few regeneration time. The study of real-time dynamics of cell division showed that bacteria add a constant mass in successive divisions, and the size becomes comparable to the control cells with generations regardless of the size at birth. These studies might help to understand the size control and homeostasis system for mammalian cells.

The fifth part of the project was to examine the temperature dependence of multistability in the lactose utilization network of *E. coli*. Lactose utilization network exhibited bistability in the presence of glucose and lactose in the media. The bistable behavior depended on the temperature and repression factor, the ratio of maximum to basal activity of the polymerase. At low temperatures, the bistable system changed to a monostable system due to a decrease in the repression factor. The switching from bistable to monostable system is applicable to building biological switches.

## Appendix B

### Executive Summary of Newly Created Intellectual Property

The newly created intellectual property during the course of research are listed below:

1. The numerical simulation method to study the cell division.

2. The method to extract the cell length and study of the cell division processes in control and stressed environments.

# Appendix C

## Potential Patent and Commercialization Aspects of Listed Intellectual Property Items

### C1 Patentability of Intellectual Property

The newly created intellectual properties in Appendix B are modified from existing methods, mathematical equations, and algorithms. Hence, these items can not be patented.

### C2 Commercialization Prospects

Not applicable

### C3 Possible Prior Disclosure of IP

Not applicable

# Appendix D

## Broader Impact of Research

### D1 Applicability of Research Methods to Other Problems

Bacteria can grow at diverse environmental conditions. The methods used to study the response of bacteria under extreme conditions is useful to investigate the stress response of bacteria at several other stresses like pH, temperature, antibiotics, and radiation. The study of gene expression at high salt concentration shows the upregulation of the genes related to transporter of thiosulfate and osmotic stress response. A similar method can be adopted to study the gene expression of other genes associated with the synthesis of RpoS, H-NS, and LrP. The cell division models discussed have a wide range of applications. The models are equally applicable to yeast and mammalian cells. The temperature dependence bistability implies that the metabolism of bacteria is temperature dependent. Similar methods can be used to study the metabolism in other several stresses present in the natural environment.

### D2 Impact of Research on US and Global Society

The research conducted here has wide application. The study was carried out using *Escherichia coli* as a model organism to study the cellular processes. The cell division study might be applicable to understand the somatic cell division and growth process of several organs in higher organisms. Studies on extreme conditions are important to understand the possibility of life on extraterrestrial bodies including Mars, Europa, Ceres, and Enceladus. These studies are also important from the planetary protection perspective. Furthermore, these studies might help understanding the evolution and adaptation of living organisms.

### D3 Impact of Research on the Environment

The research carried out during the project has no known harmful or positive effects on the environment.

## Appendix E

## Microsoft Project for MicroEP PhD Degree Plan

| | Task Name | Duration | Start | Finish |
|---|---|---|---|---|
| 41 | **Research** | **1295 days** | **Thu 10/1/15** | **Mon 9/14/20** |
| 42 | Define Experiments | 3 mons | Thu 10/1/15 | Wed 12/23/15 |
| 43 | Make sample ready | 4 mons | Thu 12/24/15 | Wed 4/13/16 |
| 44 | Check the reliability of the samples | 1 mon | Thu 4/14/16 | Wed 5/11/16 |
| 45 | **Perform Experiments** | **1065 days** | **Tue 6/28/16** | **Thu 7/23/20** |
| 46 | Experiment 1(Cell division of bacteria | 150 days | Tue 6/28/16 | Mon 1/23/17 |
| 47 | Experiment 2 ( Characterization of ba | 250 days | Tue 6/6/17 | Mon 5/21/18 |
| 48 | Experiment 3( Cell division of bacteri | 175 days | Tue 5/22/18 | Thu 1/17/19 |
| 49 | Experiment 4 (Lactose utilization net | 200 days | Tue 2/12/19 | Mon 11/18/19 |
| 50 | Experiment 5(Adaptive evolution of b | 178 days | Tue 11/19/19 | Thu 7/23/20 |
| 51 | **Analyze Results** | **1013 days** | **Mon 10/31/1** | **Mon 9/14/20** |
| 52 | Experiment 1(Cell division of bacteria | 100 days | Mon 10/31/1 | Wed 5/17/17 |
| 53 | Experiment 2 ( Characterization of ba | 200 days | Thu 7/27/17 | Wed 1/30/19 |
| 54 | Experiment 3( Cell division of bacteri | 200 days | Tue 5/1/18 | Mon 10/14/19 |
| 55 | Experiment 4 (Lactose utilization net | 80 days | Tue 11/5/19 | Mon 2/24/20 |
| 56 | Experiment 5(Adaptive evolution of b | 200 days | Tue 12/10/19 | Mon 9/14/20 |
| 57 | **Write Dissertation** | **227 days** | **Thu 9/12/19** | **Fri 7/24/20** |
| 58 | Chapter 1: Introduction | 43 days | Thu 9/12/19 | Mon 11/11/19 |
| 59 | Chapter 2: Cell division of bacteria at hig | 20 days | Wed 11/13/1 | Tue 12/10/19 |
| 60 | Chapter 3: Characterization of bacteria a | 20 days | Wed 12/11/1 | Tue 1/7/20 |
| 61 | Chapter 4: Cell division of bacteria at hig | 35 days | Fri 1/10/20 | Thu 2/27/20 |
| 62 | Chapter 5: Lactose utilization network | 45 days | Tue 3/3/20 | Mon 5/4/20 |
| 63 | Chapter 6: Conclusion | 10 days | Tue 5/5/20 | Mon 5/18/20 |
| 64 | Chapter 7: Future work | 10 days | Wed 5/20/20 | Tue 6/2/20 |
| 65 | Appendix | 10 days | Thu 6/4/20 | Wed 6/17/20 |
| 66 | Dissertation revision | 12 days | Thu 7/9/20 | Fri 7/24/20 |
| 67 | **END GAME** | **1 day** | **Fri 7/24/20** | **Fri 7/24/20** |
| 78 | Graduate | 1 day | Fri 7/24/20 | Fri 7/24/20 |

**Microsoft Project for MicroEP PhD Degree Plan (Contd.)**

| | Task Name | Duration | Start | Finish |
|---|---|---|---|---|
| 41 | **Research** | **1295 days** | **Thu 10/1/15** | **Mon 9/14/20** |
| 42 | Define Experiments | 3 mons | Thu 10/1/15 | Wed 12/23/15 |
| 43 | Make sample ready | 4 mons | Thu 12/24/15 | Wed 4/13/16 |
| 44 | Check the reliability of the samples | 1 mon | Thu 4/14/16 | Wed 5/11/16 |
| 45 | **Perform Experiments** | **1065 days** | **Tue 6/28/16** | **Thu 7/23/20** |
| 46 | Experiment 1(Cell division of bacteria | 150 days | Tue 6/28/16 | Mon 1/23/17 |
| 47 | Experiment 2 ( Characterization of ba | 250 days | Tue 6/6/17 | Mon 5/21/18 |
| 48 | Experiment 3( Cell division of bacteri | 175 days | Tue 5/22/18 | Thu 1/17/19 |
| 49 | Experiment 4 (Lactose utilization netv | 200 days | Tue 2/12/19 | Mon 11/18/19 |
| 50 | Experiment 5(Adaptive evolution of b | 178 days | Tue 11/19/19 | Thu 7/23/20 |
| 51 | **Analyze Results** | **1013 days** | **Mon 10/31/1** | **Mon 9/14/20** |
| 52 | Experiment 1(Cell division of bacteria | 100 days | Mon 10/31/1 | Wed 5/17/17 |
| 53 | Experiment 2 ( Characterization of ba | 200 days | Thu 7/27/17 | Wed 1/30/19 |
| 54 | Experiment 3( Cell division of bacteri | 200 days | Tue 5/1/18 | Mon 10/14/19 |
| 55 | Experiment 4 (Lactose utilization netv | 80 days | Tue 11/5/19 | Mon 2/24/20 |
| 56 | Experiment 5(Adaptive evolution of b | 200 days | Tue 12/10/19 | Mon 9/14/20 |
| 57 | **Write Dissertation** | **227 days** | **Thu 9/12/19** | **Fri 7/24/20** |
| 58 | Chapter 1: Introduction | 43 days | Thu 9/12/19 | Mon 11/11/19 |
| 59 | Chapter 2: Cell division of bacteria at hig | 20 days | Wed 11/13/1 | Tue 12/10/19 |
| 60 | Chapter 3: Characterization of bacteria a | 20 days | Wed 12/11/1 | Tue 1/7/20 |
| 61 | Chapter 4: Cell division of bacteria at hig | 35 days | Fri 1/10/20 | Thu 2/27/20 |
| 62 | Chapter 5: Lactose utilization network | 45 days | Tue 3/3/20 | Mon 5/4/20 |
| 63 | Chapter 6: Conclusion | 10 days | Tue 5/5/20 | Mon 5/18/20 |
| 64 | Chapter 7: Future work | 10 days | Wed 5/20/20 | Tue 6/2/20 |
| 65 | Appendix | 10 days | Thu 6/4/20 | Wed 6/17/20 |
| 66 | Dissertation revision | 12 days | Thu 7/9/20 | Fri 7/24/20 |
| 67 | **END GAME** | **1 day** | **Fri 7/24/20** | **Fri 7/24/20** |
| 78 | Graduate | 1 day | Fri 7/24/20 | Fri 7/24/20 |

## Appendix F

### Identification of All Softwares Used in Research and Dissertation Generation

Computer #1: Personal laptop

Model Number: MacBook Pro (Retina, 13 inch, Early 2015)

Serial Number: C17QC8ZXFVH3

Location: Personal

Owner: Sudip Nepal

Software #1:

Name: Microsoft Office 365

Purchased by: Free download for the students provided by University of Arkansas

Software #2:

Name: Dropbox

Purchased by: Free version for personal use

Software #3:

Name: TexShop

Purchased by: Free version for personal use

Software #4:

Name: Texmaker

Purchased by: Free version for personal use

Software #5:

Name: MATLAB

Purchased by: Free download for the students provided by University of Arkansas

Software #6:

Name: ImageJ

Purchased by: Free version for personal use

Software #7:

Name: Grace

Purchased by: Free version for personal use

Software #8:

Name: Prism 8

Purchased by: Purchased by Pradeep Kumar

Software #9:

Name: Keynote

Purchased by: Free version for personal use

Software #10:

Name: Preview

Purchased by: Free version for personal use

Software #11:

Name: Microsoft Project

Purchased by: Free download for the students provided by University of Arkansas

Computer #2: Personal Desktop Computer

Model Number: HP All in One

Serial Number: 8CC7331BWG

Location: Personal

Owner: Pradeep Kumar

Software #1:

Name: Microsoft Office 365

Purchased by: Free download for students provided by University of Arkansas

Software #2:

Name: Dropbox

Purchased by: Free version for personal use

Software #3:

Name: TexShop

Purchased by: Free version for personal use

Software #4:

Name: texmaker

Purchased by: Free version for personal use

Software #5:

Name: ImageJ

Purchased by: Free version for personal use

Computer #3: Personal Desktop Computer

Model Number: N/A (Custom built)

Serial Number: N/A (Custom built)

Location: PHYS 126

Owner: Pradeep Kumar

Software #1:

Name: Microsoft Office 365

Purchased by: Free download for students provided by University of Arkansas

Software #2:

Name: ImageJ

Purchased by: Free version for personal use

Software #3:

Name: Micro-Manager-1.4

Purchased by: Free version for personal use

Software #4:

Name: MATLAB

Purchased by: Free download for students provided by University of Arkansas

Software #5:

Name: SPOT software 5.1

Purchased by: Pradeep Kumar

## Appendix G

## All Publications Published, Submitted, and Planned

1. **Published**

    - **Sudip Nepal** and Pradeep Kumar. Growth, Cell Division, and Gene Expression of *Escherichia coli* at Elevated Concentrations of Magnesium Sulfate: Implications for Habitability of Europa and Mars. *Microorganisms* 8.5 (2020): 637.
    - **Sudip Nepal** and Pradeep Kumar. Dynamics of phenotypic switching of bacterial cells with temporal fluctuations in pressure. *Physical Review E* 97.5 (2018): 052411.
    - Navita Sinha, **Sudip Nepal**, Timothy A Kral, and Pradeep Kumar, Survivability and growth kinetics of methanogenic archaea at various PHs and pressures: Implication for deep subsurface life on Mars. *Planetary and Space Science* 136 (2017): 15-24.
    - Navita Sinha, **Sudip Nepal**, Timothy A Kral, and Pradeep Kumar. Effect of temperature and high pressures on the growth and survivability of methanogens and stable carbon isotope fractionation: Implication for deep subsurface life on Mars. *International Journal of Astrobiology* (2018):1-7.

2. **Planned**

    - **Sudip Nepal**, Khanh Nguyen, and Pradeep Kumar. Constant Mass Addition and Symmetric Cell Division Drive Size Homeostasis in Filamentous Cells Obtained at High Concentration of Magnesium Sulfate.
    - **Sudip Nepal** and Pradeep Kumar. Temperature dependence of multistability of the lactose utilization network of *Escherichia coli*.
    - **Sudip Nepal**, Khanh Nguyen, Steven Murray, and Pradeep Kumar. Temporal dynamics of adaptive evolution of *Escherichia coli* at high hydrostatic pressure: A

phenotypic and genotypic study.

# Appendix H

## IBC Protocol


June 3, 2016

MEMORANDUM

| | |
|---|---|
| TO: | Dr. Pradeep Kumar |
| FROM: | Ines Pinto, Biosafety Committee Chair |
| RE: | New Protocol |
| PROTOCOL #: | 16039 |
| PROTOCOL TITLE: | Adaptive evolution and stochastic gene regulation in bacteria under fluctuating environment |
| APPROVED PROJECT PERIOD: | Start Date May 12, 2016 Expiration Date May 11, 2019 |

The Institutional Biosafety Committee (IBC) has approved Protocol 16039, “Adaptive evolution and stochastic gene regulation in bacteria under fluctuating environment”. You may begin your study.

If modifications are made to the protocol during the study, please submit a written request to the IBC for review and approval before initiating any changes.

The IBC appreciates your assistance and cooperation in complying with University and Federal guidelines for research involving hazardous biological materials.

# Appendix I

## Codes

### I1 MATLAB Code to Extract Length of Bacteria

```
clear all
%Choose a cutoff length for bacteria
cutoffL2=40;
cutoffL1=1.0;
scale40x=8; % The images are 8 pixel per micron
%Number of bacteria detected for each image files
nBacFound=1;
%Loop for number of images
for nimage=1:100
 nimage
 imfile = sprintf('Image%d.tif', nimage);
  BW=imread(imfile);
   BW=1-BW;
 [B,L,N,A] = bwboundaries(BW,'noholes');
arcL = zeros(1,N);
for i=1:N
 d=cell2mat(B(i));
 minY = min(d(:,1));
 maxY = max(d(:,1));
 maxX = max(d(:,2));
 minX = min(d(:,2));
 dX = maxX-minX;
 dY = maxY-minY;
 if(dX>=dY & dX>2)
    lengthX = maxX-minX+1;
    meanYvals = zeros(lengthX,1);
    n=1;
    for k=minX:maxX
```

```
    idx = find(d(:,2)==k);
    yVals = d(idx);
    diam(n) = length(min(yVals):max(yVals));
    meanYvals(n) = sum(min(yVals):max(yVals))/(length(min(yVals):max(yVals)));
    % take the average y-values for a given x
    n=n+1;
   end
% now we have y as a function of x for each connected component of the
% image.
X = minX:maxX;
X=X';
Y = meanYvals;
 %determine the order of polynomial
nOrder = floor(dX/200)+2;
parFit = polyfit(X,Y,nOrder);
derL=0;
func = 0;
for np=1:nOrder
    derL = derL+(nOrder-np+1)*parFit(np)*X.^(nOrder-np);
end
for np=1:nOrder+1
    func = func + parFit(np)*X.^(nOrder-np+1);
end
arcL(i) = sum(sqrt(1+derL.*derL));
arcL(i) = arcL(i)/scale100x;
meanDiam(i) = mean(diam)/scale100x;
end
if(dY>dX & dY>2)
   lengthX = maxY-minY+1;
   meanYvals = zeros(lengthX,1);
   n=1;
   for k=minY:maxY
    idx = find(d(:,1)==k);
```

```
    yVals = d(idx,2);
    meanYvals(n) = sum(min(yVals):max(yVals))/(length(min(yVals):max(yVals)));
    % take the average y-  %values for a given x
    diam(n) = length(min(yVals):max(yVals));
    n=n+1;
   end
% now we have y as a function of x for each connected component of the image.
X = minY:maxY;
X=X';
Y = meanYvals;
%determine the order of polynomial
nOrder = floor(dY/200)+2;
parFit = polyfit(X,Y,nOrder);
derL=0;
func = 0;
for np=1:nOrder
    derL = derL+(nOrder-np+1)*parFit(np)*X.^(nOrder-np);
end
for np=1:nOrder+1
    func = func + parFit(np)*X.^(nOrder-np+1);
end
arcL(i) = sum(sqrt(1+derL.*derL));
arcL(i) = arcL(i)/scale100x;
meanDiam(i) = mean(diam)/scale40x;
end
end
% arcL contains the length of all the bacteria. Now choose only the
% bacteria which are properly oriented. For that we will choose a cutoff
% length (unless otherwise one is looking at a different bacteria).
n=1;
for k=1:length(arcL)
    if(arcL(k)>cutoffL2)
        imfile
```

```
        break;
    end
    if(arcL(k)>cutoffL1 && arcL(k)<cutoffL2)
    realL(n)=arcL(k);
    bacLength(nBacFound)=realL(n);
    nBacFound = nBacFound+1;
    n=n+1;
    end
 end
end
% fill the array of lengths with the length found for each image files
%fill the connected components with different color
imshow(label2rgb(L, @jet, [.5 .5 .5]))
hold on
l=bacLength;
seconorder=mean(l.^2);
forthorder=mean(l.^4);
x=bacLength';
phiL=(forthorder/(3*(seconorder)^2))-1
% measure of non Gaussianity of the distribution of the bacterial length
meanL=mean(bacLength)  % measures average length of bacterial cells
varL=var(bacLength)  % measures variance of bacterial length
skL=skewness(bacLength) % measures skewness of bacterial cells
kurtL= kurtosis(bacLength) % measures kurtosis
save('MG1655_MgSO4_2.5per_length.dat','x','-ASCII')
figure
hist(x,50)
data=zeros(5,1);
data(1)=meanL;
data(2)=varL;
data(3)=phiL;
data(4)=skL;
data(5)=kurtL;
```

```
save('MG1655_MgSO4_2.5per_statpar.dat', 'data', '-ASCII');
% Save the length parameter data file on local directory.
```